Master Thesis, Department of Geosciences

Monitoring CO_2 behaviour during injection into reservoir sandstone

Truong Xuan Tran

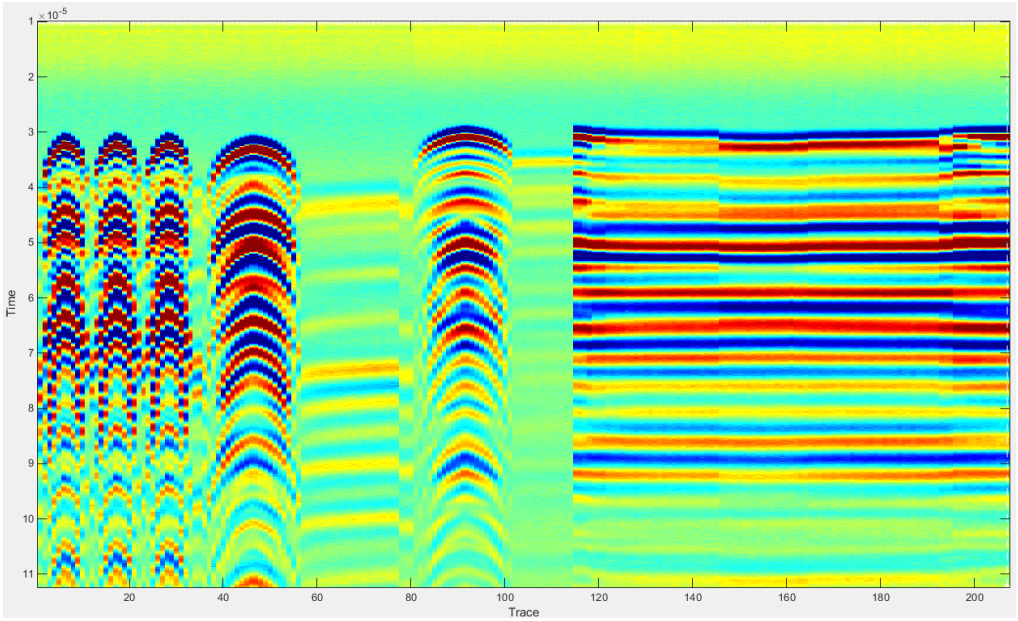

UNIVERSITY OF OSLO

FACULTY OF MATHEMATICS AND NATURAL SCIENCES

Monitoring of CO_2 behaviour during injection into reservoir sandstone

Truong Xuan Tran

Master Thesis in Geosciences

Discipline: Geophysics

Department of Geosciences

Faculty of Mathematics and Natural Sciences

University of Oslo

June, 2015

Preface

This thesis is a part of collaboration between the University of Oslo (UiO) and the Norwegian technical institute (NGI) for FME Subsurface CO_2 storage – Critical Elements and Superior Strategy (SUCCESS), project number 193825. Submission will be done to the Department of Geoscience at University of Oslo for candidacy of M.Sc. in Geophysics.

Laboratory work was done at Norwegian Geotechnical Institute (NGI) and results analyzed at the Department of Geoscience. Time period for this work was August 2014 – June 2015 supervised by Dr. Nazmul Haque Mondol, Associate Professor, Department of Geoscience, UiO, Norway and Dr. Øistein Johnsen, Senior Scientist, Polytec R&D Institute.

Acknowledgments

I would like to express my gratitude to my supervisors Dr. Nazmul Haque Mondol and Dr. Øistein Johnsen for their continuous support, encouragement and guidance. Discussions with them have always brought forth improvement of my thesis.

My sincerely thanks staff at NGI Dr. Joonsang Park for support and encouragement, Magnus Soldal for guiding me through the laboratory experiment and improving my thesis, Heidi Debreczeny Wilkinson for fixing the many problems in the lab, Guillaume Sauvin and Inge Viken for helping to improve acoustic measurements.

I would like to thank my lab partner Lamech Omondi Omolo for interesting discussions during and after laboratory work.

Thanks to Maarten Aerts for XRD analysis and Berit Løken Berg for her help with SEM analysis.

Lastly I would like to thank my family for their support to finish my thesis.

Abstract

Storing CO_2 in deep subsurface aquifers is considered to be a good solution for reducing the increasing atmospheric emissions of CO_2. To mitigate the possibility of stored CO_2 leaking out to the atmosphere, geophysical monitoring techniques are applied. These techniques must be able to detect small and big changes in CO_2 saturation. In this thesis acoustic and electrical resistivity measurement will be used to detect and monitor the injection of CO_2 into three brine saturated samples.

Two sandstones from the Gres des Vosges formation with different orientation relative to bedding and one Berea sandstone were selected. Each sample is in turn placed in a nitrile sleeve with piezo-elements for acoustic and resistance measurements. A hydrostatic pressure vessel is used to simulate reservoir condition by using pumps to apply an effective pressure of 15MPa on the sample and 10MPa pore pressure when saturated. These samples are will undergo several experiment exposing them to different conditions. Each sample undergoes a set series of loading cycles (dry, fully CO_2 and full brine saturated) before drainage and imbibition. In drainage CO_2 is injected from the top and pushed downwards and in imbibition brine is injected from the bottom. Pressure and temperature are assumed constant during drainage and imbibition.

For Gres des Vosges (drilled perpendicular to bedding) two additional drainage and imbibition experiments were done to asset flow rate influence on CO_2 injection.

Rock physical and pore fluid analysis were used to interpret acoustic velocity and electrical resistivity measurements. Analysis shows CO_2 saturation and front movement are affected by injection flow rate, orientation of beddings, permeability and prior injection experiments.

Acoustic velocities in axial direction decreases by 7.8%, 7.4% and 4.8% for respectively Gres des Voges drilled perpendicular to bedding, parallel to bedding and Berea. For saturation of CO_2 passes 20%, the acoustic velocity has little to no significant changes.

Front movement of CO_2 can be seen on both acoustic and resistivity measurement. At high saturation of CO_2 resistivity can be used to estimate saturation. Saturations found for Gres des Voges in axial direction are 60% for perpendicular to bedding and 49% for parallel to bedding.

An increase in flow rate decreases the saturation of CO_2 shown constant flow rate from start to finish of 2.5mL/min results in 57% while 0.5mL/min results in 58%. Results from Gres des Voges suggest a continuous usage after first drainage and imbibition alters permeability of the sample.

Table of contents

List of Figures

Chapter 2

Chapter 3

Chapter 4

Chapter 5

Chapter 6

List of tables

Chapter 2

Chapter 3

Chapter 4

Chapter 5

Chapter 6

Chapter 1: Introduction

1.1. Background and motivation

Average global temperature has varied predictably before the industrial revolution then accelerated after. Scientists have linked this change in temperature and weather conditions to the increase in accumulated carbon dioxide (CO_2) concentration from hydrocarbon (HC) usage. Extreme weather such as heat waves and flooding is predicted to likely become more frequent and last longer (IPCC, 2013).

One possible solution to reduce the CO_2 emission while continuing use of HC as a main energy source is carbon capture and storage (CCS). This technology will enable capturing CO_2 at its source and injecting into a subsurface geological formation for permanently storage. CCS will make it possible to continuously use HC while reducing the CO2 emission.

Saline aquifers are considered to be good candidates to permanently store CO_2 in a geological storage. Indirect monitoring techniques (i.e. acoustic and electrical resistivity) can used to observe the changes fluids in the subsurface. This makes it possible to look for leakages from the aquifer and study the how the CO_2 will behave and where it is moving after being injected. Laboratory experiments (Alemu et al., 2013; Onishi et al., 2006) have been conducted on the behavior of CO_2 injected into a brine saturated sandstone. This study will use of a multi directional array of sensors to measure both acoustic and electrical resistivity along the length of the sample. Difference in flow rate, type of sandstone and permeability will be tested.

1.2. Research objectives

The research objective for this thesis is to understand and see how injecting CO_2 into a brine saturated sample affects acoustic and resistivity measurements in a lab environment. A set-up enabling multi directional measurement, one axial and three radial at different angles and positions, is used on the sample. Several steps are used to reach this objective:

- Select samples for experiments and characterize them from literature
- Define the experimental procedure
- Define pore fluids needed for the experiments
- Get an overview of theoretical framework needed for analysis of data
- Execute the experiment and collect data
- Process data with Matlab scripts and excel sheet
- Analyse processed data and compare with literature

1.3. Database and software

1.3.1. Sandstone samples

Sandstone selected to represent geological storages in this study are Gres des Voges and Berea sandstone.

Gres des Voges is a sandstone from The Vosges Mountains in the eastern France. It is of Triassic or Permian formation and with a rose color. Gres des Vosges was selected after considering available sandstones at NGI. Core samples were drilled perpendicular and parallel to bedding.

Berea sandstone is from Ohio in the US. A high permeable plug of Berea was bought from Berea Sandstone Petroleum Cores and cut at NGI to core samples for experimental use. One core sample drilled vertical to bedding is used. This sample is from the Mississippian formation and consists mainly of quartz.

1.3.2. Software

Modlab was used for instrumental control and data acquisition, NGI PS-waves for acoustic and Resistivity_test for electrical resistivity measurements during the whole experiment. All measured data are written out to text files.

Mechanical data from Modlab were written to text files which were loaded and processed in excel This excel file is developed by NGI to do corrections on data and rock properties. From here the processed mechanical data was given out as an output excel file.

The Matlab script time_picker by Inge Viken at NGI was used to pick the arrival time for acoustic measurement. This script allows for a semi-automatic pick of first arrival time for P- and S-waves. The script gives a visual presentation of traces for a single channel using a color bar to differentiate top (blue) and bottom (red) peak, in addition to show original traces. Time_picker works by first loading acoustic data in, select control points for arrival time and let the script calculate where the other picks should be. Corrections can be done by adding more control points. The final picks can then be saved to a text file.

A self-developed Matlab script was made to combine the acoustic and electrical resistivity data with the mechanical data excel file. This script is seen in appendix (A8.2), it works by reading the text file of either acoustic picks or resistivity measurements and compare the time stamp in text file with the time in excel. Measurements of acoustic and resistivity are put into the excel sheet when correct time has been found, this allows for studying the all the data together at the right condition. This script only read, find and write data. All the calculations are done inside the excel file where all equations and coefficients are extensively quality controlled.

1.4. Limitation and future works

Laboratory measurements are a small scale test compared to what would happen during a real injection into a saline aquifer. In these laboratory experiments the sandstones are fairly homogenous without any visible fractures, and they are both permeable and porous. An experiment such as this is easier to control when the known parameters are limited. Several additional parameters need to be mapped out when dealing with field experiments.

An aquifer for storage of CO_2 should be of significant size and be underlying a tight cap rock. Such an aquifer will have a considerable bigger extent and thickness than the sample core. Parameters like fractures, one or more shale layers in between and different types of brines with varying properties are among parameters which need to be accounted for to have reliable measurements which can be transferred from laboratory to the field.

Future work should involve testing with different parameters to see how they affect the acoustic and electrical measurements. Parameters like sample heterogeneity and different fluids (i.e. use different brines), temperature (i.e. gas or supercritical CO_2) and flow rates will be relevant to study.

1.5. Chapter description

Chapter 1 gives a general background for this thesis including the motivation and research objective. Sandstone samples and software used for possessing the measured data are also given as well as the limitation of this thesis.

Properties of pore fluids are presented in Chapter 2 with equations used for analyzing measured data. Most of the information is from published work.

Three samples used in the experiments are characterized in Chapter 3 with the use of XRD, SEM and available literature.

These samples will undergo experiments elaborately explained in the experimental procedures in Chapter 4.

Chapter 5 presents the results from acoustic velocity and electrical resistivity measurements analysis.

A discussion is given in Chapter 6 regarding the results from Chapter 5.

Chapter 7 summarizes this thesis with conclusions will at the end.

Chapter 2: Theoretical background and methodology

2.1. Work flow

Fig. 2.1 describes the work flow of the whole thesis. A literature study is done to get background information about experimental procedure, sample characterization and equations used for analyzing the results. Experiments are executed simultaneously as the samples undergoes characterization processes, results from both are used to analyze the behavior of CO_2.

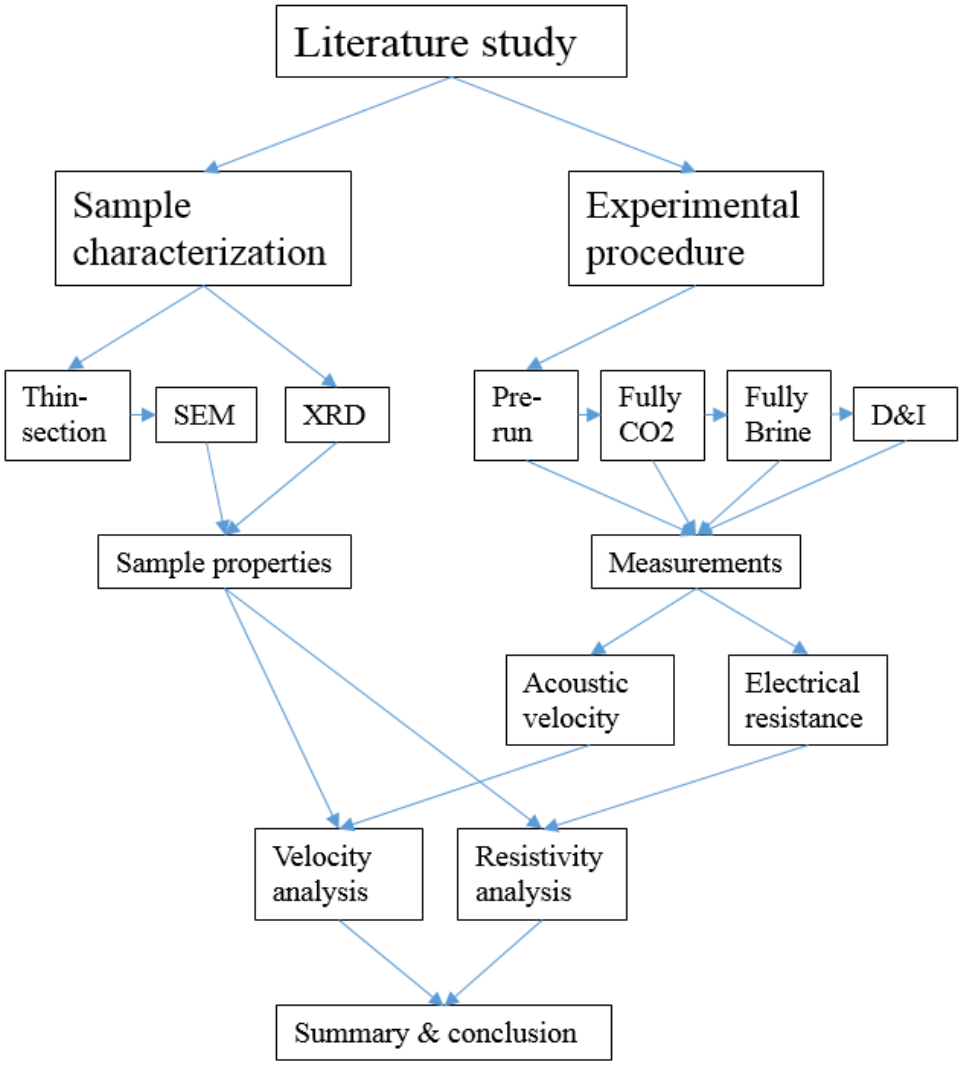

Fig. 2.1 Work flow for thesis

2.2. Pore fluids

Two fluids are used for this study, liquid CO_2 and brine under a pressure of 10MPa and temperature at 22°C. Density, bulk modulus and viscosity for these fluids will defined.

2.2.1. Carbon dioxide (CO_2)

CO_2 is a natural molecule consisting of one carbon atom bounded to two oxygen atoms. It can be found in the atmosphere where it acts like an absorber and re-emitter of infrared (IR) energy. This makes the CO_2 an excellent heat-trapper for the IR radiation emitted from the Earth. As the concentration of CO_2 increases, more IR energy will be trapped resulting in increase of the Earth's temperature.

Processes involving burning fossil fuel and cement production are some of the sources of CO_2 emission. Volcanic and hotspot activities are examples of big natural sources which also can release big amount of CO_2 over one or several periods of time.

CO_2 can change phases by changing pressure and temperature. Fig. 2.2 shows four different phases which are gas, liquid, solid and a midway phase between gas and liquid at the critical point (also known as supercritical CO_2). Supercritical CO_2 is a fluid phase when temperature and pressure of CO_2 are above the critical point. Above this point the CO_2 will adapt to have properties between gaseous and liquid phases.

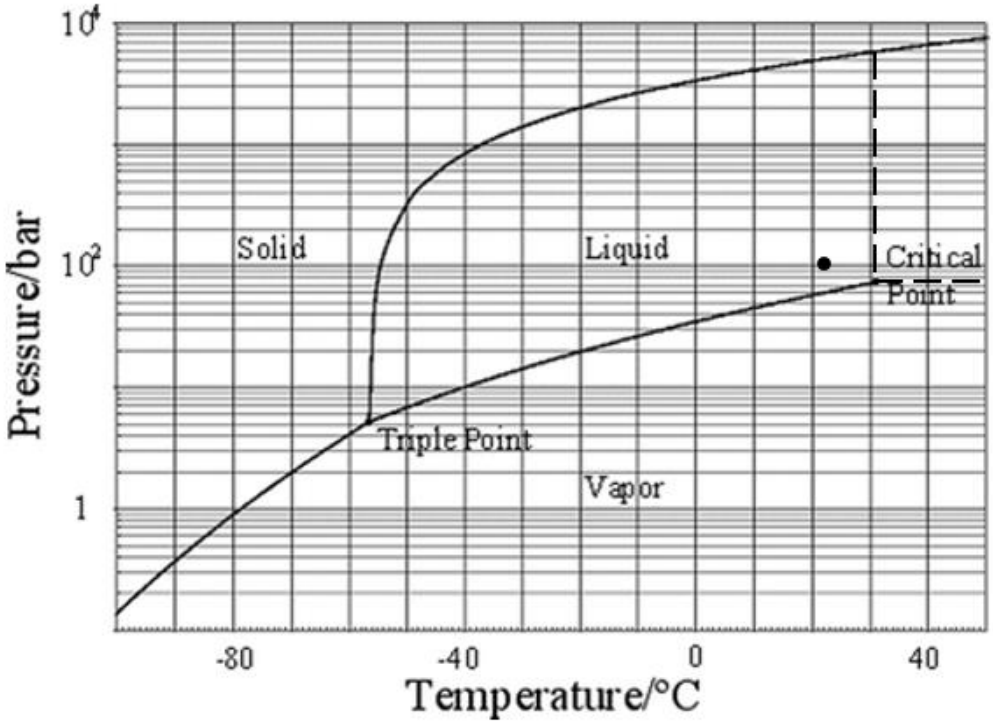

Fig. 2.2 Modified CO_2 phase diagram from McKenzie et al. (2004), black dot marks the temperature and pressure conditions for CO_2 in this study

Table 2.1 Properties of CO2 for different temperatures at 10MPa (Linstrom and Mallard)

Temperature (C)	Pressure (MPa)	Density (g/cm3)	Sound Spd. (m/s)	Phase
20	10	0.856	478.84	liquid
21	10	0.849	469.78	liquid
22	10	0.841	460.6	liquid
23	10	0.833	451.3	liquid
24	10	0.825	441.87	liquid
25	10	0.817	432.31	liquid

The National Institute of Standards and Technology (NIST) chemistry web book is used to get the properties of the liquid CO_2 as seen in Table 2.1. Speed of sound and density are used to calculate the bulk modulus for CO_2.

2.2.2. Brine

Pure deionized water is used together with sodium chloride (NaCL) to make a 30g/L NaCl brine solution. Properties from brine can be calculated by use of empirical equations from Batzle and Wang (1992) as shown below.

The brine velocity is given by equation 2.1 in m/s while 2.2 give the density in g/cm^3.

$$V_B = V_W + S*(1170 - 9.6T + 0.055T^2 - 8.5*10^{-5}T^3 + 2.6P - 0.0029TP - 0.0476P^2) + S^{1.5}(780 - 10P + 0.16P^2) - 820S^2 \quad 2.1$$

$$\rho_b = \rho_w + S\{0.668 + 0.44S + 10^{-6}[300P - 2400PS + T(80 + 3T - 3300S - 13P + 47PS)]\} \quad 2.2$$

V_w is the pure water velocity in m/s and can be calculated through equation 2.1 with help of Table 2.2.

$$V_w = \sum_{i=0}^{4}\sum_{j=0}^{3} w_{ij}T^iP^j \quad 2.1$$

Where T is the temperature and P is the pressure given in degree Celcius and MPa respectively. S is the weight fraction of NaCL in the solution in ppm/1000000 and ρ_w is the density of pure water in g/cm^3 calculated by equation 2.2 and shown in Table 2.3.

$$\rho_w = 1 + 10^{-6}(-80T - 3.3T^2 + 0.00175T^3 + 489P - 2TP + 0.016T^2P - 1.3 * 10^{-5}T^3P - 0.333T^3 - 0.002TP^2) \quad 2.2$$

Table 2.2 Coefficients for water properties calculations (Batzle and Wang, 1992)

$w_{00} = 1402.85$	$w_{02} = 3.437 \times 10^{-3}$
$w_{10} = 4.871$	$w_{12} = 1.739 \times 10^{-4}$
$w_{20} = -0.04783$	$w_{22} = -2.135 \times 10^{-6}$
$w_{30} = 1.487 \times 10^{-4}$	$w_{32} = -1.455 \times 10^{-8}$
$w_{40} = -2.197 \times 10^{-7}$	$w_{42} = 5.230 \times 10^{-11}$
$w_{01} = 1.524$	$w_{03} = -1.197 \times 10^{-5}$
$w_{11} = -0.0111$	$w_{13} = -1.628 \times 10^{-6}$
$w_{21} = 2.747 \times 10^{-4}$	$w_{23} = 1.237 \times 10^{-8}$
$w_{31} = -6.503 \times 10^{-7}$	$w_{33} = 1.327 \times 10^{-10}$
$w_{41} = 7.987 \times 10^{-10}$	$w_{43} = -4.614 \times 10^{-13}$

Table 2.3 Calculated properties for pure water and brine solution

		pure water		brine		
T Celcius	P Mpa	V m/s	density g/cm3	V m/s	density g/cm3	Bulk modulus Gpa
20	10	1514.93	1.0021	1548.45	1.022793	2.452338
21	10	1518.02	1.001893	1552.05	1.022583	2.463262
22	10	1521.03	1.00168	1554.85	1.022368	2.471619
23	10	1523.98	1.001461	1557.57	1.022149	2.479755
24	10	1526.85	1.001236	1560.22	1.021926	2.48767
25	10	1529.65	1.001005	1562.81	1.021698	2.495366

2.2.3. CO_2 in contact with brine

CO_2 in contact with brine can cause salt precipitation and anhydration effect (Alkan et al., 2010). Salting-out will decrease the permeability and porosity at the injection point. Reduced permeability and porosity results in higher injection pressure needed due to increase in capillary pressure.

2.2.4. Viscosity of brine

Viscosity of brine has been studied by several authors, a recent study by Francke and Thorade (2010) compares different methods of calculating dynamic brine viscosity. The general finding were an increase in viscosity with increasing NaCl in solution.

2.2.5. Capillary and viscous fingering regime

Capillary fingering regime has been studied extensively (Méheust et al., 2002). This regime dictates the fluid distribution and flow when a non-wetting fluid invades a porous medium saturated with wetting fluids, where the non-wetting fluid has lower viscosity. Neglecting gravity gives two cases, very low and high flow rates. In very low flow rates capillary pressure dominates over viscous forces (Capillary fingering regime), thus the displacement pattern depends on the distribution of throats. In high flow rates the viscous forces dominates over capillary and gravity effects (Viscous fingering regime), the displacement is dependent on which of the fluids is more viscous. When the invading fluid is less viscous than fluid in the pores, the displacement is unstable. A more viscous fluid invading a less viscous fluid will have a stabilizing front.

2.3. Acoustic velocity

Acoustic measurements involves the use of compressional and shear waves from which velocities, Vp and Vs, is determined. This can give information about the change of pore fluids in the subsurface where direct monitoring cannot be done (Siggins et al., 2010).

2.3.1. Relationship between elastic waves and moduli

Compressional and shear-wave velocities are functions of elastic moduli, porosity and pore fluids (Batzle and Wang, 1992; Benson and Wu, 1999). Equation 2.3 and 2.4 shows this relationship.

$$V_p = \sqrt{\frac{K^* + \frac{4}{3}G^*}{\rho^*}} \quad 2.3$$

$$V_s = \sqrt{\frac{G^*}{\rho^*}} \quad 2.4$$

Where K^*, G^* and ρ^* is the effective bulk modulus, shear modulus and density of the saturated sample.

Effective values are used to simplify the estimation of sample properties containing more than one type of mineral. "The Voigt and Ruess averages are interpreted as the ratio of average stress and average strain within the composite" (Mavko). Voigt is the upper bound and assumes a uniform strain while Reuss is the lower bound assuming a uniform stress. For the samples an average of Voigt's and Reuss is used known as the Hill's average. A geometrical illustration Voigt and Reuss can be seen in Fig. 4.3 where a is the Reuss and b is Voigt's when pressure is applied from top and bottom.

$$K_s = \frac{1}{2}(K_v + K_r) \textit{ (Hill's average)} \quad 2.5$$

$$K_v = \sum_{i=1}^{n} f_i K_i \textit{ (Voigt's average)} \quad 2.6$$

$$K_r = \left(\sum_{i=1}^{n} \frac{f_i}{K_i}\right)^{-1} \textit{ (Reuss average)} \quad 2.7$$

fi is the volume fraction of the mineral in the sample with bulk modulus *Ki*. Shear modulus is calculated the same way as bulk, for fluids Reuss will be used due to the isostress assumption (2.12) and Voigt's for density.

Sample characterization and acoustic measurements will be used to find saturation during fluid substitution. Uniform and patchy saturation will be considered.

Gassmann (1951) equation is used for uniform saturation of a sample. Three assumptions are essential:

- All pores are connected (total porosity = effective porosity)
- All grains have the same properties
- Pore fluid distribution is homogenous and fully saturates the pore space

Chemical interactions and effect of surface tension, attenuation and dispersion are not considered in Gassmann (Biot, 1956; Geertsma, 1961).

Equation 2.13 gives the effective bulk modulus for a saturated sample with one or more pore fluids. Keff is a function of Kf (2.14) which is also a function of saturation as density is, thus be varying the saturation a Vp can be calculated to match the measured Vp.

$$K_{eff} = K_d + \frac{\left(1-\frac{K_d}{K_s}\right)^2}{\frac{\emptyset}{K_f}+\frac{1-\emptyset}{K_s}-\frac{K_d}{K_s^2}} \quad 2.8$$

K_f is the bulk modulus of the fluid saturating the sample 2.9, K_d is the bulk modulus of the dry rock frame, ϕ is the effective porosity and K_s is the bulk modulus of solid grains.

$$K_f = \left(\sum_{i=1}^{n} \frac{S_i}{K_i}\right)^{-1} \quad 2.9$$

S_i is the saturation fraction of fluid i with bulk modulus K_i.

$$\rho = \rho_s * (1 - \emptyset) + \emptyset * (\rho_{brine} * S_w + \rho_{CO2} * S_{CO2}) \quad 2.10$$

Gassmann equation can be used to find the K_d by rearranging 2.8 to 2.11. Using measurements from Vp and sample characterization, the only unknown is K_d. Note measurements from dry or a sample saturated with one fluids are needed.

$$K_d = \frac{K_{eff}\left(\emptyset\frac{K_s}{K_f}+1-\emptyset\right)-K_s}{\emptyset\frac{K_s}{K_f}+\frac{K_{eff}}{K_s}-1-\emptyset} \quad 2.11$$

Bulk and shear modulus can be found by use of grain properties and empirical equations. Several authors have tried to find this relationship.

Hamilton (1970) studied a series of reports sound velocities and properties of marine sediments proposed equation 2.12 for the dry bulk modulus using logarithm. The test conditions was done under a pressure of 1 atm and 23°C.

$$log\left(\frac{K_d}{K_s}\right) = -4.25\emptyset \quad 2.12$$

Nur et al. (1995) presented a model based on critical porosity ($\emptyset_c$) as seen in equation 2.13 and 2.14. Critical porosity is the maximum porosity of a sample with its grains still in contact with each other.

$$K_d = K_s\left(1 - \frac{\emptyset}{\emptyset_c}\right) \quad 2.13$$

$$G_d = G_s\left(1 - \frac{\emptyset}{\emptyset_c}\right) \quad 2.14$$

K_d and G_d is the bulk and shear modulus for the dry rock while K_s and G_s is for the solid grains. Typical value for $\emptyset_c$ is about 40% for sandstones.

Geertsma (1961) suggest a near linear relationship for consolidated sandstone:

$$(\frac{K_s}{K_d} - 1) = 50\emptyset \quad 2.15$$

Krief et al. (1990) used Biot (1941) and Gassmann (1951) theory to express the following equation for the dry bulk modulus with the Biot factor, β_B.

$$K_d = K_s(1 - \beta_B) \quad 2.16$$

By use of β_B, effective bulk modulus can be calculated without K_d:

$$K_{eff} = K_s(1 - \beta_B) + \beta^2 M \quad 2.17$$

M depends on porosity and bulk modulus of solids and fluid

$$\frac{1}{M} = \frac{(\beta_B - \emptyset)}{K_s} + \frac{\emptyset}{K_{fl}} \quad 2.18$$

Data from Raymer et al. (1980) was used by Krief et al. (1990) to find a relationship between β_B and porosity:

$$(1-\beta_B) = (1-\emptyset)^{\frac{3}{1-\emptyset}} \quad 2.19$$

Krief et al. (1990) used Pickett (1963) observations to derive the equation for shear modulus with Biot factor:

$$G_d = G_s(1-\beta_B) \quad 2.20$$

A special version of equation 2.8 can be used for fluid substitution without the need for dry elastic moduli:

$$\frac{K_{f1}^*}{K_s - K_{f1}^*} - \frac{K_{f1}}{\emptyset(K_s - K_{f1})} = \frac{K_{f2}^*}{K_s - K_{f2}^*} - \frac{K_{f2}}{\emptyset(K_s - K_{f2})} \quad 2.21$$

Here K_{fi}^* is the effective bulk modulus of the saturated sample and K_{fi} is the bulk modulus of the fluid.

Changes in bulk and shear modulus can be used to explain the changes in the acoustic velocities during increase and decrease in effective pressure. Zhang and Bentley (1999) found an empirical relation for bulk and shear modulus of dry sample when effective pressure changes and temperature at 22ºC:

$$\frac{dK_d}{dP} = 0.746e^{-0.0773P} \quad 2.22$$

$$\frac{dG_d}{dP} = 0.372e^{-0.0791P} \quad 2.23$$

Patchy saturation a displacement model for when there are residual fluids (patches) after a displacement is done, Fig. 2.4d illustrates it with CO_2 not displacing all the brine. For patchy saturation Johnson (2001) present an equation with the use of Hill's theorem (Hill, 1963, 1964):

$$\left(K_{patchy} + \frac{4}{3}G_d\right)^{-1} = S_1\left(K_1^* + \frac{4}{3}G_d\right)^{-1} + S_2\left(K_2^* + \frac{4}{3}G_d\right)^{-1} \quad 2.24$$

K_i^* is the effective bulk modulus of a fully saturated sample with fluid i.

Fig. 2.3 illustrates how saturation can be estimated from acoustic measurement when sample and fluid properties are known. It works by both for homogenous and patchy saturations.

Effective bulk modulus is calculated based on zero CO_2 saturation, then a temporary velocity (Vp,c) is calculated. If Vp,c is greater or equal then if will go to the next measured Vp resetting CO_2 saturation to zero , if not 1% is added to the CO_2 saturation and a new effective bulk modules is calculated and so on.

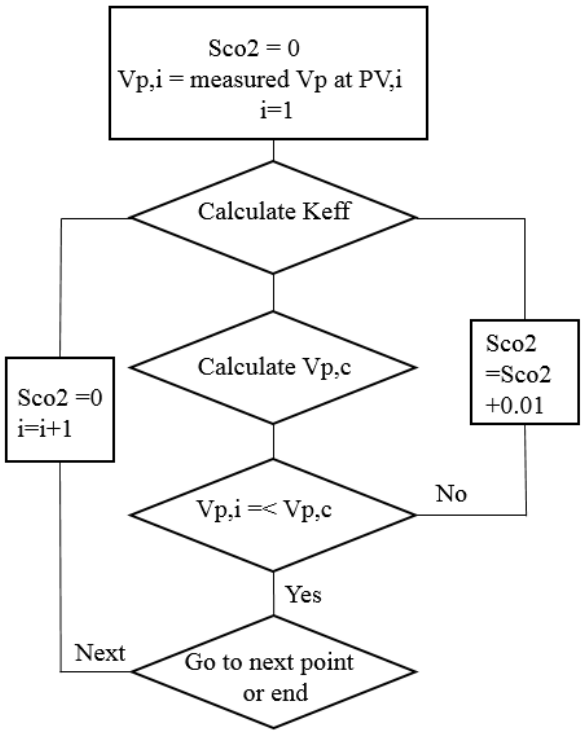

Fig. 2.3 Iteration schematic for saturation estimation

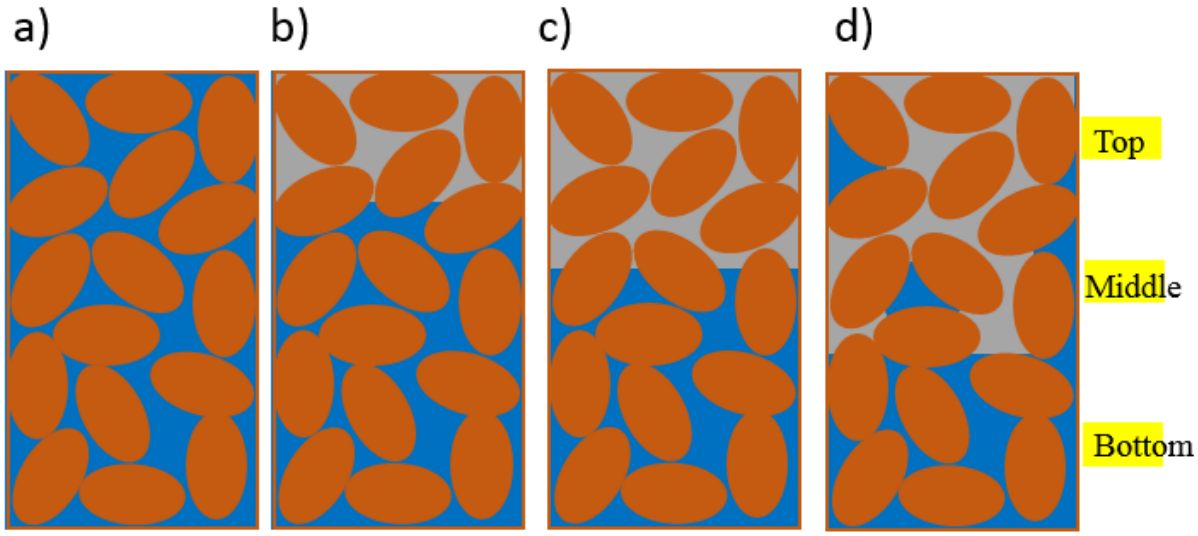

Fig. 2.4 a) fully brine, b) and c) homogenous saturation with moving front of CO2 and d) patchy saturation

Table 2.4 Mineral properties

Minerals	Bulk modulus [GPa]	Shear modulus [GPa]	Density [kg/m^3]	Source
Quartz	37	44	2.62	Carmichael (1989)
Mica 2M1	42.9	22.2	2.79	Carmichael (1989)
Kaolinite	1.5	1.4	1.58	Woeber et al. (1963)
Calcite	73	32	2.71	Gebrande et al. (1982)
Albite	75.6	22.6	2.63	Woeber et al. (1963)
Ankerite	91	45*	2.97	Ross and Reeder (1992)
Microcline	55.8	27.2	2.56	Alexandrov et al. (1966)

*No shear modulus for Ankerite was found, value from Dolomite is used as they resembles each other.

Table 2.4 shows the mineral properties needed to calculate the bulk modulus of the sample. Effective bulk modulus for a saturated sample depends on the fluid occupying the pore space as shown in 2.8, 2.17 and 2.24. The difference in bulk modulus in brine and CO_2 is greater than in their densities, which implies that Vp will change more than Vs when brine is replaced by CO_2 and vice versa. This makes the acoustic measurement useful in detecting changes in fluid properties and saturation in the subsurface.

Elastic moduli for the solid grains are calculated using XRD results (Table 3.5) and Table 2.4 together with equation 2.5 to 2.7, the results are as shown in Table 2.5.

Table 2.5 Elastic moduli for Gres des Vosges and Berea

	Bulk [Gpa]		Shear [Gpa]	
	GDV	Berea	GDV	Berea
Reuss	34.304	25.578	28.694	26.709
Voigt	44.808	37.585	36.853	41.114
Hill	39.556	31.582	32.773	33.911

2.4. Resistivity

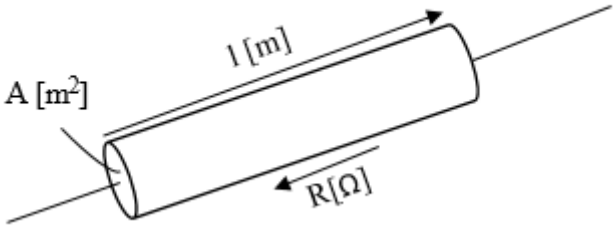

Fig. 2.5 Electrical current through a cylindrical medium

Resistivity is a measurement of how strong a material opposes the change in electrical current illustrated by Fig. 2.5. Brine has ions and will be more conductive than the liquid CO_2, thus the resistivity will increase with higher concentration of CO_2 and decrease with higher brine concentration. The change in resistivity will be an indication of the change in fluid saturations and/or distribution. Resistance is measured during the experiment, thus an equation to obtain resistivity is needed (2.25). A test was conducted to measure the resistance of wires by use of an aluminum dummy places inside the nithril sleeve, which resulted in 1Ω for all wires. Any value over 1Ω is due to the sample and fluid composition.

$$R^* = \frac{R * A}{l} \qquad 2.25$$

Where R^* is the resistivity [Ω*m], R is the electrical resistance [Ω], A is the cross section area of receiver/source [m^2], and l is the length which the electrical current has traveled[m]

A correction factor (F_{corr}) is needed for the radial measurement since the all the electrical current from the source dose not go straight to the receiver, thus does not give a right value assuming a straight field . Fig. 2.6 shows an illustration of the electrical current for radial measurement.

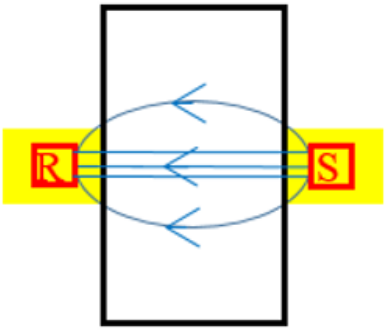

Fig. 2.6 Illustration of electrical current in radial direction

The correction factor takes into the account of anisotropy between axial and radial measurement, where axial values do not need correction. To find this factor, manual iterations are used with the start point as Rv/Rh = 1. Fig. 2.7 is provided by Jung Chan Choi at NGI. Multiplying equation 2.25 with the correction factor gives the corrected resisitivity value.

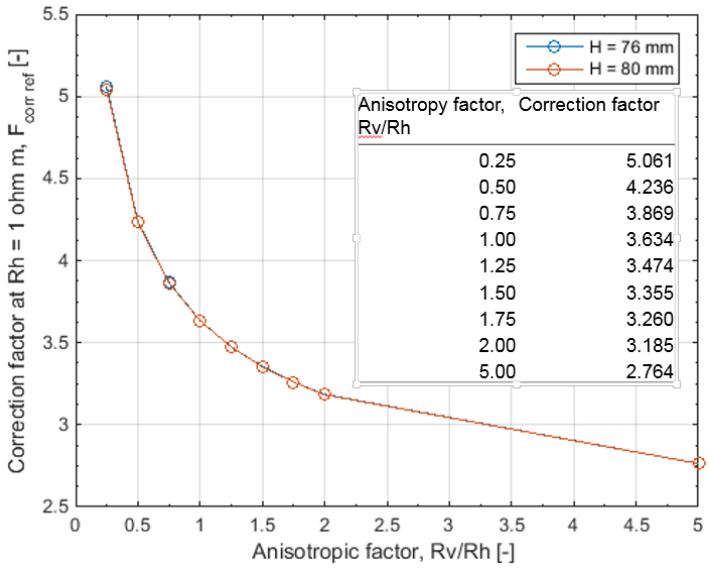

Fig. 2.7 Table with correction factor with corresponding plot

Resistance values for brine are used to find the correction factors when the pores are filled with only one fluid. This iteration is done in excel by first using F_{corr} as 3.634, then calculate Rv/Rh to find the F_{corr} from Fig. 2.7. Repeat until F_{corr} used to get Rv/Rh is the about the same as the one read from table/chart. Using trend line for Rv/Rh 0.5 to 2 to get the equation $y=3.6679x^{-0.221}$, where y is F_{corr} and x is Rv/Rh, makes this iteration faster as Rv/Rh do not exceed 2.

For the purpose of CO_2 injection, correction factor at effective pressure of 15MPa is found and shown in Table 2.6.

Table 2.6 Correction factors for radial measurements

Sample	Top		Middle		Bottom	
	Rv/Rh	Fcorr	Rv/Rh	Fcorr	Rv/Rh	Fcorr
GDV_V	0.770354	3.8856	0.959094	3.7019	0.748421	3.9105
GDV_H	1.051149	3.6276	0.881309	3.7717	0.796811	3.8567

Archie's equation is used to find the saturation from resistivity assuming a clean sandstone by combining equation 2.26 with 2.27 to get 2.28.

$$R_t = a\emptyset^{-m}S_w^{-n}R_w \quad 2.26$$

$$F = \frac{a}{\emptyset^m} = \frac{R_o}{R_w} \quad 2.27$$

$$S_w^n = \frac{R_o}{R_t} \quad 2.28$$

Here R_t, R_o and R_w is the resistivity of saturated sample, fully brine saturated sample and brine respectively, while $\emptyset$, m, n, a and S_w is the porosity, cementation exponent, saturation exponent tortuosity factor and water saturation respectively. To find the CO_2 saturation the relation $1 = S_w + S_{CO2}$ will be used. As seen in equation 2.28 many of the unknown factors falls away. R_o and R_t are measured, typical saturation exponent for sandstone is 2 (Onishi et al., 2006).

Chapter 3: Sample characterization

3.1. Sandstone samples

Two Gres des Vosges and one Berea 400mD sandstone samples were used in this study. One Gres des Vosges (GDV_V) and the Berea is drilled vertical, i.e. perpendicular to bedding while the other Gres des Vosges (GDV_H) is drilled horizontal, i.e. parallel to bedding. In addition two Red Wildmoor sandstones and a Berea 20mD samples are studied by Omolo (2015) for the same typ of experiments. Fig. 3.1 shows the two Gres des Voges and Berea samples used in this study.

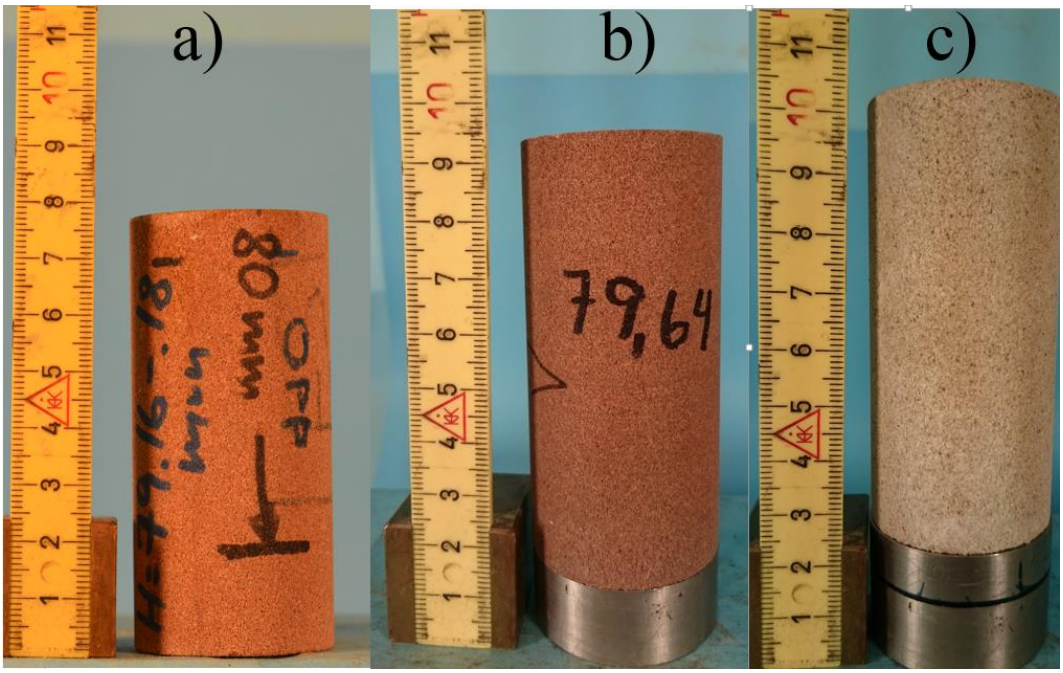

Fig. 3.1 Sandstone samples (a) GDV_H, (b) GDV_V and (c) Berea 400mD

Both types of sandstones are known permeable sedimentary rocks which have been studied and used in various experiment (Andre et al., 2010; Sarda et al., 1998). All sandstones samples have been Computed Tomography scanned (CT-scan), made into thin-sections for Scanning Electron Microscopy (SEM) and analyzed thoroughly using X-ray Diffraction (XRD) to characterize their properties. Table 3.1 shows the sample dimensions measured in the laboratory.

Table 3.1 Sample dimensions

	Length [mm]	Diameter [mm]
GDV_V	80	38
GDV_H	80	38
Berea	79	37

3.1.1. CT-scan

CT-scan uses multiple X-ray images acquired from all angles (0-360^{o}) to produce a tomographic image of the sample. This scan provides images from any angles in full 3D. Density distribution of the samples can be seen with CT images as variation in grey level intensity and is used to look for heterogeneities and structures of samples.

Fig. 3.2 is modified and shows the CT-scan of all three samples, from top and one of the side view cross sections are shown. Original images including two more side views can be seen in Fig. A1.4, Fig. A1.5 and Fig. A1.6 for GDV_V, GDV_H and Berea respectively. These images shows mostly homogenous samples as the gray levels are quite uniformly distributed in one sample. Minor darker and whiter spots can be observed as heavier or lighter minerals. Darker color indicates higher density and whiter lower. GDV_H images displays the beddings in the top view as stripes going from upper right corner to down left corner, on the side view these stripes goes from top to bottom. Observing beddings on vertical drilled samples are harder, the top only shows the top of the sample which is one layer. The side view does not clearly show the layers stacked up vertically, but these layers can be seen clearer on Berea images than GDV_V.

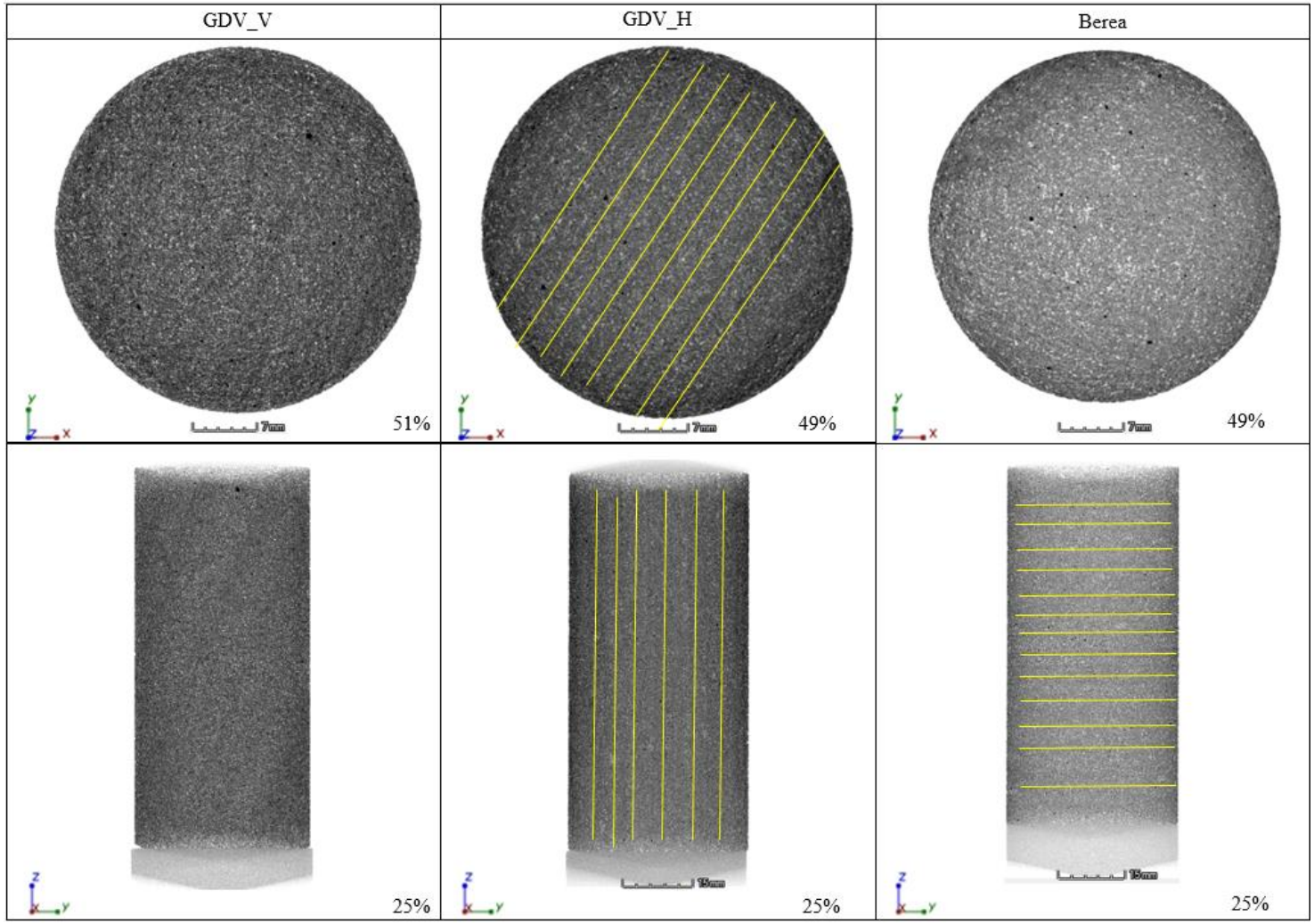

Fig. 3.2 CT-scan of samples, first row shows the top and second row shows one of the sides, yellow line drawn on is guidelines showing the sample structure. GDV_V has the same structure as Berea, but shows diagonal lines, these lines might be the after-effect of drilling the sample.

3.1.2. Thin section

A thin section is made by cutting a slice from the sample with diamond saw, by so obtaining a very thin disk with a flat surface which is polished to make a smooth flat surface. This flat side is then mounted to a flat glass with a colorless and isotropic cementing agent. When the piece is stuck to the glass, the final cutting of the piece is done to make it as thin as possible. To finish it, the new cut surface is polished down to obtain a thickness of about 30µm, cleaned and then sealed with epoxy.

3.1.3. Scanning electron microscope (SEM)

SEM provides a high resolution image of a solid sample by using the secondary or backscattered electron signal. For this analysis a type JEOL JSM-6460LV SEM, with LINK INCA Energy 300 (EDS) from Oxford Instrument was used. This device uses a standard wolfram filament (15 kV) and has detectors for secondary electrons (SEI), back-scattered electron (BEI), cathodoluminescenes C and X-Ray detector for elemental determination and mapping. Analyzing the pore system and estimating the amount of each mineral can be done by using SEM on a thin-section of the sample. In SEM, the lighter minerals will appear darker than heavier minerals. Quartz looks darker than K-feldspar in Fig. 3.3 due to the difference in unit weight. Heavy minerals such as Zircon, apatite and iron oxide was also found in small amounts as was kaolinite.

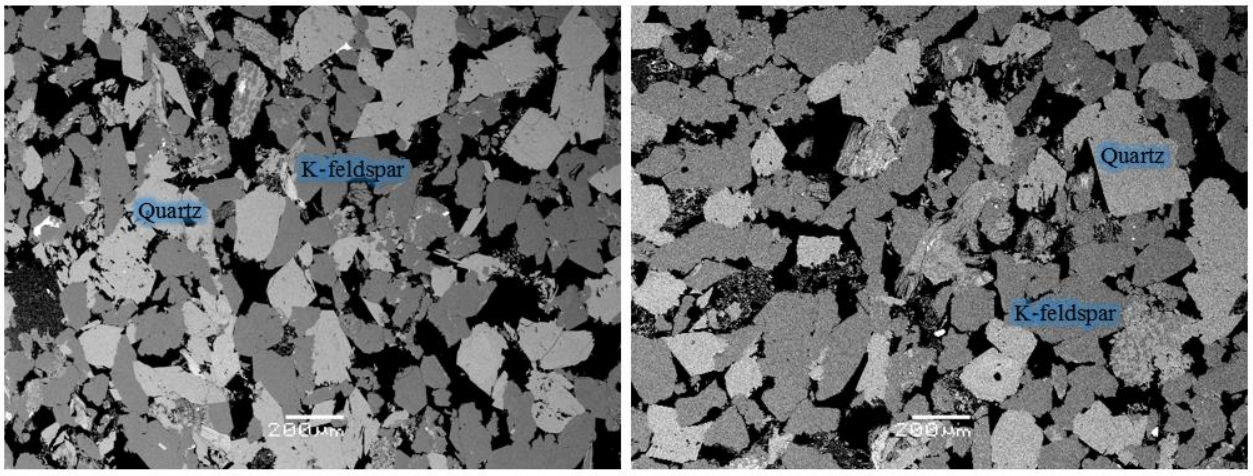

Fig. 3.3 Thin-section of Gres des Vosges, vertical sample to the left and horizontal sample to the right

Three images for the horizontal sample and two for the vertical sample were taken at the same magnification, but at different positions in the thin-section. Table 3.2 shows the summary of the mineral composition of the samples. The analyzed report of the thin-sections in Fig. 3.3 can be seen in the appendix (Fig. A1.7 and Fig. A1.8). Note that SEM reports provides the porosity + sum of mineral fractions = 1. Table 3.2 gives the mineral fractions as volume of individual minerals divided by total volume of only minerals. These porosities are measured in 2D.

Table 3.2 Mineral composition of Gres des Vosges from SEM

Gres des Vosges [%]					
Porosity	Kaolinite	Quartz	K-feldspar	Heavy minerals	Orientation
21.2	8.0	52.6	39.4	0.3	H
21.4	6.3	68.5	25.3	0.3	H
19.1	5.3	65.1	29.6	0.2	H
20.8	4.5	71.8	23.6	0.1	V
22.6	5.8	64.1	30.1	0.3	V

As seen in Table 3.2 the local porosity varies from 19.1% till 22.6%. These porosities are in the same range as found in literature, where porosity is measured in 3D. Sarda et al. (1998) used two Gres des Vosges samples with porosities of 19.5% and 17%, while Andre et al. (2010) used one with porosity of 21.8%. Based on SEM results and these authors, the porosity of both Gres des Vosges samples will be set to be 20%.

Porosity can be estimated by use of the weight of dry sample before the experiment and the brine saturated sample after. By rearranging equation 2.29 an estimation of porosity can done as shown in equation 2.30.

$$\rho_{sat} = \emptyset\rho_{fluid} + (1 - \emptyset)\rho_{solid} = \emptyset\rho_{fluid} + \rho_{dry} \quad 2.29$$

$$\emptyset = \frac{\rho_{sat} - \rho_{dry}}{\rho_{fluid}} \quad 2.30$$

where ρ is the density in kg/m^3 and ϕ is the porosity.

Table 3.3 shows the porosity estimation based on equations 2.7. The estimated porosity for Gres des Vosges is lower than what SEM indicates but close to the samples used by Sarda et al. (1998). The porosity from SEM may represent the total porosity while the estimated is the effective porosity. Measurements on the samples were done in an approximate temperature of 22^{o}C and standard pressure. Air density is negligible as it is very small compared to the grain densities. Dry

densities shown in Table 3.3 are assumed to be for the sandstone in vacuum. Measurements for dry samples were done prior to the experiments. Samples were dried out after the experiments and showed increase in weight, GDV_V measured 181.79g, GDV_H 179.51g and Berea 174.24g. This increase is assumed to be mainly due to salt.

Table 3.3 Estimate of porosity

Direction of sample	Dry		wet		Volume of sample [m3]	Fluid density [g/cm3]	Porosity
	mass [g]	density [g/cm3]	weight [g]	density [g/cm3]			
GDV Vertical	181.37	2.004	196.53	2.172	90.5	1.022	16.4 %
GDV Horizontal	179.28	1.996	195.8	2.180	89.8	1.022	18.0 %
Berea vertical	174.07	2.052	187.77	2.213	84.8	1.022	15.8 %

SEM can also be used on a small chunk of the sample as shown in Fig. 3.4 for Berea, where quartz and k-feldspar are identified on the surface of the chunk. Here the porosity can not be estimated, but the grain growth and size is visible. Other minerals as kaolinite, lillite and iron oxide were also found see (Fig. A1.1 to Fig. A1.3) in appendix. Several authors have used Berea sandstones in their experiment or study as shown in Table 3.4. As there are no thin-section of Berea sandstone, a porosity of 20% will be assumed based on the permeability of 400 mD and the Table 3.4.

Table 3.4 Berea properties from literature

Perm	Φ[%]	Mineral composition [%]							Ref.
mD		Quartz	Feldspar	Clay	Calcite	Mica	Ankerite	Other	
n/a	21	75	10	10	5	n/a	n/a	n/a	[1]
1100	23	n/a	n/a	n/a	n/a	n/a	n/a	n/a	[2]
n/a	n/a	90.6	4.1	1.6	trace	trace	0.4	3.6	[3]
2.8	14.8	72.3	3.6	9.8	0.2	3.2	5.2	5.4	[4]
40.6	17	72.5	2.9	11.3	0.1	3.9	3.2	5.7	[4]
1.5	10.4	69.1	2.6	10	0	1.1	10.3	6.6	[4]
26.2	15.7	72	3.1	10.9	0.1	3.3	4.6	5.7	[4]
1.7	12.6	63.6	2.6	14.6	0.5	4.5	7.9	6	[4]
3.7	15.2	74	2.8	10.3	0.1	2.8	4.5	5.1	[4]
102.3	22.7	74	3.2	10.1	0.1	3	2	7.4	[4]
24.10	16.3	72.3	2.9	10.9	0.2	3	4.5	5.8	[4]
172.5	24.3	n/a	n/a	9.3	8	n/a	n/a	n/a	[5]
240	24	n/a	n/a	n/a	n/a	n/a	n/a	n/a	[6]
300	22	n/a	n/a	n/a	n/a	n/a	n/a	n/a	[7]

[1] Zhang et al. (1990)
[2] Hazlett (1995)
[3] Dawson et al. (2014)
[4] Balthazor (1991) *note that TABLE uses mineral composition instead of average composition which includes inter- and intra-granular porosity.
[5] Baraka-Lokmane et al. (2007)
[6] Geertsma (1961)
[7] Garg et al. (1996)

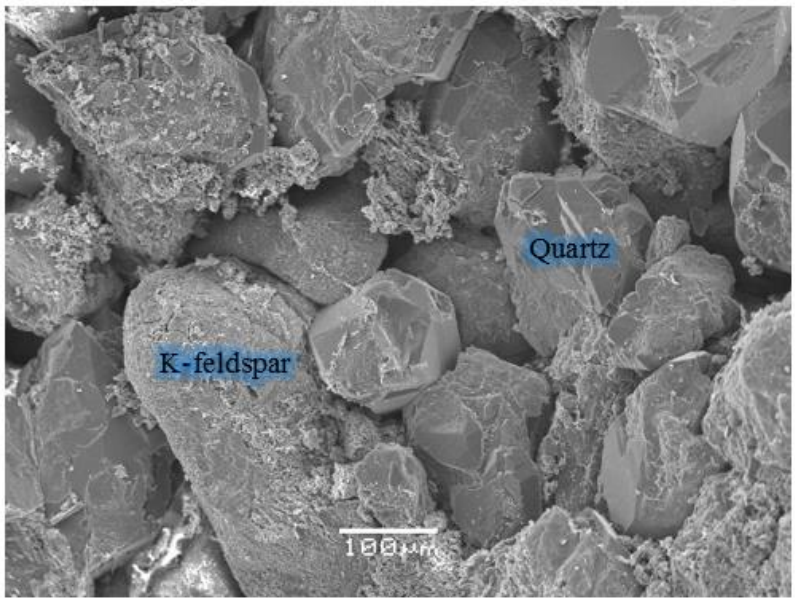

Fig. 3.4 Berea sandstone

3.1.4. X-ray diffraction (XRD)

Bruker D8 Apex 3-circle diffractormeter is utilized to identify the amount of minerals in a sample with the use of X-rays. A piece of each sample is taken and pulverized separately (grains size in the order of micro meters, 10^{-6}m). The pulverized sample is put into three different containers and inserted into the diffractormeter. Here each container will be exposed to a series of X-Ray beams which diffracts upon contact with the powder and are recorded. These diffracted rays are studied closer in a software where it will be compared to a known database to identify and quantify the minerals. Table 3.5 shows the results from the XRD analysis.

Table 3.5 XRD result for Gres des Vosges (GDV) and Berea sandstone

Mineral	GDV[%]	Berea[%]
Quartz	60.7	87.18
Kaolinite	0.9	2.136
K-feldspar	28.2	2.783
Albite	6.8	0.402
Mica 2M1	3.4	3.18
Calcite	0	0.58
Ankerite	0	3.73

The dominating minerals found in SEM (Table 3.2) are visible in XRD, i.e. quartz and K-feldspar. SEM provides three local (zoomed in) estimations of mineral fractions. The average values from these reports are 6%, 64.4%, 29.6% and 0.2% for Kaolinite, Quartz, K-feldspar and heavy minerals respectively. SEM analysis do resembles the XRD, with some over and under estimation on kaolinite, quartz and heavy minerals. The difference is due to the nature of the analysis. SEM gives local estimation in a small restricted area while XRD gives a broader view. A good representation of mineral is needed to properly do XRD, thus more of the sample is pulverized than necessary. XRD results will be used as the mineral composition of grains. Small traces of minerals like zircon, apatite and iron oxide are not visible on XRD as higher amount is needed.

Chapter 4: Experimental setup

4.1. Triax system

Fig. 4.1 shows the summary for the experimental equipments. Up to three GDS pumps and an ISCO pump is used. Experiments are conducted inside a pressure vessel simulating pressure at reservoir condition. A GDS pump (Cpump) is used to control the confinement pressure created by silicon oil. The sample is enclosed with a nitrile sleeve and placed inside the pressure vessel between a top and bottom pedestal. During drainage an ISCO pump (CO_2 pump) is used to introduce CO_2 at the top of the sample while a Brine pump will act as a backpressure pump countering the pressure build-up at the top. Brine pump is a GDS pump connected to a cylinder containing 50 mL brine and 450 mL silicon oil. In imbibition CO_2 pump will act as the backpressure pump and Brine pump will inject brine from the bottom where pressure will build up. The cylinder in brine pump contains only brine. A second cylinder (separator) is used to separate CO_2 from brine as fluids leaves the sample from the top. This separator is placed between the top outlet from the sample and CO_2 pump, thus only allow CO_2 into the pump.

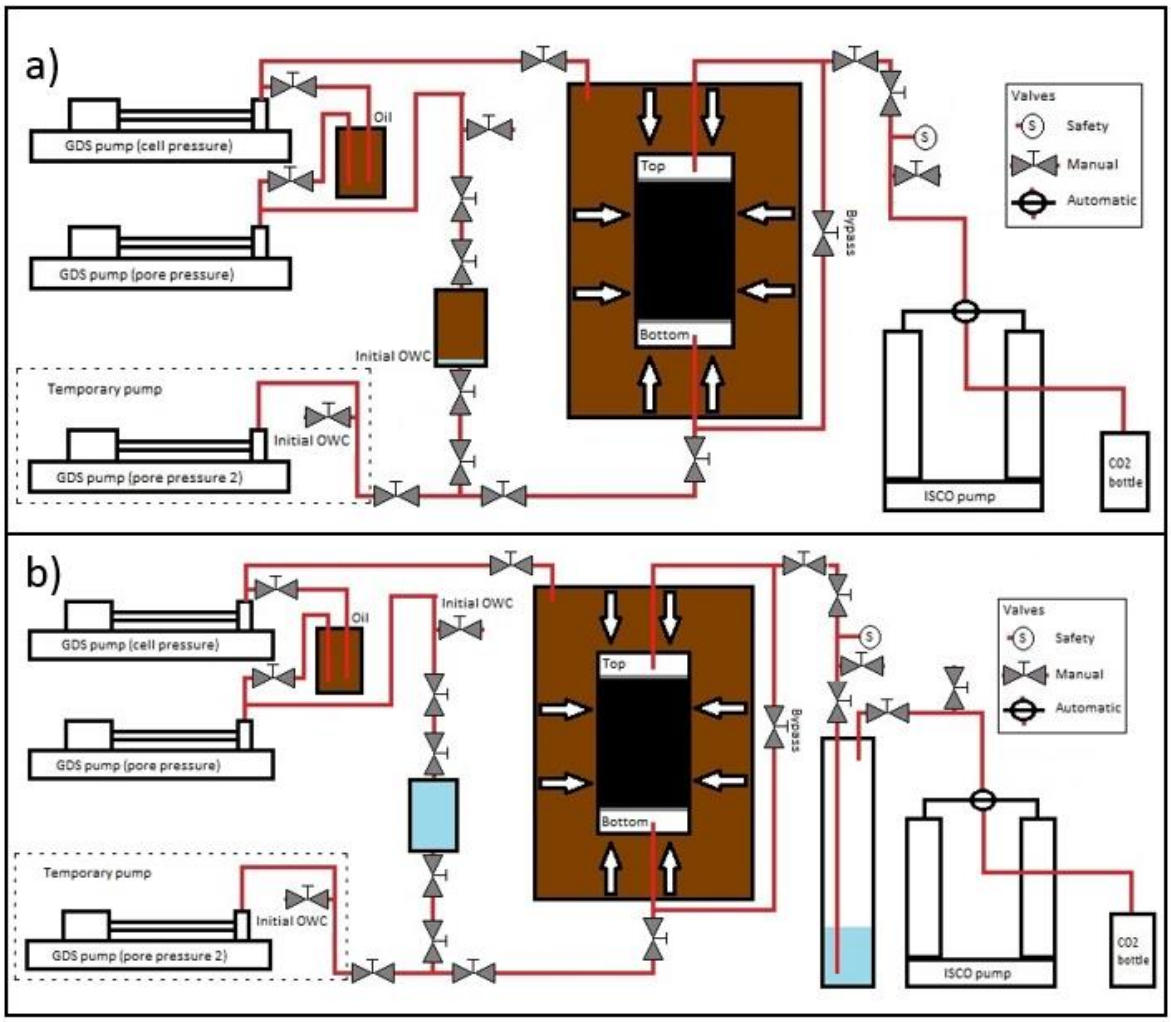

Fig. 4.1 Setup for (a) drainage and (b) imbibition

4.2. Sleeve configuration

A special made nitrile sleeve with sensors is used for acquiring acoustic velocities and electrical resistances from the sample placed inside. The main purpose of the sleeve is to isolate the sample from surrounding silicon oil. As seen on Fig. 4.2 the sleeve is equipped with three radial couples of sensors and receivers of the type P-wave piezo-ceramic crystals, and one sensor for measuring radial deformation. The three radial geophysical sensors will be referred to as top, middle and bottom from their physical position. This sleeve enables multidirectional measurement of acoustic velocities and resistance along the sample height. Fig. 4.2 the sleeve containing a sample mounted and wired inside a pressure vessel. The sleeve with a sample is placed between a top piece and bottom pedestal which is used for axial measurements and to channel fluids through the sample. Two axial deformation sensors are mounted on the top piece and measures the change in sample height during the experiments. Fig. 4.3 shows an illustration on how piezo-elements can be placed in regards to orientation of bedding in the sample. The relationship between orientation of sensors and bedding plane is not known and can only be speculated upon.

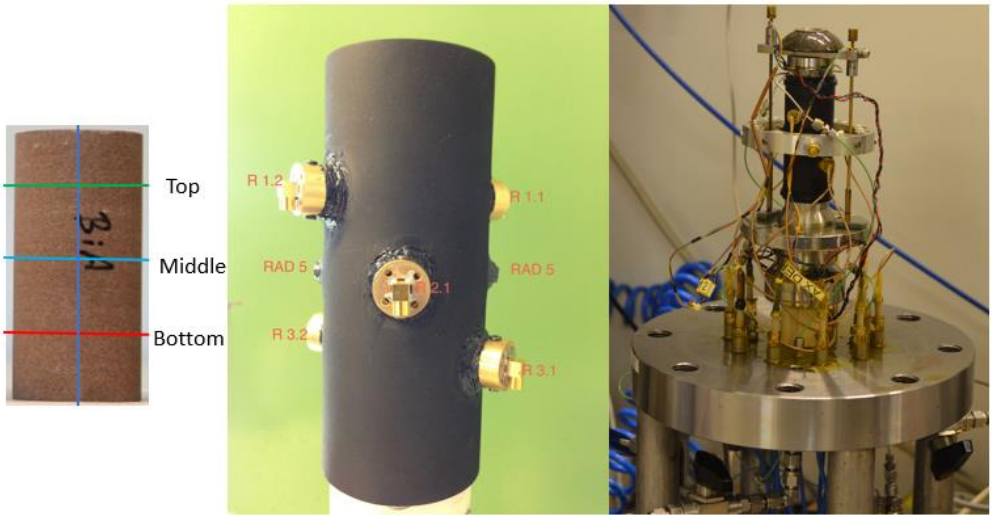

Fig. 4.2 (left) illustration of multi-directional measurement, (middle) Nitrile sleeve with sensors, (right) mounted sleeve with sample and deformation sensors

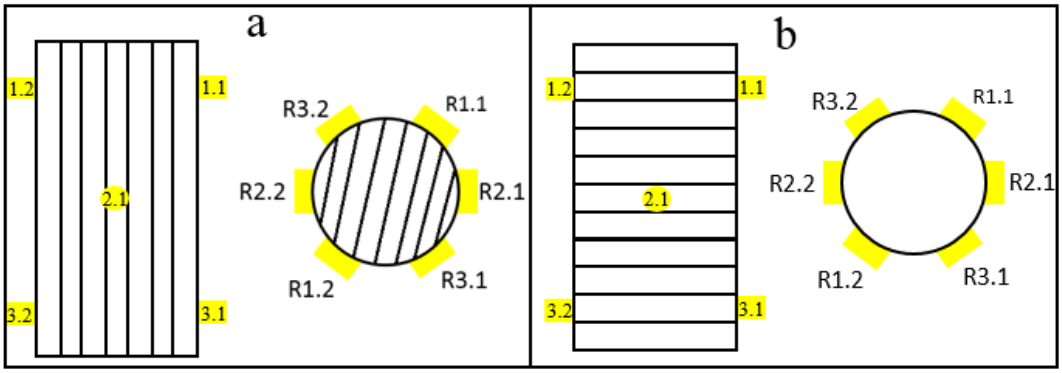

Fig. 4.3 illustration on piezo-element setup with sample from the side and top, a) horizontal drilled sample and b) vertical drilled sample

4.3. Acoustic velocity correction

The sources and receivers are not directly in contact with the sample, thus need a correction to get the velocities of the sample from measurements. Fig. 4.4 shows how the sensors and receivers are placed. There are three radial sensor and receiver pairs, but only one is shown here to simplify the figure. Red arrows show the time the signal takes from the source to arrive at the receiver, this is the measured signal. While blue arrows show what is desired, the time for the signal to travel past the sample.

Axial correction are done by first removing the sample, then press the top and bottom piece together with about 15MPa pressure, and lastly make a measurement for the Vp and Vs (Fig. 4.5). From these measurements t_0 for axial Vp and Vs is found by picking the first arrival, seen as green vertical lines in the figure. As seen there are two S-axial picks, this is due to measurement of the actual experiments. Fig. 4.7 shows the acoustic data measured for dry, fully brine, fully CO_2 and all three drainage and imbibition experiments. Choosing to follow the S-axial will result in decrease in Vs with increasing PV for drainage and increasing Vs with increasing PV for imbibition. According to equation 2.4 Vs will increase with decreasing density, thus a displacement of brine with CO_2 must give a higher Vs. Picking the arrival at a later time, S-axial 2, the observed Vs will behave as expected. GDV_V and Berea uses the time picks from S-axial 2 while GDV_H uses the S-axial.

An aluminum dummy is used to find the t0 for radial Vp measurements. The dummy is places inside the sleeve and pressurized to 15MPa, then a measurement is done for all channels as seen in Fig. 4.4. T0 for Vp axial is found as indicated above and used to find the velocity inside the dummy with the P-axial pick and its dimensions. The aluminum dummy is assumed to be homogenous, thus the Vp velocity in radial direction is the same. This velocity is used with the diameter of dummy to find the time it takes from one point to another. T0 is found by subtracting the time calculated from the time measured in radial direction. All three radial measurements have same t0.

Fig. 4.6 displays date from Vs measurement for GDV_V. Red dots indicated the manual time picks for Vs, while the white line is the automatically time picks. The image seen is a results of stacking wave forms from acoustic measurements vertically next to each other. Once one or more arrival times have been picked (red dots) a function can be used to make the white line. This function will used red dots as a reference and find the closes match on the surrounding

waves. D&I stands for drainage and imbibition, here more manual picks were necessary to ensure a good quality analysis as the fluid mixture of brine and CO_2 does not give a clear signal.

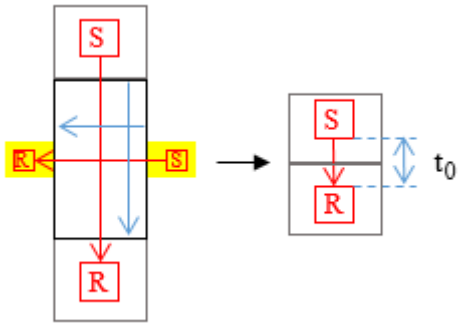

Fig. 4.4 Schematic of travel time for acoustic waves from sensors to receiver with dummy to the left and without dummy to the right.

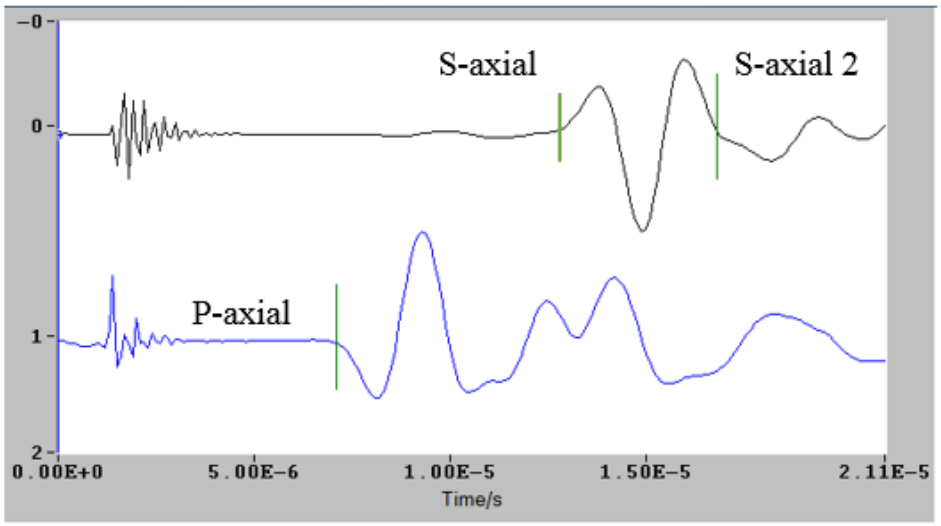

Fig. 4.5 Vp and Vs axial readings when top and bottom piece are in contact under a pressure of 15MPa

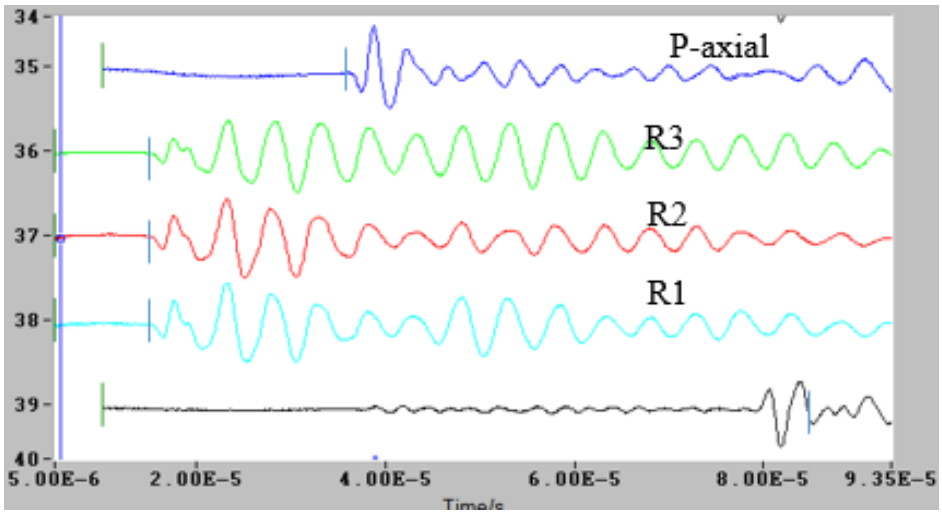

Fig. 4.6 Wave forms for all channels with an aluminum dummy, vertical green lines indicates first arrival of wave, placement of sensors are seen in Fig. 4.3

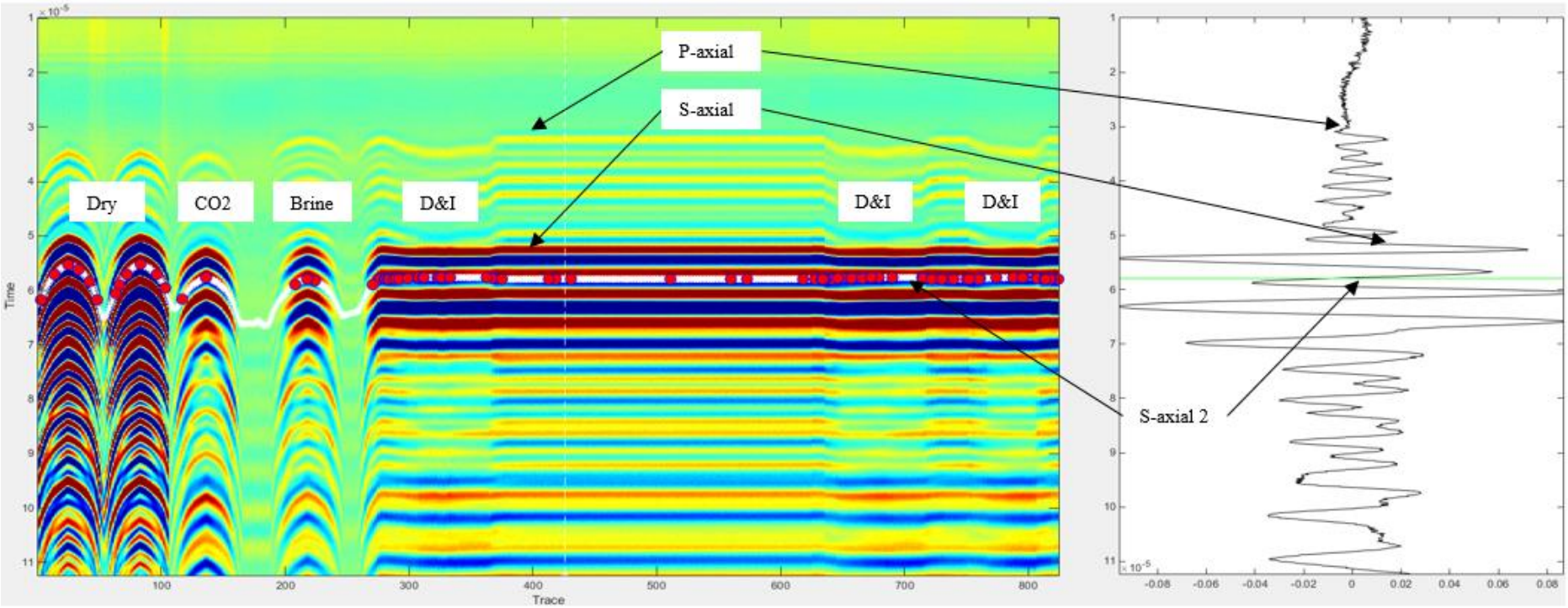

Fig. 4.7 Screenshot from the Matlab script time_picker

4.4. Experimental protocol

Experiments are done in a fixed order of five steps. These steps are presented below with their setup. Fig. 4.8 show the how the confinement pressure (CP) and pore pressure (PP) changes for all five steps.

Experimental steps:

1. Dry run
2. Loading and unloading of fully liquid CO_2 saturated sample
3. Loading and unloading of fully brine saturated sample
4. Brine drainage by CO_2 injection
5. Brine imbibition by brine injection

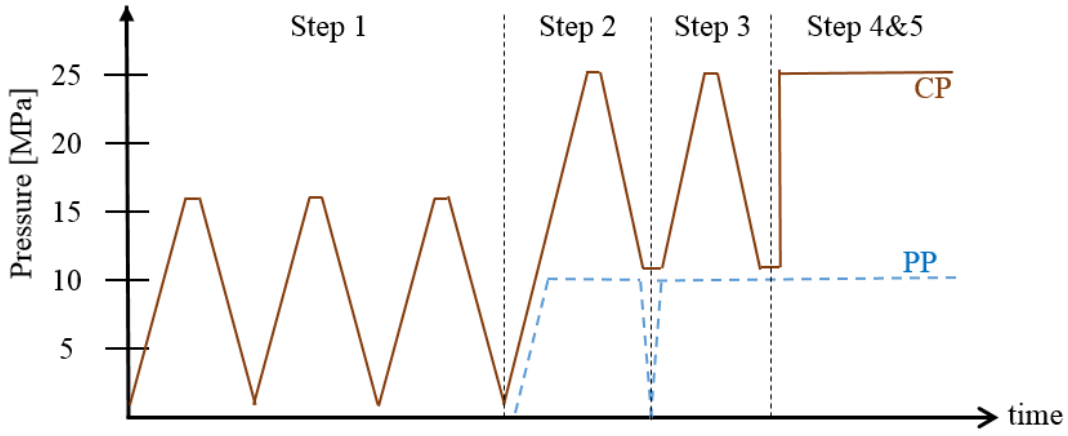

Fig. 4.8 Pressure devlopment

4.4.1. Dry run

Initially three cycle of isotropic loading and unloading of the sample is conducted to ensure good quality of mechanical measurements during the experiments (i.e removing false deformation caused by sensor seating to sample). Loading and unloading is done in two set, first the effective pressure is increased from 1 MPa to 15 MPa in seven hours, it will stay here for 30 mins then decreased to 1 MPa in seven hours. The pore pressure (PP) is zero. Mechanical data and acoustic velocity measurements are collected to study the sample properties. Vacuum inside the sample is achieved with the use of a vacuum pump, thus the pores are empty. Fig. 4.9 illustrates how the piezo-element is in contact with the sample wall before and after these three cycles. Sensors in full contact with the sample will give more accurate measurements.

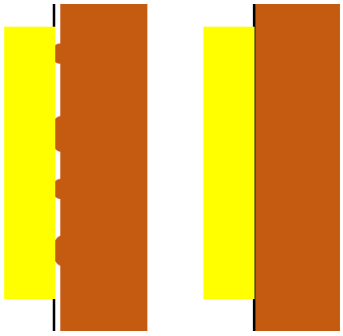

Fig. 4.9 (right) sensor resting on a few sand grains and (left) sensor in full contact with the sample

4.4.2. Fully CO_2 saturated

In step 2 the sample is saturated by allowing liquid CO_2 to enter the sample through bottom and top pedestal. Liquid CO_2 is provided by a CO_2 pump connected to a CO_2 bottle. A vacuum pump is used to empty the tubes between the sample and the CO_2 pump, ensuring only CO_2 is saturating the sample. The bottom valve is closed while bypass and top valves are open.

Loading and unloading cycle is the same as in step 1, seven hours for effective pressure to go from 1 MPa to 15 MPa, half an hour hold time and lastly unloads back to 1 MPa in seven hours. The CO_2 pump is connected to ensure a constant pore pressure of 10 MPa for the whole duration of this step. Mechanical and acoustic velocities are also measured here.

4.4.3. Fully brine saturated

For step 3 the CO_2 from step 2 needs to be replaced by brine. CP is set to 13 MPa while pore pressure is reduced slow and steadily to 0.5 MPa. CO_2 from the sample will flow into the CO_2 pump as the pressure is reduced. A high cell pressure prevents bubbles caught in the sleeve making it not tight for the next step. These bubbles are from CO_2 as it changes from liquid to gasses phase at around 6-5 MPa at ~22^{o}C (Fig. 2.2). CO_2 at 0.5 MPa is let out to empty the sample. A vacuum pump is used to obtain vacuum in the tubing and sample.

A brine pump is providing brine which will saturate the sample from both top and bottom of the sample. CP is lowered from 13 to 11 MPa while the PP is at 10 MPa. Loading and unloading cycle will be the same as for step 2. Electrical resistivity is measured in addition to mechanical and acoustic velocity.

4.4.4. Fluid substitution by drainage

Drainage is the process of the non-wetting fluid (CO_2) displaces the wetting fluid (brine). This process is done by injecting CO_2 from the top of the sample and push fluids downwards to avoid gravity segregation.

CO_2 pump is filled with ~230mL liquid CO_2 and put under constant flow rate (FR) when injection starts. Maximum injected pore volume (PV) is achieved when the brine pump is full or CO_2 is empty. Further injection can be done switching out brine pump or refill CO_2 pump. The brine pump is initially almost empty of silicon oil, during drainage it has to reduce pressure at the bottom to maintain a PP of 10MPa. This reduction of pressure allows the CO_2 to enter the GDS pump, thus when it is full the PP can not be maintained at 10MPa.

One measurement of acoustic velocity and resistivity is performed before injection as a reference. Drainage of brine is done by injection a pre-determined volume of CO2, stop and take three measurements of acoustic velocity and one electrical resistivity before continuing with next volume. The injection schedule is given in Table 4.1 and shows cumulative PV and flow rate. The volume of the tubing from top valve until top of sample is included during injection (~2mL). Additional injection is needed when maximum saturation is not achieved. Maximum saturation is seen when resistivity measurements slightly changes despite.

Table 4.1 Injection schedule

PV	0	0.1	0.2	0.3	0.4	0.5	0.6	0.7	0.8	0.9	1	2	4	6	8
FR [mL/min]	0	0.5	0.5	0.5	0.5	0.5	0.5	0.5	0.5	0.5	0.5	2.5	2.5	2.5	2.5

4.4.5. Fluid substitution by imbibition

The final step is the imbibition where the wetting phase (brine) is replacing the non-wetting phase (CO_2). This process is done by injecting brine from the bottom of the sample, thus pushing out a mixture of CO_2 and brine out from the top. Imbibition is done when only brine left in the sample.

For imbibition a GDS pump (Tpump) is used to maintain a PP of 10MPa while changing equipments. Tpump is disconnected when the cylinder in brine pump is switched out and separator is in place. CO_2 pump will be used as a backpressure pump so PP is kept at 10MPa. The brine pump can provide 10PV of brine without refilling. Injection is done from the bottom and the schedule is as for drainage (Table 4.1).

Chapter 5: Results

Results for both acoustic velocity and electrical resistivity are presented below. Pore volume for Gres des Vosges samples are 18,14mL and for Berea 17mL.

5.1. Acoustic measurements

Acoustic measurements are used to study the fluid substitution by sending a signal (either P- or S-wave) through a sample and measure the time it takes from the source to the receiver on the opposite side. Arrival time of these waves are semi-automatically picked with a Matlab script. These time picks are corrected to only include travel time through the sample, lastly the velocity is calculated using the dimensions of the sample.

Results presented here are data processed in Excel and plotted with Matlab. An overview of the compressional and shear wave velocities is given with saturation estimates from acoustic measurements for every increment of injected PV, with more detail in the range 0 to 1PV range. Velocities for a fully brine saturated and fully CO_2 saturated sample were calculated from the measurements. These velocities are shown as broken horizontal lines in the plots of drainage and imbibition for Vp. The picking error estimate is about +/- 15m/s.

A sample drilled perpendicular to bedding can be represented as a Reuss model in the axial direction and Voigt in radial. Elastic moduli would be default be higher when calculated by Voigt than Reuss, thus Vp in the radial direction is higher than in axial. Is the opposite for sample drilled parallel to bedding.

5.1.1. Vertically drilled Gres des Voges (GDV_V)

Three experiments were conducted on the vertical drilled plug of Gres des Vosges. The first experiment followed the protocol as given in Chapter 4. Drainage and imbibition were repeated two more times to test for flow rate influence by keeping a constant flow rate for the whole duration of the experiment. Table 5.1 shows the different flow rate for drainage and imbibition.

Table 5.1 Overview of flow rates for drainage and imbibition

	Experiment flow rates [mL/min]					
	Drainage			Imbibition		
	1st	2nd	3rd	1st	2nd	3rd
0-1PV	0.5	2.5	0.5	0.5	2.5	2.5
1-9 PV	2.5	2.5	0.5	2.5	2.5	2.5

Fig. 5.1 shows the measured Vp for all channels (one axial and three radial directions) for all three experiments. Injection of CO_2 from the top is seen as radial measurement of Vp is decreasing at R1. CO_2 will keep flowing through the sample with increase PV as observed with the decrease in velocity at R2 and R3. Only $Vp_{,top}$ in all three drainage experiments displays a lower measured Vp than measured on a fully CO_2 saturated sample under the same pressure and temperature conditions.

Vp at the end of drainage are the same as Vp at the start of imbibition, thus no change has happened while switching equipment. Measurement at the end of imbibition are closely the same as for a fully brine saturated sample with same pressure and temperature conditions. Table 5.2 shows the decrease in Vp at the end of drainage in percent. The 1st experiment does have the highest decrease in Vp.

Table 5.2 Decrease in Vp for all three experiments in percent. 1st experiment flow rate of 0.5ml/min from 0PV to 1PV, then changed to 2.5mL/min till the end, 2nd experiment constant 2.5mL/min and 3rd constant 0.5mL/min for drainage and 2.5mL/min for imbibition

	Axial	Top	Middle	Bottom
1st	7.80 %	10.07 %	7.98 %	7.08 %
2nd	7.46 %	9.36 %	8.72 %	7.00 %
3rd	7.73 %	9.36 %	8.74 %	6.46 %

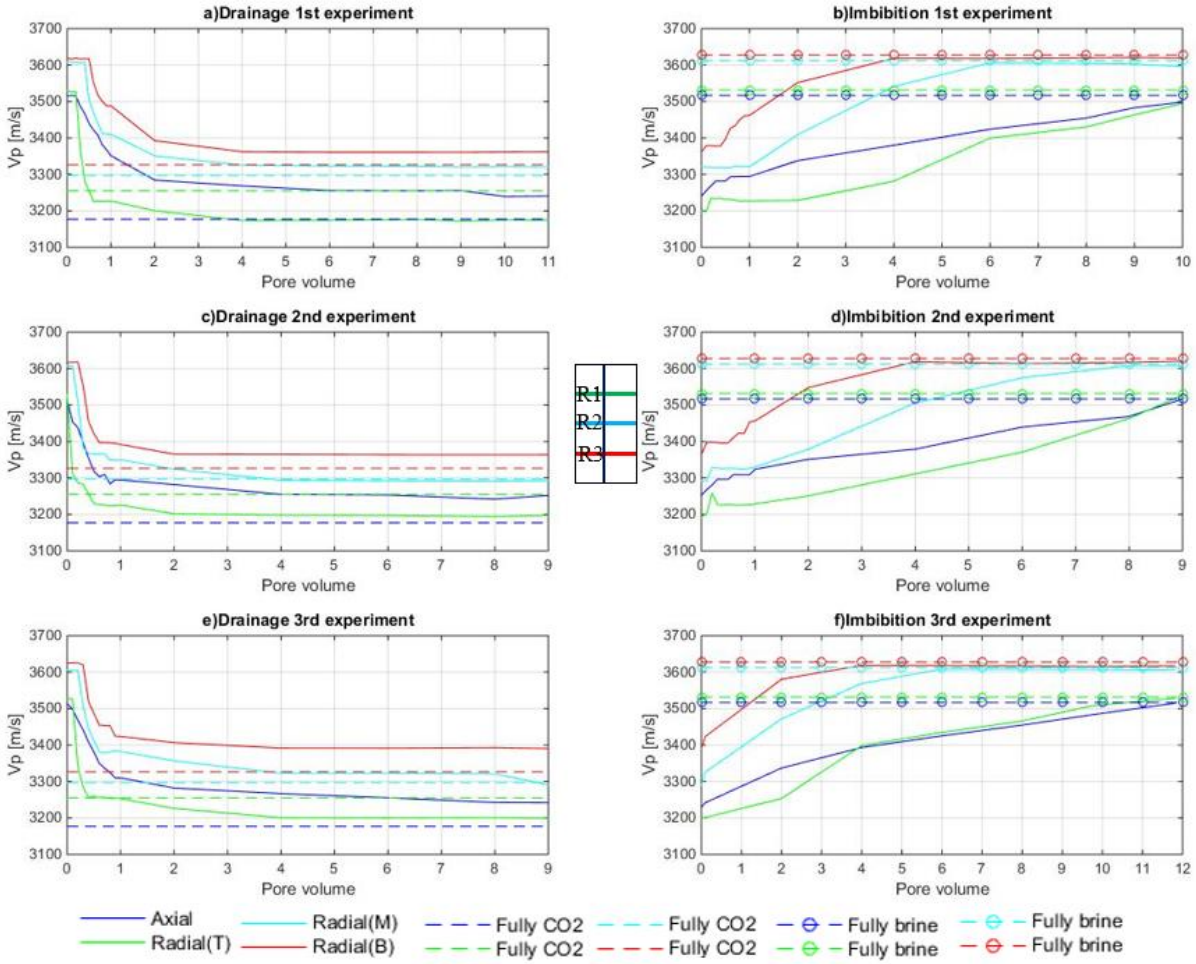

Fig. 5.1 Vp measurements, 1st experiment flow rate of 0.5ml/min from 0PV to 1PV, then changed to 2.5mL/min till the end, 2nd experiment constant 2.5mL/min and 3rd constant 0.5mL/min for drainage and 2.5mL/min for imbibition

Acoustic velocities are most sensitive to injected CO_2 during the first injected pore volume. During 0-1PV the CO_2 has entered to sample from the top and flowed through it. The movement of the CO_2 front be observed with radial measurement. In Fig. 5.1a CO_2 front reaches R1 at 0.3PV ($Vp_{,top}$ decreases), R2 after 0.5PV ($Vp_{,middle}$ decreases) and R3 at 0.6PV ($Vp._{bottom}$ decreases). At 0.6PV the CO_2 front should have already or is close to leave the sample (breakthrough point). For the reaming two experiments the breakthrough points are at 0.3PV and 0.4PV for 2nd and 3rd respectively.

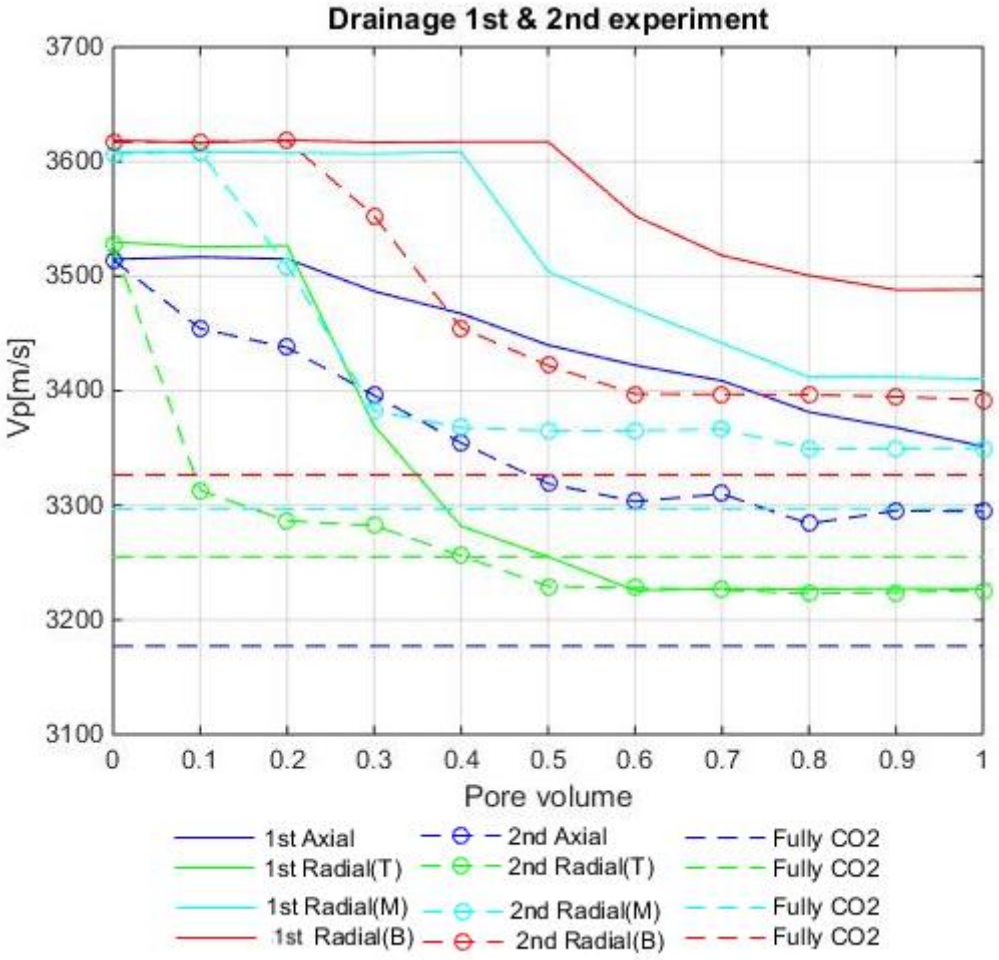

Fig. 5.2 Comparison between Fig. 5.1a and c. 1st experiment flow rate of 0.5ml/min from 0PV to 1PV and 2nd experiment constant 2.5mL/min

Fig. 5.2 shows the comparison between Vp measurements of 1st and 2nd flow rate schedule form 0-1PV. The injected CO_2 is detected earlier in all radial channels when the flow rate is increased. CO_2 is detected at PV 0.1, 0.2 and 0.3 for respectively $Vp_{,top}$, $Vp_{,middle}$ and $Vp_{,bottom}$ instead of at PV of 0.3, 0.5 and 0.6 for 1st. After 0.6PV the $Vp_{,top}$ is the same independent of flow rate. Axial, middle and bottom Vp are lower with the increased in flow rate. The lower velocities in 2nd than 1st show a higher saturation with higher injection rate. This only applies until the sample is filled up.

The same flow rate of 0.5mL/min from 0-1PV is shown in Fig. 5.3 the difference is the sample has undergone two set of drainage & imbibition before conducting the 3rd experiment. Injected

CO_2 is detected earlier in 3rd than 1st despite same flow rate. R1 and R2 detects CO_2 at 0.2PV and R3 at 0.3PV. These results suggest previous experiments affect the later ones. CO_2 flows easier by creating a flow path through the sample twice. This pre-made path might have enabled the CO_2 to travel faster through the sample, thus explaining the difference. Higher Vp indicates lower CO_2 saturation. The CO_2 which would stay at top in 1st experiment has now moved downwards. This development can be observed as the middle and bottom velocities decreases faster and ends up at lower velocities in the 3rd than in the 1st experiment.

Changes in Vs are not big compared to Vp (+/- 20m/s for Vs and +/- 300 m/s for Vp). Vs only affected by fluid through density change in the pore fluids (Eq. 2.25). As for Vp, the results from 1st experiments stands out of the three. The difference is 5 m/s after 4PV between these experiments. 1st and 2nd resemble each other, but in 2nd CO_2 flows easier through the sample than in 1st, less accumulation of CO_2 decreases Vs. The 3rd experiment indicates something has changed as Vs reaches the end velocity before 1PV when 4PV and 2PV were needed for 1st and 2nd respectively. CO_2 is observed to flow easier through the sample. As seen in Fig. 5.4, the start in drainage and end in imbibition are closely the same.

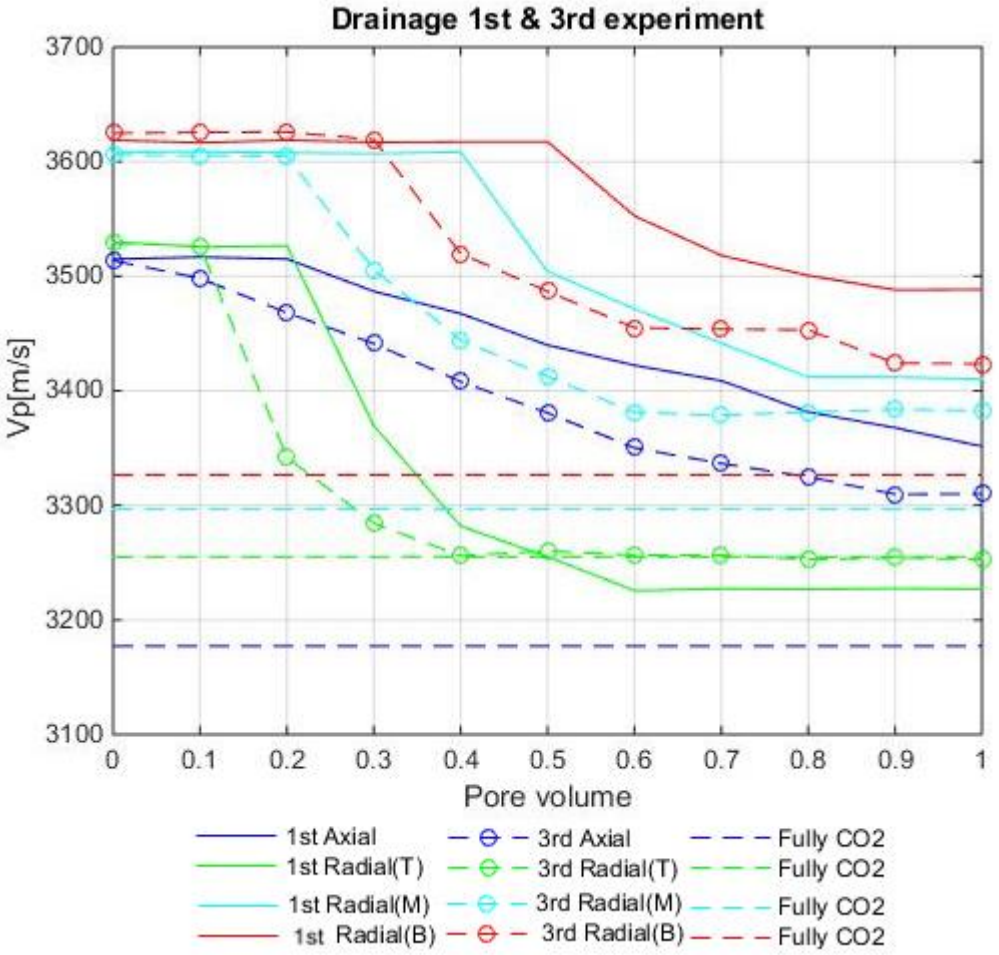

Fig. 5.3 Comparison between Fig. 5.1a and e, 1st experiment flow rate of 0.5ml/min from 0PV to 1PV and 3rd constant 0.5mL/min

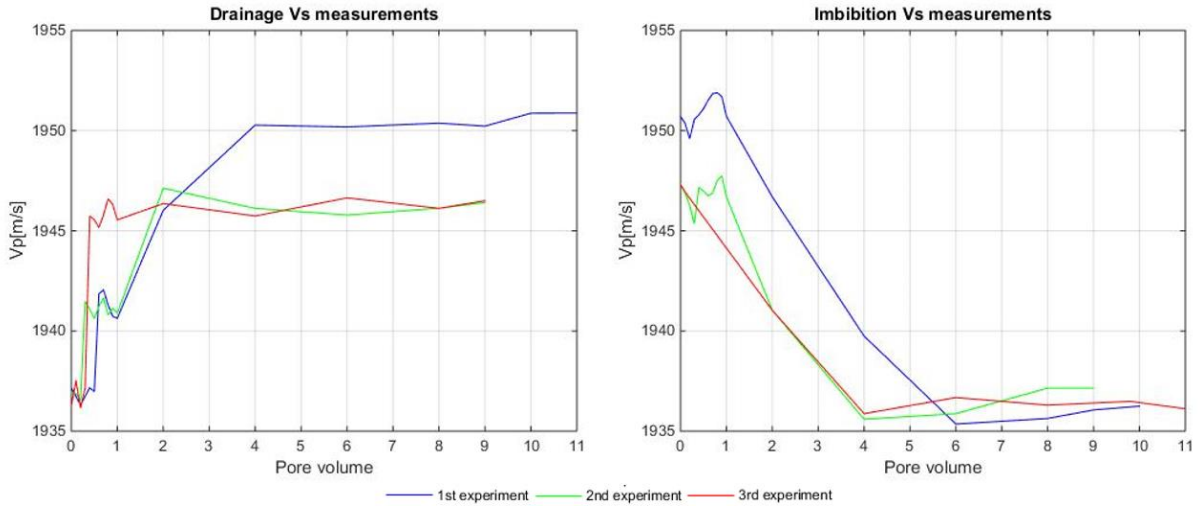

Fig. 5.4 Vs [m/s] vs PV for all three experiments

5.1.2. Horizontal drilled Gres des Voges (GDV_H)

Experiments done on GDV_H follows the protocol from Chapter 3, with drainage and imbibition flow rate 0.5mL/min from 0-1PV and 2.5mL/min for 1-9PV. Fig. 5.5 and Fig. 5.7 shows velocities for every increment of PV during drainage and imbibition of the sample.

Fig. 5.6 shows the CO_2 front moving fast through the sample, already at 0.1PV R1 and R2 have detected CO_2 (Vp decrease). The front has reached R3 at 0.2PV, thus the breakthrough point is here. $Vp,_{middle}$ and $Vp,_{bottom}$ are similar while $Vp,_{top}$ is higher. The reason for not being the same might be due to the placement of the piezo-elements. Placement of the piezo-elements aligned with the layers was not considered when setting up the sleeve, thus creates an uncertainty of how the acoustic wave travels through the sample. An example of the setup with sample is shown in Fig. 4.3b.

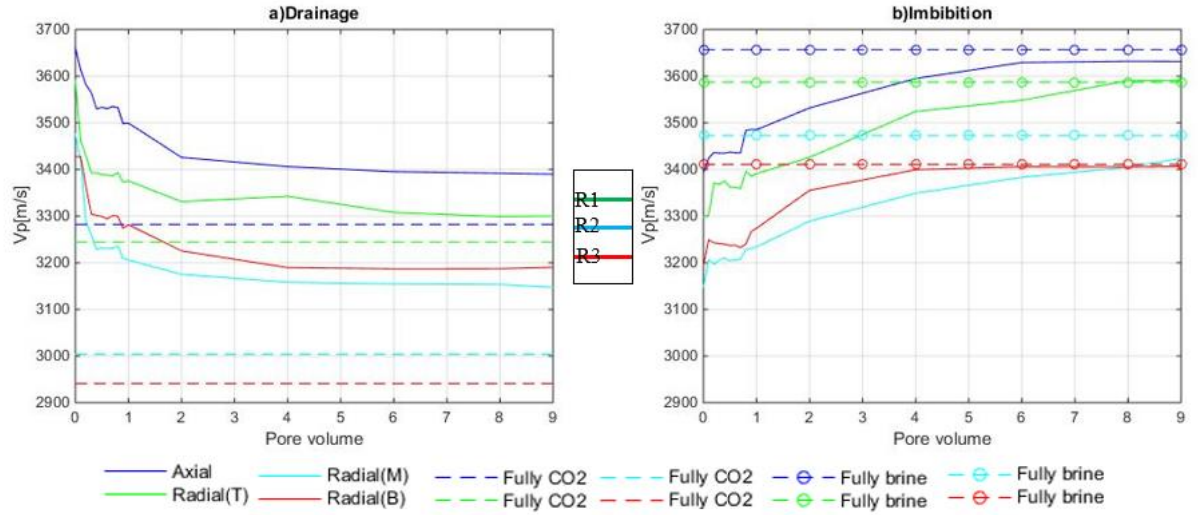

Fig. 5.5 Vp measurements for GDV_H

The highest saturation is found locally at the top of the sample close to the injection point. This is seen as $Vp_{,top}$ is the velocity closes to the its fully CO_2 saturated line. Changes in Vp is insignificant after 2PV, thus the highest detectable saturation of CO_2 is here. Table 5.3 shows the decrease of Vp for all channels at the end of drainage in percent.

An almost fully brine saturated sample is achieved after imbibition with indication of residual CO_2. This observation is based on Vp axial after imbibition is close, but not equal to the fully brine line. The CO_2 seems to be trapped in the middle of the sample as its Vp is the only one which is not at the line of fully brine.

A closer look on Vp during drainage is shown in Fig. 5.6 from 0 to 1PV, here the it is clearly seen that it takes more only 0.2PV of CO_2 for a reduction in Vp bottom. Saturation in the middle is higher than bottom due to the difference in velocities, $Vp_{,middle}$ was higher than $Vp_{,bottom}$ at the start.

Changes in Vs are seen in Fig. 5.7 on about 10m/s from about 1943m/s to 1953m/s. As expected Vs is nearly not affected by fluid substitution.

Table 5.3 Decrease in Vp at the end of drainage for GDV_H

	Axial	Top	Middle	Bottom
GDV_H	7.39 %	8.08 %	9.46 %	6.92 %

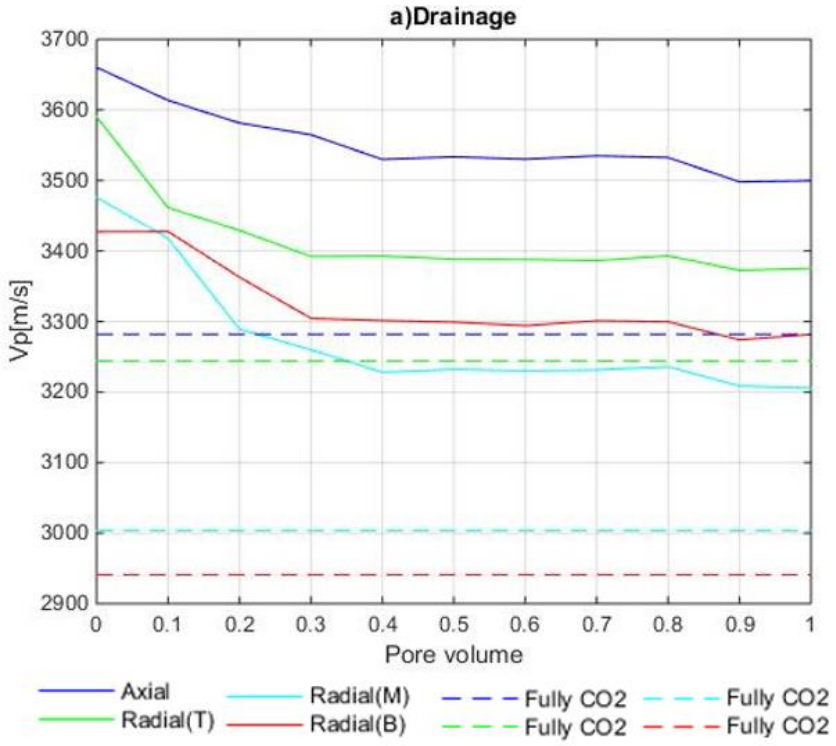

Fig. 5.6 Vp plotted between 0-1PV for drainage of GDV_H

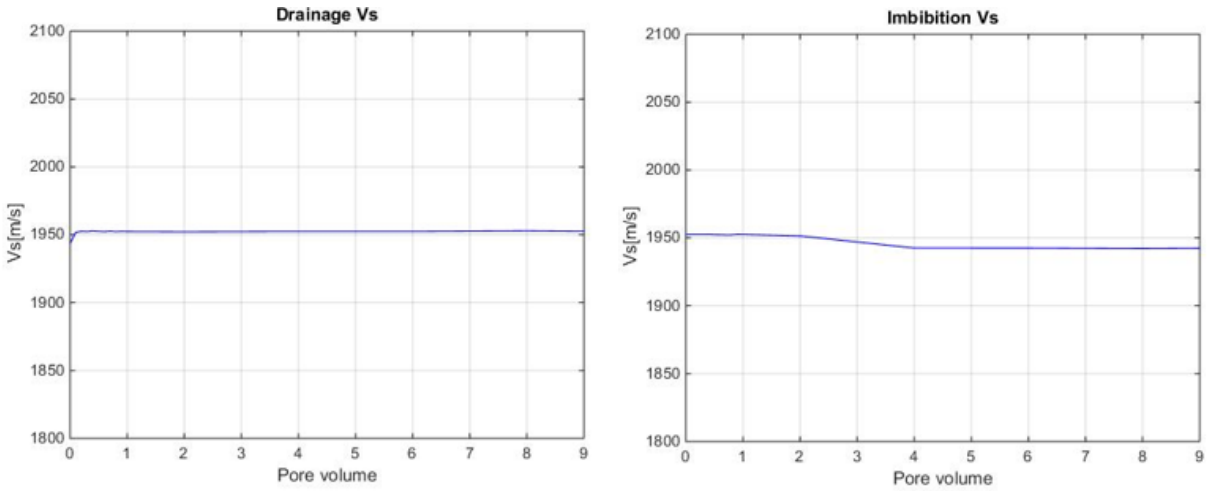

Fig. 5.7 Vs measurements for GDV_H

5.1.3. Berea

Berea was drilled perpendicular to beddings, thus radial Vp are higher than axial Vp (Fig. 5.8). Vp measurements for Berea indicates a homogenous sample as radial velocities at the start of drainage is about the same. The CO_2 front moves fast through the sample due to Berea's high permeability. After 0.2PV the front has pass the top and reached the middle measurement at 0.3PV. The top part is the closes to be fully saturated with CO_2 as it is closes to its full CO_2 line. The difference between $Vp_{,middle}$ and $Vp_{,bottom}$ before and after 1PV is significant. The increase in flow rate decreases this difference until they are almost equally at 4PV. Velocities are nearly unchanged after 4PV, indicating the highest saturation seen by acoustic is here. Fig. 5.8 shows a fully brine saturated sample is achieved after imbibition as the Vp for each channel corresponds to their lines.

Constant Vp achieved at low PV (0.6 to 1PV) is likely due to the high permeability allowing CO_2 quickly fill the pores and move one, by so hindering high accumulation of CO_2 (Fig. 5.9). An increase in injection rate will make it possible for the CO_2 to bypass the smaller throats, thus increasing the saturation in the sample and lowers the Vp.

Vs measurements shown in Fig. 5.10 increases from the first injected 0.1PV of CO_2, with no change in Vs is seen until the increase in flow rate from 1 to 2PV. These changes in Vs are relative small compared to Vp, which is as expected.

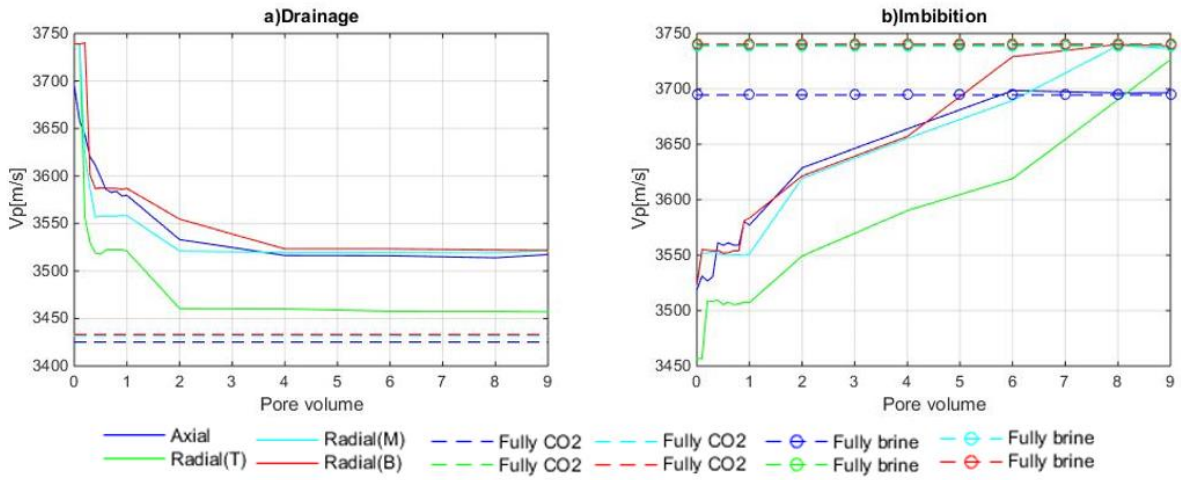

Fig. 5.8 Vp measurement for Berea

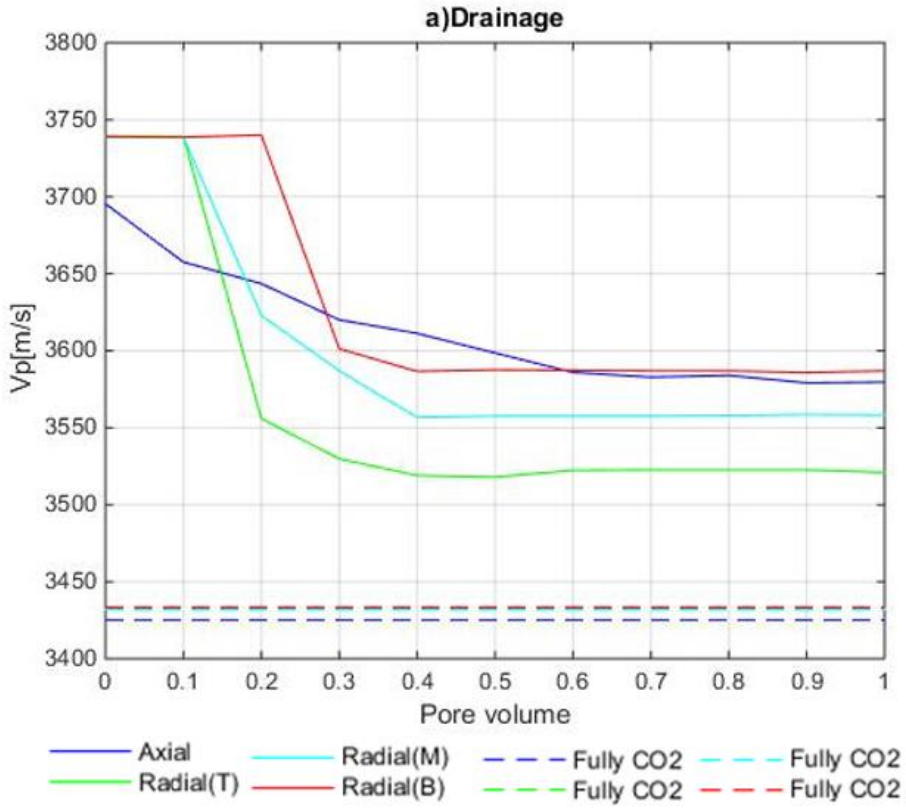

Fig. 5.9 Vp plotted for 0-1PV, drainage of Berea

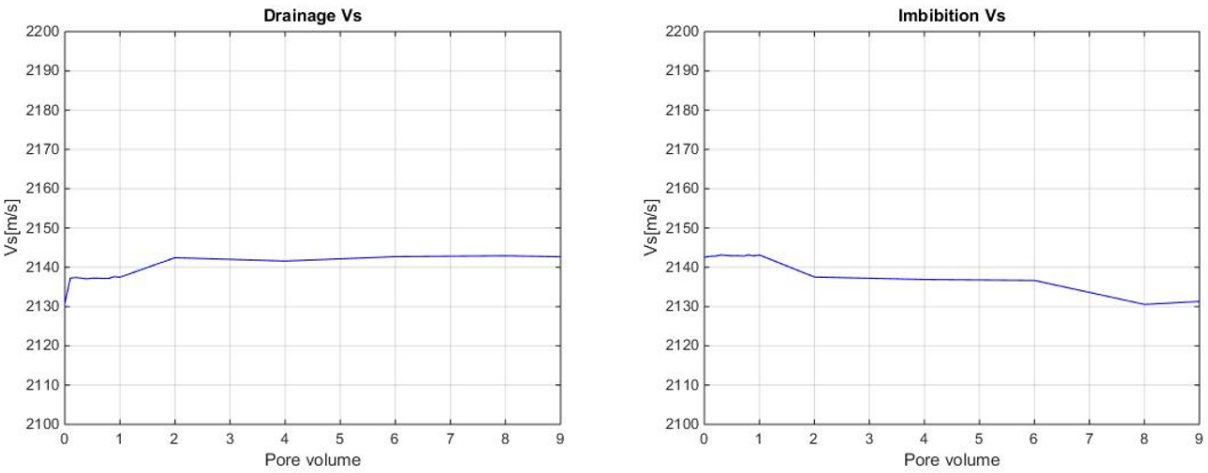

Fig. 5.10 Vs measurement for Berea

5.1.4. Saturation estimation

Using Vp and Vs measurements from previous steps, i.e. completely CO_2 and brine saturated, the dry bulk modulus can be estimated with the use of grain bulk modulus, densities and porosities. Total porosity will be the same as effective porosity of 20%. Temperature is set to 22ºC and pore pressure of 10MPa. The process of estimating saturation is described by iteration in Fig. 2.3. When an estimate of saturation can not be found through Gassmann, the previous estimate is used.

Saturation estimation strongly depend on acoustic measurement, thus will reflect the interpretation of Vp. Patchy saturation gives a linear solution and depend accurate measurement of fully brine and fully CO_2 saturated samples. Using patchy saturation gives higher estimation than using Gassmann for all samples. The end Vp is the same independent on which saturation type is used. Gassmann has a curve before it flattens out, thus will give a lower saturation than for a straight diagonal as patchy saturations gives.

GDV_V

Elastic moduli are calculated as shown in Table 5.4 for GDV_V. Shear modulus is calculated from Eq. 2.4 and where Vs is nearly not affected by fluids. Dry rock moduli should be the same independent a sample is saturated or not. Elastic moduli calculated from these three phases are not equal to each other, thus an average value between brine and CO2 saturated sample is used in the estimation of saturation. Saturation estimations for GDV_V are seen in Fig. 5.11.

Table 5.4 Dry bulk modulus estimation

	Density [g/cm3]		Shear[GPa]	Dry bulk modulus [GPa]			
	liquid	sat. Core	ax	ax	rB	rM	rT
Dry	0.000	2.080	8.937	9.789	11.963	11.861	10.869
CO2	0.841	2.248	8.514	10.846	13.098	12.637	12.012
Brine	1.022	2.284	8.573	11.394	13.938	13.686	11.762

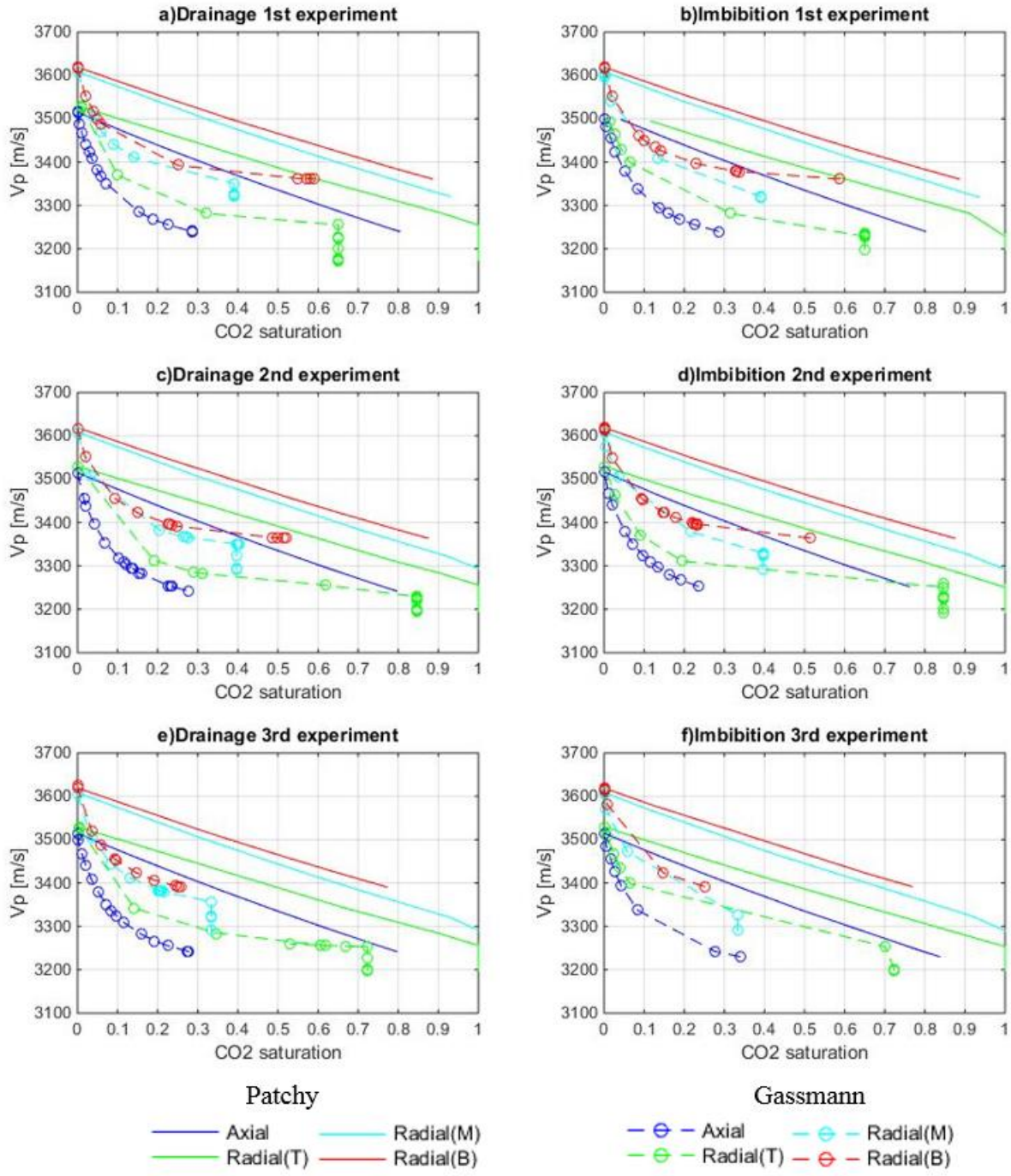

Fig. 5.11 Acoustic estimation of CO2 saturation for GDV_V. 1st experiment flow rate of 0.5ml/min from 0PV to 1PV, then changed to 2.5mL/min till the end, 2nd experiment constant 2.5mL/min and 3rd constant 0.5mL/min for drainage and 2.5mL/min for imbibition

Patchy displacement shows saturation up to 100% which is higher than Gassmann for all experiments. Gassmann equation has problem estimating CO_2 saturation at high injected PV when the velocity decreases with about 300 m/s. The last estimated saturation is seen as a vertical line at the end of the graph for both top and middle measurements. This vertical line is when saturation can not be calculated while the velocity still decreases. In general drainage and imbibition graph follows the same pattern. All experiment shows small difference between

drainage and imbibition. Table 5.5 shows the maximum estimated CO_2 saturation and saturation at 1PV for all three experiment.

Table 5.5 CO2 saturation at 1PV and at end of drainage. 1st experiment flow rate of 0.5ml/min from 0PV to 1PV, then changed to 2.5mL/min till the end, 2nd experiment constant 2.5mL/min and 3rd constant 0.5mL/min for drainage and 2.5mL/min for imbibition

	Patchy				Gassmann			
	Axial	Top	Middle	Bottom	Axial	Top	Middle	Bottom
Max 1st	80.4 %	100.0 %	92.8 %	88.2 %	28.7 %	65.0 %	39.0 %	57.0 %
Max 2nd	76.2 %	100.0 %	100.0 %	87.4 %	23.6 %	84.5 %	39.6 %	51.4 %
Max 3rd	79.6 %	100.0 %	100.0 %	77.2 %	27.7 %	72.4 %	33.4 %	25.7 %
1st (1PV)	45.1 %	100.0 %	61.1 %	42.0 %	7.1 %	65.0 %	14.0 %	6.0 %
2nd (1PV)	62.6 %	100.0 %	82.3 %	76.6 %	13.7 %	84.5 %	39.6 %	24.9 %
3rd (1PV)	57.7 %	100.0 %	70.7 %	65.0 %	11.4 %	72.4 %	20.4 %	14.8 %

GDV_H

Elastic moduli for GDV_H are shown in Table 5.6, as there are difference in elastic moduli for all condition of the sample. An average value between a brine and CO_2 saturated sample will be used for saturation estimation.

Table 5.6 Elastic moduli for GDV_H

	Density [kg/m3]		Shear[GPa]	Dry bulk modulus [GPa]			
	liquid	sat. Core	ax	ax	rB	rM	rT
Dry	0.00	0.00	8.68	12.58	7.03	8.12	11.11
CO2	841.53	2248.45	8.57	12.57	7.57	8.45	11.99
Brine	1022.37	2284.62	8.63	14.76	8.71	10.23	13.06

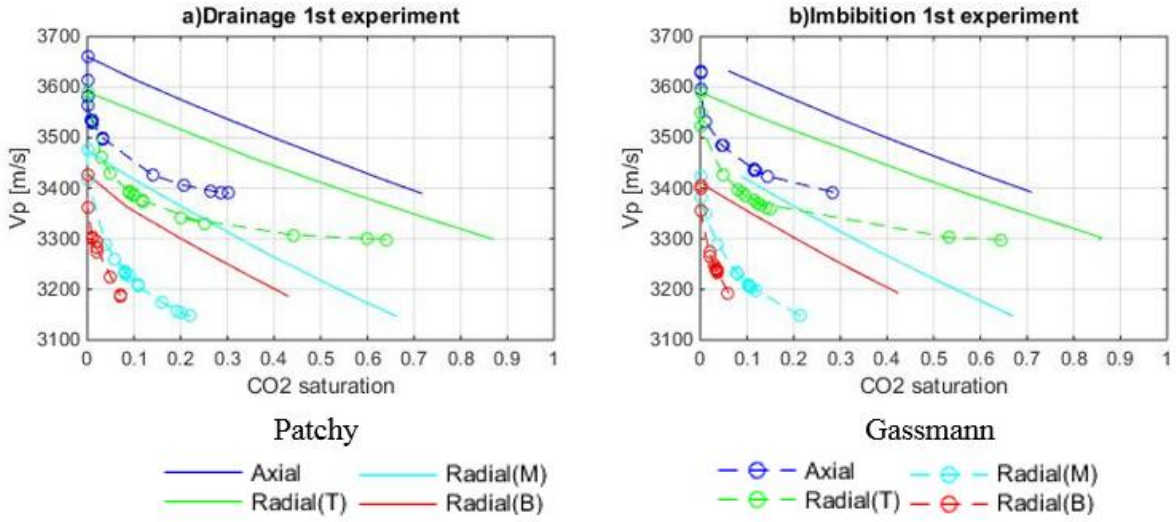

Fig. 5.12 Acoustic estimation of CO2 saturation for GDV_H

Fig. 5.12 shows CO_2 for GDV_H. Patchy displacement has a higher estimate on CO_2 saturation than Gassmann. Drainage and imbibition shows similar trend, the exceptions are patchy axial and middle estimates are not equal to zero at the end of imbibition whereas Gassmann estimate are zero for all channels. Table 5.7 shows the estimated saturation at end of drainage and 1PV.

Table 5.7 CO2 saturation at 1PV and end of drainage for GDV_H

	Patchy				Gassmann			
	Axial	Top	Middle	Bottom	Axial	Top	Middle	Bottom
Max	70.9 %	85.4 %	66.9 %	42.3 %	28.4 %	64.5 %	21.4 %	6.0 %
At 1PV	40.0 %	61.4 %	52.6 %	23.7 %	3.3 %	12.0 %	11.0 %	2.0 %

Berea

Table 5.8 shows the elastic moduli for Berea. Calculations show different value for conditions of dry, CO_2 and brine saturated sample. Since the dry elastic moduli are not constant independent of saturation, an average value between CO_2 and brine will be used.

Table 5.8 Elastic moduli for Berea

	Density [g/cm3]		Shear[GPa]	Dry bulk modulus [GPa]			
	liquid	sat. Core	ax	ax	rB	rM	rT
Dry	0.00	2.066	10.55	11.04	11.06	10.32	10.32
CO2	0.841	2.235	10.50	12.00	12.12	12.10	12.11
Brine	1.022	2.271	10.32	13.66	14.83	14.78	14.81

Patchy and Gassmann displacement for Berea sandstone are shown in Fig. 5.13. Radial saturations are closely the same after 4PV of injected CO_2. Top measurement shows an increase in saturation to 51% before being reduced to about 45% where stays unchanged while Vp is decreasing. Patchy displacement gives higher saturation than Gassmann, but the saturation does

not reach 100% at any point in the sample during the experiment. Saturations at 1PV and end of drainage are given in Table 5.9.

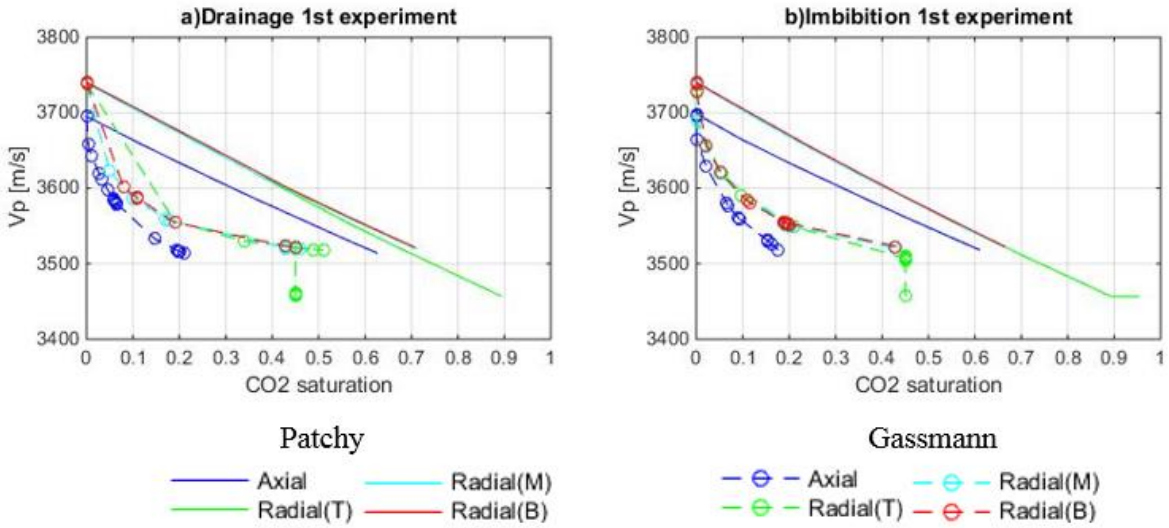

Fig. 5.13 CO2 saturation from acoustic measurement for Berea

Table 5.9 Saturation at 1PV and end of drainage for Berea

	Patchy				Gassmann			
	Axial	Top	Middle	Bottom	Axial	Top	Middle	Bottom
Max	60.9 %	95.1 %	66.5 %	66.4 %	20.9 %	45.0 %	42.5 %	43.0 %
At 1PV	38.7 %	67.3 %	57.2 %	47.9 %	6.5 %	45.0 %	17.0 %	11.0 %

5.2. Resistivity measurements

Resistivity measurements can be used to detect and observe changes in the pores while brine is being replaced with CO_2. Replacing brine with CO_2 will increase the resistivity as the latter is less conductive. Resistance is the measured value. Resistance is calculated by use of sample dimensions and correction factor as shown in Eq.2.5.

Electrical resistivity are presented for all three samples with a closer look from 0 to 1PV. Berea and GDV_H was done with another setup, thus yields different result than GDV_V. After testing and changing out equipment an improved electrical measurement was obtained as shown in the re-testing of GDV_H and GDV_V. A re-testing of Berea was not done due to time issues. Saturation based on resistivity measurement and corresponding Vp is included for comparison with acoustic measurements.

5.2.1. Vertical drilled Gres des Vosges

Resistance measurements were done for all three cases of flow rate as for acoustic velocity. Fig. 5.14 shows the calculated resistance values. Common for all plots are closely the same start value, high local resistance (radial higher than axial) and resistivity is highest at R1 followed by R2 and R3.

A fully brine saturated sample should have the same resistivity independent of axial or radial measurements. Such a sample is observed in Fig. 5.14 as the measurements at 0PV injected shows nearly the same value for all three experiments. Differences are seen in accumulated CO_2 at the end of drainage in all experiments. Measurements at R1 and R2 are closely the same in 1^{st}, with constant flow rate the difference is increasing with decreasing flow rate. Radial resistivity are changing depending on the flow rate schedule, top and bottom are highest in 3^{rd} followed by 1^{st} and lastly 2^{nd} drainage experiment and middle in 1^{st}, 3^{rd} and 2^{nd}. Axial resistivities shows little difference compared to radial, highest in 1^{st}, then 3^{rd} and 2^{nd}.

Fig. 5.14a has a decrease in resistivity between 1PV and 2PV whereas the other two experiments are continuously increasing. Only difference in procedure here is the increase in flow rate from 0.5 to 2.5 ml/min. The increase has likely opened up new and/or enlarged pathways (throats) for the CO_2, thus the accumulated CO_2 in top and middle flows easier through.

Imbibition shows a considerable drop in resistivity during the first 0.1PV of injected brine. Resistivity drop indicates CO_2 leaving the sample.

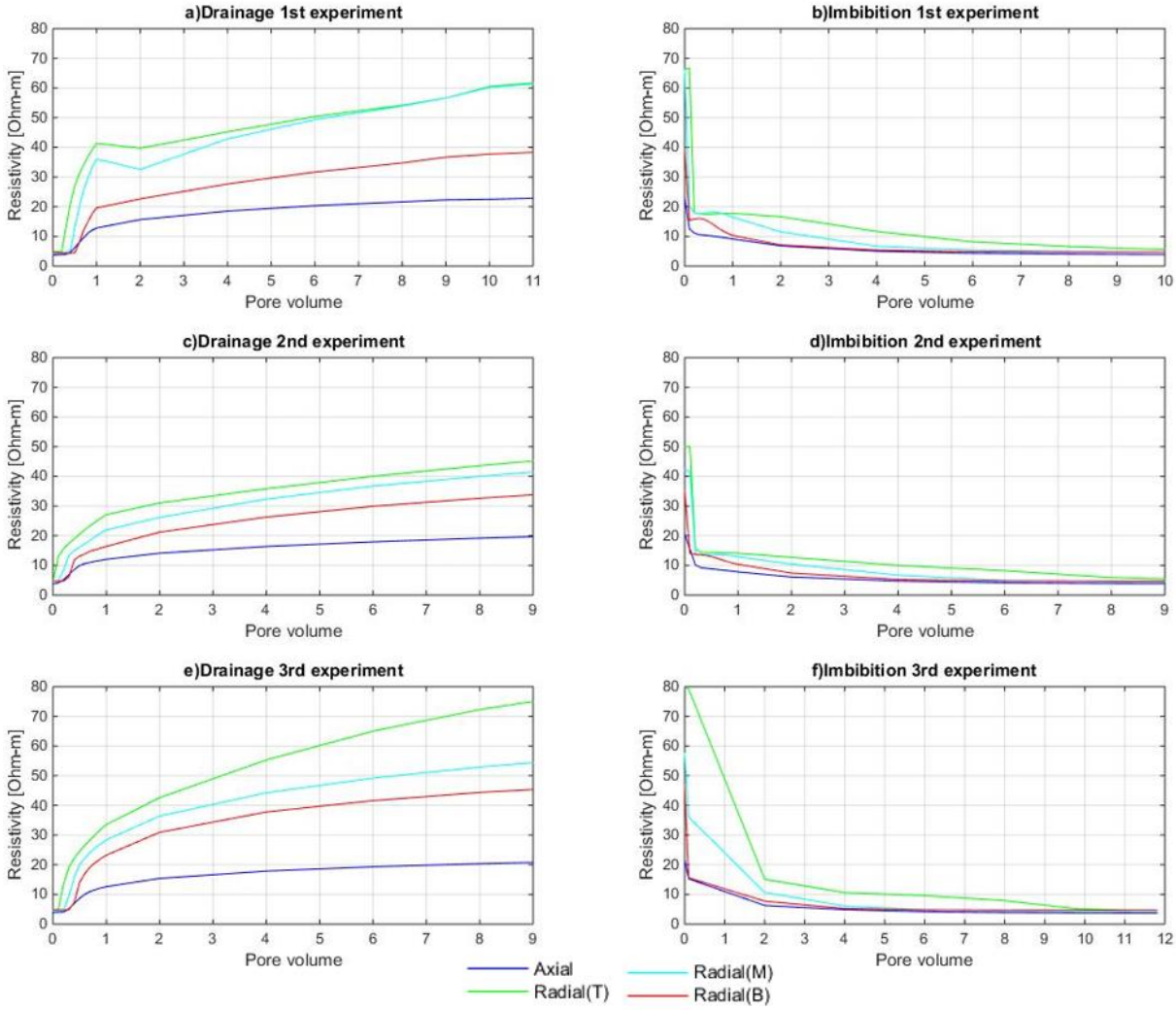

Fig. 5.14 Resistivity measurements for GDV_V. 1st experiment flow rate of 0.5ml/min from 0PV to 1PV, then changed to 2.5mL/min till the end, 2nd experiment constant 2.5mL/min and 3rd constant 0.5mL/min for drainage and 2.5mL/min for imbibition

A comparison between 1st and 2nd experiment is shown in Fig. 5.15 for 0 to 1PV. The increase in flow rate has an effect on the measurements, the detection of CO_2 is decrease from 0.2 to 0.1, 0.4 to 0.1, 0.5 to 0.2 and 0.5 to 0.4 for top, middle, bottom and axial respectively. Resistivity for the 2nd starts off higher than 1st, but when the injected PV reaches 1PV and above, the resistivity is less.

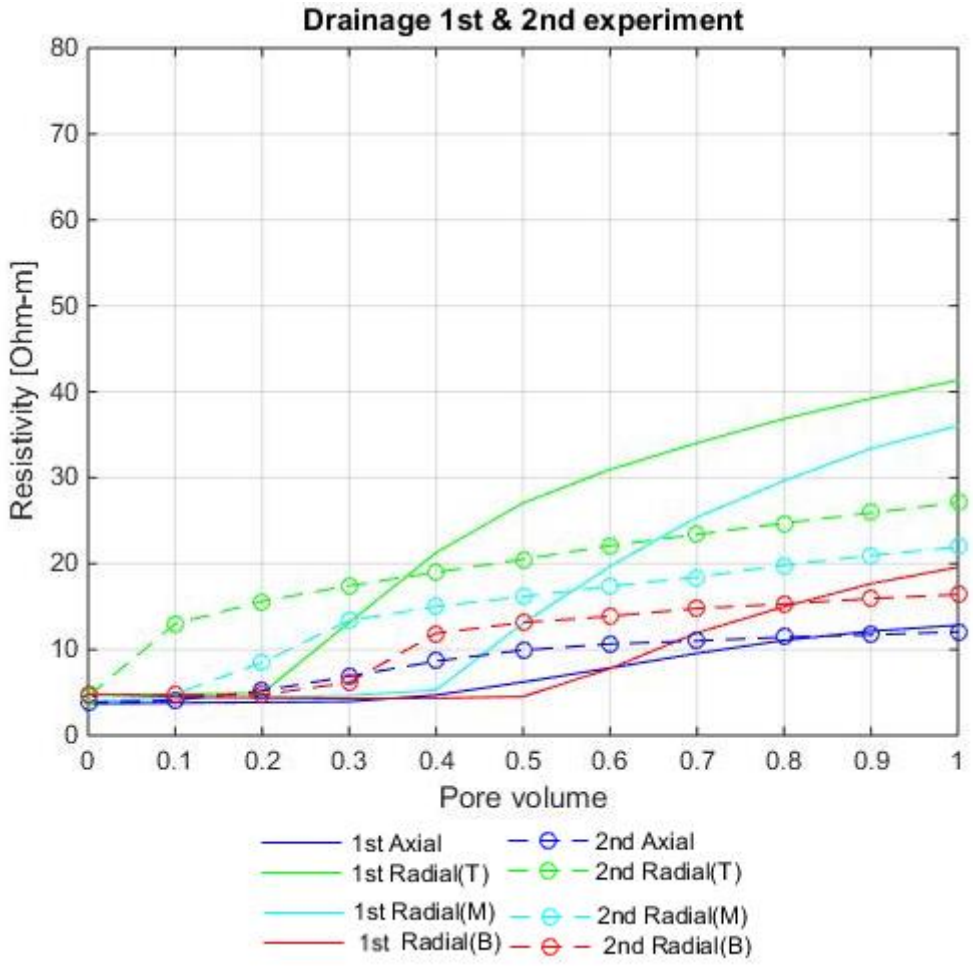

Fig. 5.15 Resistivity comparison between 1st and 2nd experiment. 1st experiment flow rate of 0.5ml/min from 0PV to 1PV, then changed to 2.5mL/min till the end and 2nd experiment constant 2.5mL/min

Fig. 5.16 shows a comparison between the 1st and 3rd experiment for 0 to 1PV. Here the flow rate are the same for this range of injected PV. The 3rd experiment shows earlier detection of CO_2 and lower value of resistivity at every measurement than 1st for radial measurement. Axial measurement shows a faster detection and higher value of resistivity in 3rd than 1st.

.

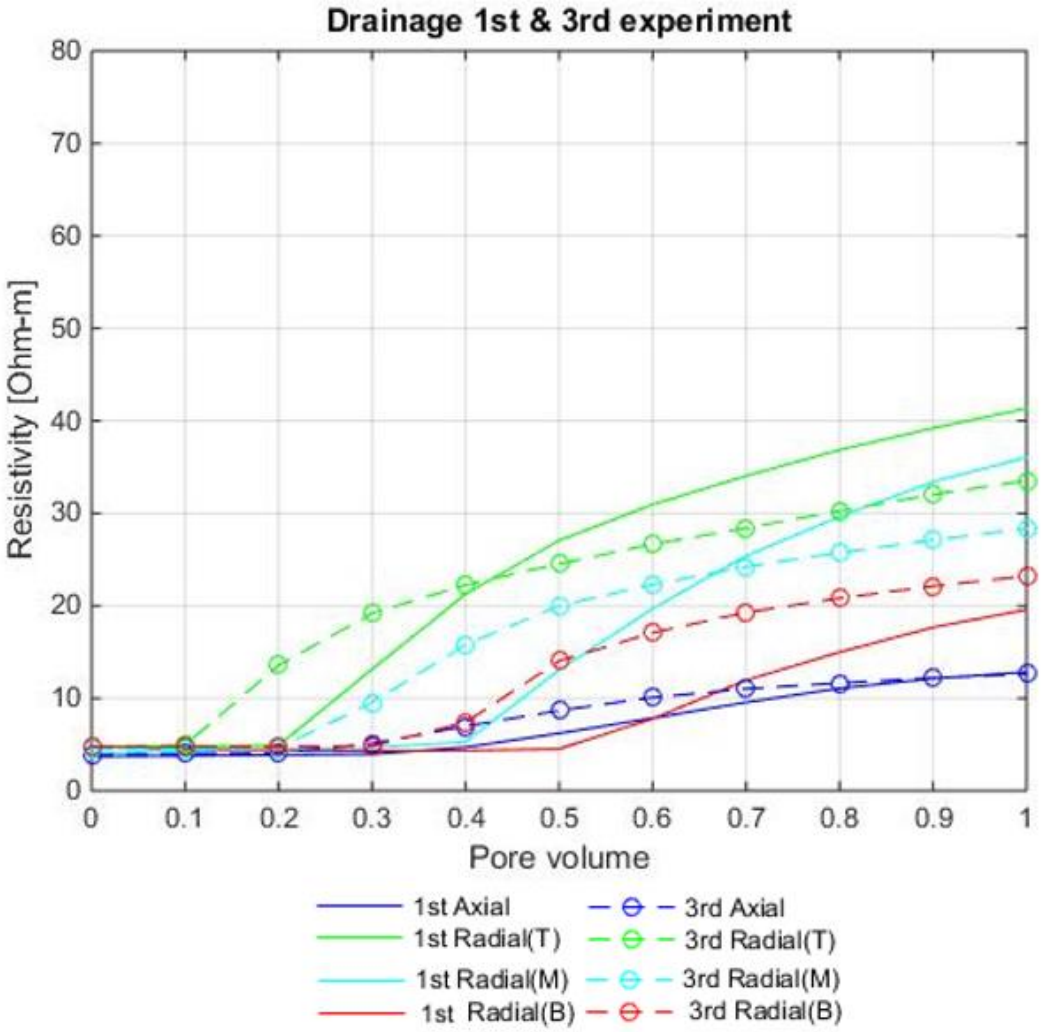

Fig. 5.16 Resistivity comparison between 1st and 3rd experiment. 1st experiment flow rate of 0.5ml/min from 0PV to 1PV, then changed to 2.5mL/min till the end and 3rd constant 0.5mL/min for drainage and 2.5mL/min for imbibition

Fig. 5.17 shows the calculated saturation for GDV_V. Max saturations is shown as 72%+/-3 for top and middle, 62% +/- 3 for bottom and 57% +/- 2 for axial measurements at the end of drainage. The lowest saturation is seen in the axial direction, for radial top and middle are about the same with bottom as the lowest. GDV_V seems to not be 100% brine saturated at the end of imbibition since in 1st only bottom is reaching zero saturation as it is in the next two. The exception is in 3rd where axial and top measurements also are zero.

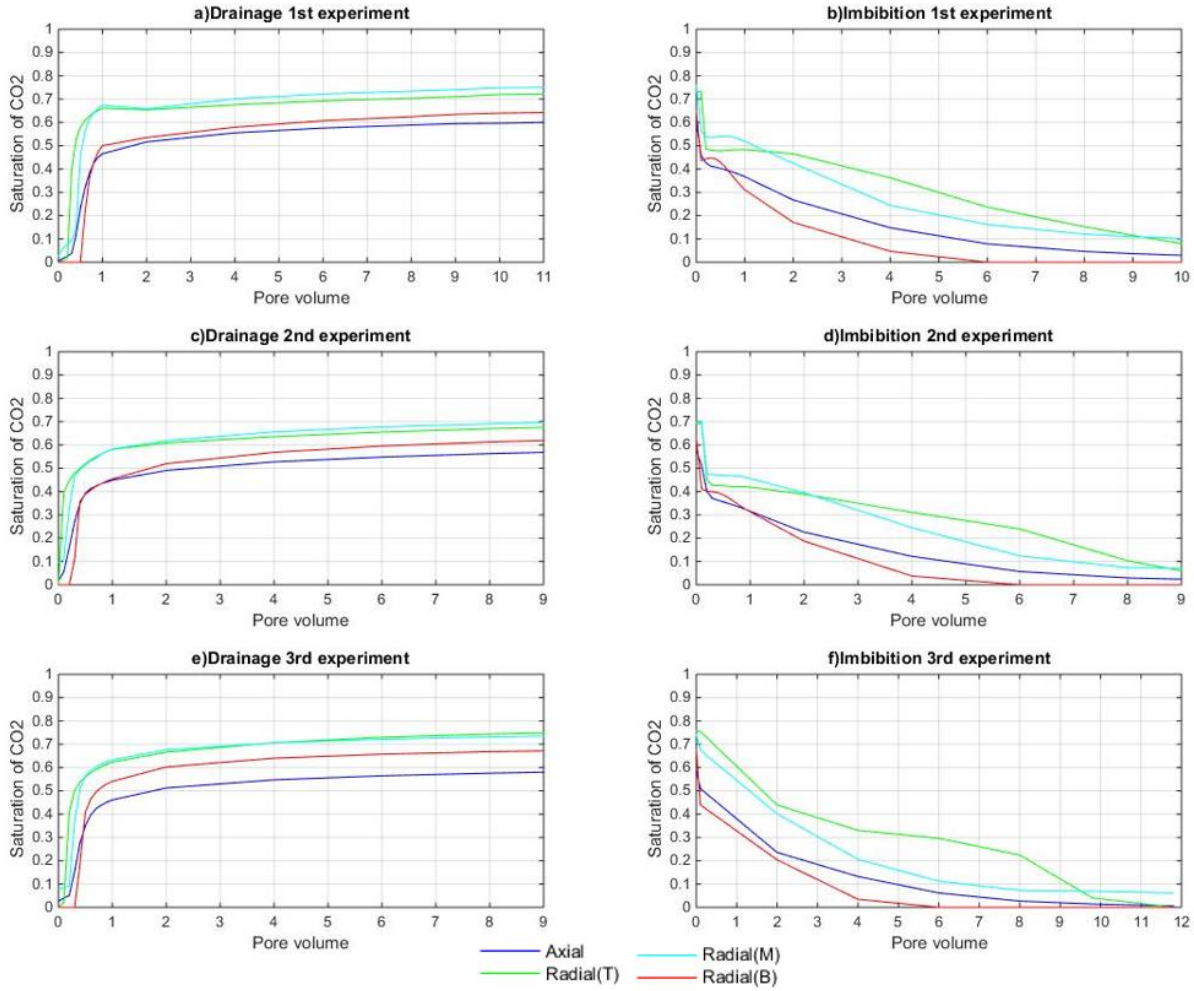

Fig. 5.17 Saturation calculated from resistivity 1st experiment flow rate of 0.5ml/min from 0PV to 1PV, then changed to 2.5mL/min till the end, 2nd experiment constant 2.5mL/min and 3rd constant 0.5mL/min for drainage and 2.5mL/min for imbibition

5.2.2. Horizontal drilled Gres des Vosges

An initial run GDV_H was done proved to give strange measurements of resistivity. Fig. 5.18 shows these values, they are normalized with the start value since it they were in the order of 1e6. The normalized values for drainage are not as expected since it initially goes down then up and at the end decrease below the start value. The values for imbibition seem more reasonable, but due to the high values as in drainage they are also normalized with the start value of imbibition.

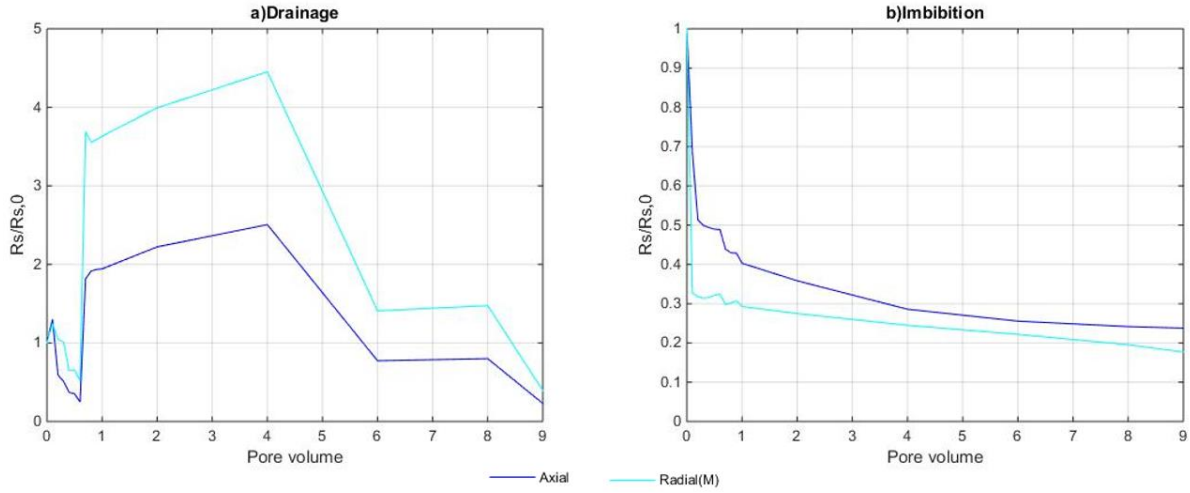

Fig. 5.18 Resistivity measurements for initial run

A second experiment was done on the GDV_H sample to verify the measurements in the initial run. The sample was washed and flushed with pure water prior to the second experiment. By using new modified equipment a different result was obtain as shown in Fig. 5.19

The new equipment makes it possible to measure in all three radial levels. Resistivity measurements are about the same for all channels at the start of drainage indicates a homogenous sample.

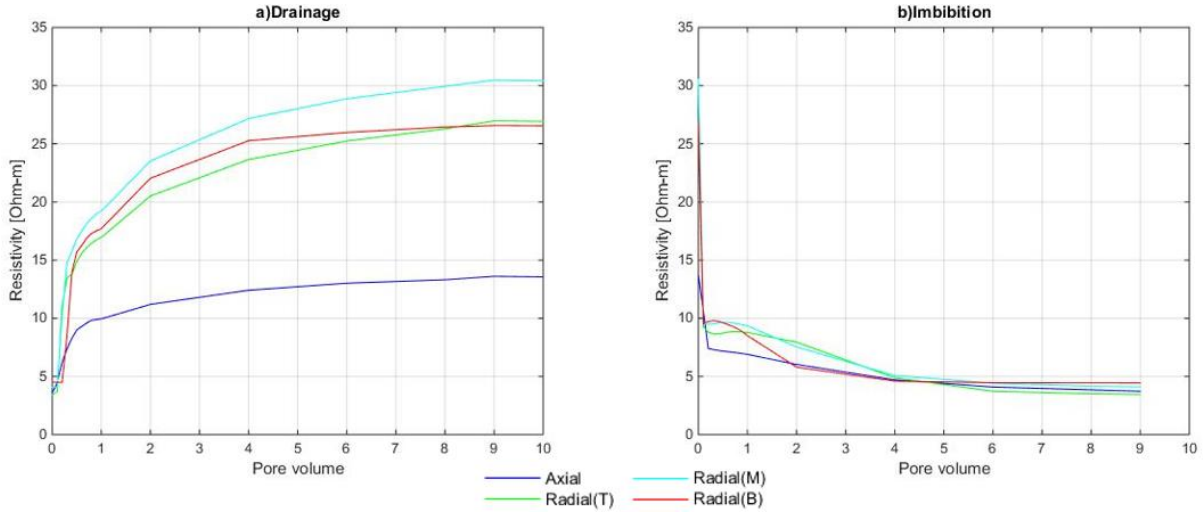

Fig. 5.19 Resistivity measurement for second experiment

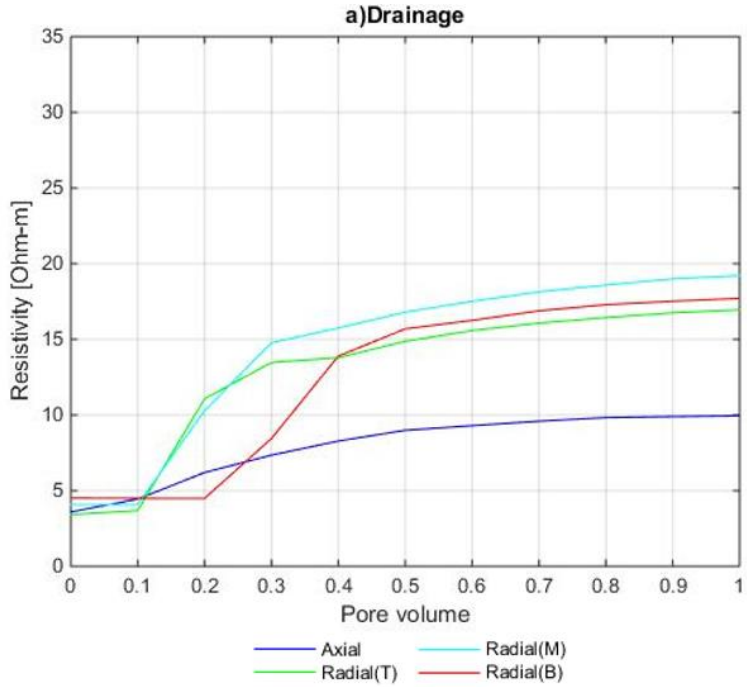

Fig. 5.20 Resistivity measurement for 0 to 1PV on second run

In Fig. 5.20 the resistivity between 0 and 1PV are plotted for GDV_H. It takes 0.2PV before CO_2 is detected on the top and middle measurements, an additional 0.1PV is needed before it reached the bottom. Axial resistivity changes from the first 0.1PV, and is significantly lower than radial. Saturation based on electrical measurement are shown in Fig. 5.21. The highest saturation is obtained in the top and middle with 65%, bottom at 59% and axial 49%. Imbibition curves indicates a nearly fully brine saturated sample.

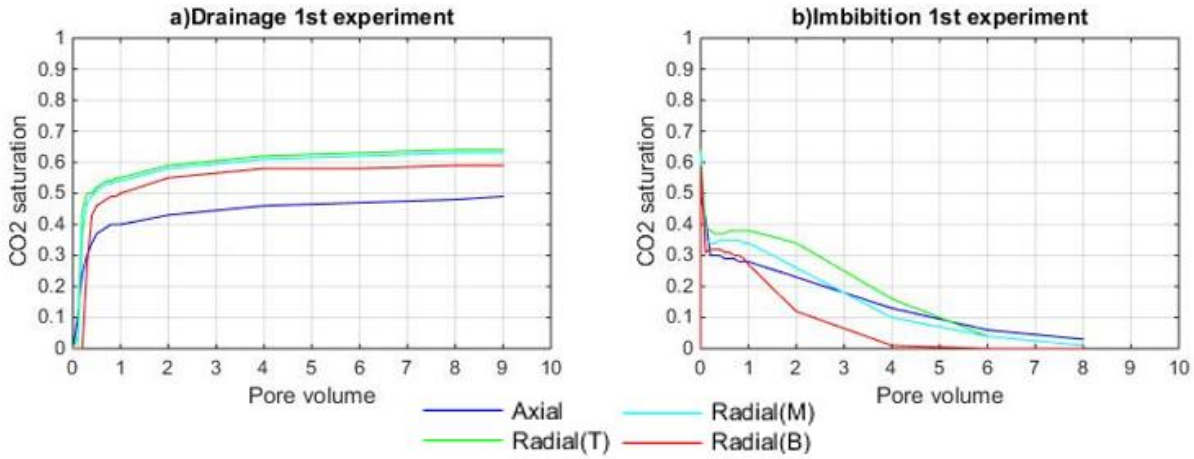

Fig. 5.21 Saturation calculated from resistivity from GDV_H

5.2.3. Berea

Berea experiment was also done with only one radial measurement. The results is shown in Fig. 5.22 as normalized values since they are high. These measurements are similar to the initial experiment for GDV_H.

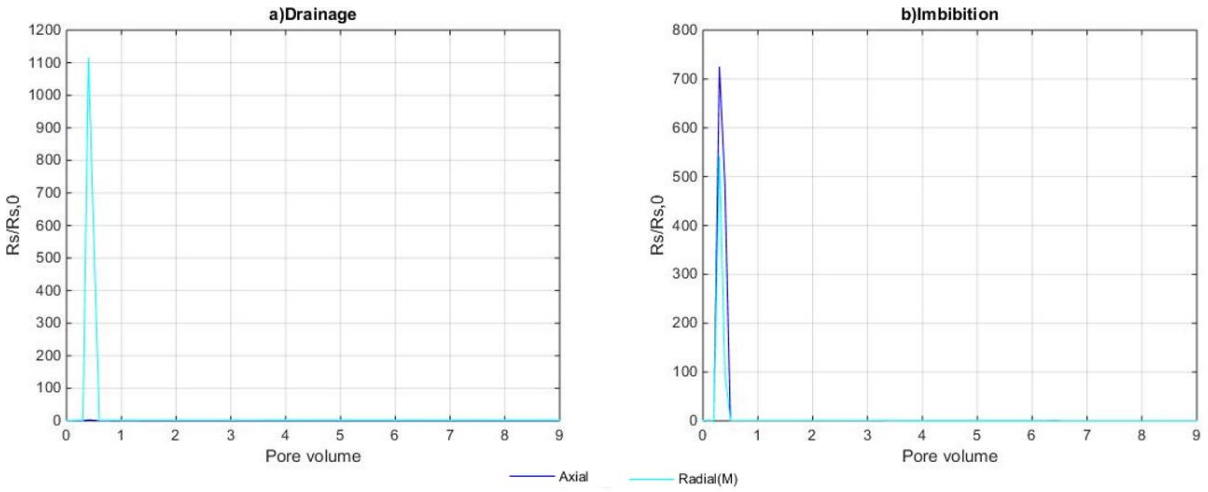

Fig. 5.22 Resistivity for Berea sample

Chapter 6: Discussion

6.1. Flow rate

Flow rate of CO_2 injection affects both electrical resistivity and acoustic velocity measurements (Kitamura and Xue, 2009; Onishi et al., 2006; Xue et al., 2009). Electrical resistivity and acoustic velocity are detecting CO_2 front at the same increment of injected PV (Table 6.1). A change in flow rate does not affect the detectability of CO_2.

Table 6.1 Detection of CO_2 front for both acoustic velocity and electrical resistivity (Fig. 5.1 and Fig. 5.14

	Acoustic[PV]			Resistivity[PV]			FR [mL/min]
	R1	R2	R3	R1	R2	R3	
1st	0.3	0.5	0.6	0.3	0.5	0.6	0.5
2nd	0.1	0.2	0.3	0.1	0.2	0.3	2.5
3rd	0.2	0.3	0.4	0.2	0.3	0.4	0.5

Experiments have been conducted on flow rate change effect on resistivity during drainage of brine saturated Berea with liquid CO_2 (Onishi et al., 2006). Results from these experiments show resistivity increase with increasing flow rate, this study (Fig. 5.14) increase in flow rate decreased the resistivity. Onishi et al. (2006) injected CO_2 from the bottom of the sample, which is the opposite direction used in this study. A fluid flow downwards with have to overcome both capillary pressure and gravity segregation, unlike fluid flow upwards where gravity is working with the flow. Gravity effect increases saturation of CO_2 to build up pressure inside the pores as it advances to the bottom.

The effect of increasing the flow rate can be explained by capillary and viscous fingering regime. A study by Méheust et al. (2002) shows how gravity, capillarity forces and viscous forces affects the invading fluid (in this case CO_2 for drainage) front. At low flow rate the capillary pressure will dominate, with injection from the top, the front will be stable. For GDV_V layering interfaces helps stabilizing the front, a stable front will increase the saturation of CO_2 in the sample. However, when increasing the flow rate viscous forces gains more influence, since brine is more viscous than CO_2 the front will be unstable (Méheust et al., 2002) causing viscous fingering. Gravity effect and layer interfaces helps stabilizing the front, but the saturation is lower as seen in GDV_V.

Continuous usage of one sample for several drainage and imbibition cycles are likely to have an effect on pore system (Fig. 5.15 and Fig. 5.16). Fig. 5.14a shows an event between 1PV and 2PV, where the resistivity suddenly drops. This event is not seen in other drainage experiments, and can not be observed for acoustic velocities. Results from the event is seen when CO_2 is detected earlier in 3rd than 1st when the flow rate is the same (Table 6.1). These changes are visible in acoustic velocities early in drainage (>1PV), at later increments of PV this effect is less. Resistivity is sensitive at all increments of PV, thus saturation at high levels of CO_2 can be estimated.

6.2. Orientation of bedding

Results from GDV_V and GDV_H shows difference due to orientation of beddings in acoustic velocity and electrical resistivity measurements. A higher saturation of CO_2 is achieved in a brine saturated sample drilled perpendicular to bedding than parallel (Alemu et al., 2013). Estimated CO_2 saturations from electrical resistivity are 60% and 49% for GDV_V and GDV_H respectively in the axial direction. Similar sandstone as Gres des Voges was used by Alemu et al. (2013) (Rothbach) resulting in an average saturation of 53% and 41% for samples corresponding to GDV_V and GDV_H respectively. Injection of CO_2 in Rothbach was from the bottom, thus previous observation may be used to explain the difference– increase in saturation of CO_2 when CO_2 injected from the top.

CO_2 injected into GDV_V will have to pass many horizontal stacked layers to get to the bottom, between each layer an interface will slow the advancement of CO_2. In each layer the CO_2 is gradually saturating the sample by building up enough pressure to overcome the interface and gravity. For GDV_H the layers are vertically stacked next to each other. Such a sample can have several beddings with higher permeability and several with low. CO_2 will flow through the high permeability zones first, then low if the conditions are right (i.e. high enough pressure to overcome the capillary pressures). This allows for channeling most of the injected CO_2 into higher permeable beddings, thus reducing the time for CO_2 to penetrate the sample. The different beddings will create zones with CO_2/brine and only brine. Electrical current sent from top to bottom will flow through the brine filled zones (less resistance) which may result in a lower resistivity value than expected. Fig. 6.1 illustrates this effect for injection of CO_2 from the bottom. CO_2 is moving faster through GDV_H than GDV_V as seen in Table 6.2. The same effected is assumed to happen with injection from above, only the saturation is higher and required PV need for breakthrough is increased. Compressional wave and electrical current travels faster in brine than in CO_2, thus making the lower CO_2 saturated layers a highway fro waves and current propagating in GDV_H.

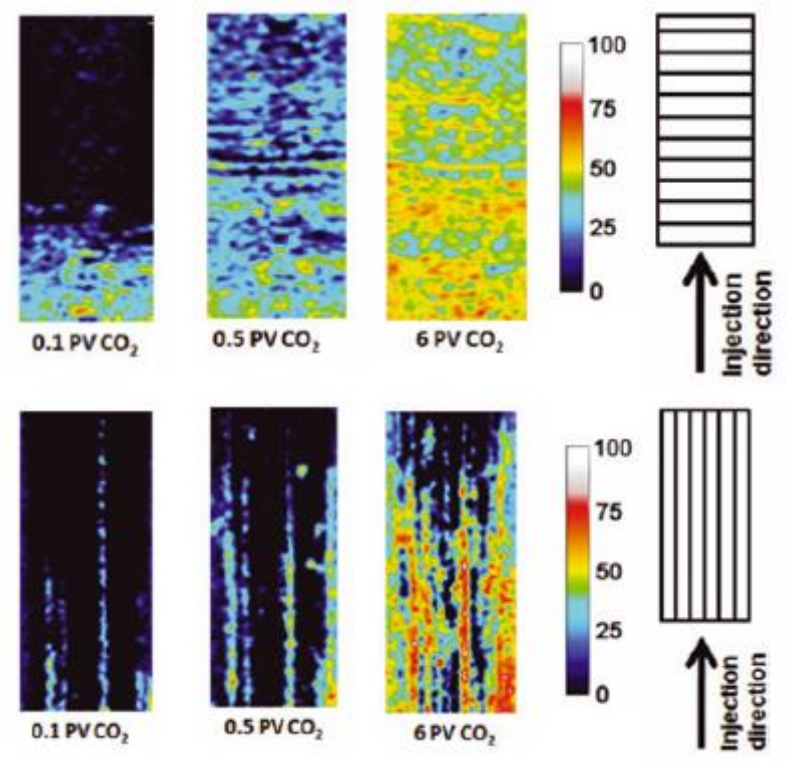

Fig. 6.1 CT-scan during injection of CO2 into brine saturated sample (Alemu et al., 2013)

Axial resistivity is low compared to radial. This behavior is due to the sample was drilled parallel to bedding plane.

Table 6.2 Detection of CO2 for GDV_H

Acoustic [PV]			FR
R1	R2	R3	
0.2	0.1	0.1	0.5

6.3. Gres des Vosges and Berea

As seen previously changing the direction of flow can speed up the movement of the injected CO_2. The same result can be done by changing to a higher permeable sandstone like Berea used in this study. As seen in Fig. 5.9 CO_2 is detected at almost the same increment as for GDV_H. Saturation in Berea at the end of drainage is expected to be higher than for GDV_H. As resistivity for fully brine saturated Berea can not be established, acoustic velocity is used to estimate CO_2 saturation.

Table 6.3 CO_2 saturation for three sample at the end of drainage, all follows protocol from Chapter 3

	Patchy				Gassmann			
	Axial	Top	Middle	Bottom	Axial	Top	Middle	Bottom
Berea	60.9 %	95.1 %	66.5 %	66.4 %	19.6 %	45.0 %	42.5 %	43.0 %
GDV_V	80.4 %	100.0 %	92.8 %	88.2 %	28.7 %	65.0 %	39.0 %	57.0 %
GDV_H	70.9 %	85.4 %	66.9 %	42.3 %	28.4 %	64.5 %	21.4 %	6.0 %

Saturation estimate from acoustic velocity shows Berea sandstone as the lowest, but it has a more even distribution of CO_2 along the sample compared to Gres des Vosges samples. Acoustic velocities are less sensitive to CO_2 injection after 1PV (Fig. 5.1, Fig. 5.5 and Fig. 5.8), thus maximum saturation estimated by Vp should be at this point. Fig. 5.11, Fig. 5.12 and Fig. 5.13 shows acoustic velocities are less sensitive to CO_2 saturation above ~20%. Saturation higher than 20% should be estimated with resistivity (Kim et al., 2009).

6.4. Anomaly

An anomaly is seen Fig. 5.1, $Vp_{,top}$ shows a lower velocity than the $Vp_{,top}$ for a fully CO_2 saturated sample. This is seen in all three experiments for GDV_V, but not for any other samples. During load and unload of fully saturated CO_2 the pore pressure is constant, but during drainage the pore pressure from injection point is increased to push the injected fluid in. The increase in pressure is needed to overcome the capillary pressure and gravity to displace brine. This may have led to CO_2 passing the smallest throats which was not possible with the constant pressure, thus increasing the saturation at the top.

Chapter 7: Summary and conclusion

CCS can be used to reduce the yearly CO_2 emissions while continuing the use of hydrocarbons. This will keep the energy production up while mitigating future problems. This study is a contribution to push CCS further and will focus on the monitoring of CO_2 as it is injected into three brine saturated sandstones.

Selected sandstones (Gres des Voges and Berea) were chosen due to their storage capacity and permeability. A literature study was conducted to investigate their properties in addition to testing them directly with available equipment at UiO and NGI. Both type of sandstones have undergone CT-scan, made into thin-sections for SEM and pulverized for a XRD analysis.

Sandstone samples were put into a nitrile sleeve equipped with three pairs of piezo-elements and a LVDT-measurement gauge for radial deformation. The sleeve with a sample is then mounted inside a hydrostatic pressure vessel. Piezo-elements are for resistance and acoustic measurements are places along the length of the sample. Two axial deformation sensors are mounted outside the sleeve. The pressure vessel is controlled by a Cpump, while injection of pore fluids from top is controlls by a CO_2 pump and from bottom Bpump. Brine is injected from the bottom while liquid CO_2 from the top. The program Modlab is used to control both Bpump and Cpump while recording mechanical data. Acoustic and resistance measurements are used to monitor the fluid change in the sample. PSwaves is used to record acoustic measurements and resistivity_test for electrical.

Condition used for the test is effective pressure of 15MPa and pore pressure of 10MPa, resulting in a maximum confinement pressure of 25MPa with a saturated sample and 15MPa for dry sample. Temperature is set to 22^{o}C. Flow rate schedule is 0.5mL/min for 0-1PV and 2.5mL/min from 1-10PV. Three measurement for acoustic and one for electrical measurement at certain injected pore fluid volumes (every 0.1PV for 0-1PV including at 0PV, then 2, 4, 6, 8 and 10PV) for drainage and imbibition.

An exception was done for Gres des Voges drilled perpendicular to beddings (GDV_V) to test for flow rate effects. One experiment was done according to protocol, to test two different flow rates the saturated sample underwent two set of drainage and imbibition experiments. Flow rate of 2.5mL/min and 0.5mL/min was tested in the second and third experiment respectively for pore volume 0-10. Acoustic and resistance measurements was done as stated above.

Mechanical data were processed by a pre-made Excel sheet Triax. Only the results was given out for analyzing purposes. Acoustic measurements were processed by the Matlab script time_picker where the arrival time of Vp and Vs waves are picked. These time picks are exported out as a text file for correction. The self-made script Combine_data is used to combine mechanical, acoustic time picks and electrical resistance data into an excel sheet for data processing and analysis.

Theoretical equations from available literature are used to find sample and fluid properties. These equations makes the foundation of calculating the acoustic velocity, electrical resistivity and estimation of saturations. Two type of saturation scenarios are considered, homogenous and patchy saturation.

Acoustic measurement analysis are done to study CO_2 front, changes in velocities, fluid displacement, estimation on rock properties (density and elastic moduli) and saturation estimation during drainage and imbibition experiments.

Resistivity measurements analysis are done to study CO_2 front, changes in resistivity and pore fluid.

Based on rock physical analysis, pore fluid properties, experimental procedure, available literature and measurement of mechanical, acoustic and resistance the following conclusions are made:

- Both acoustic and resistance measurements are affected by CO_2 injected into a brine saturated sample. It is clearly seen that acoustic velocity measurement is sensitive to CO_2 when saturation of brine is high (>~80%), resistance is sensitive to CO_2 independent of saturation.

- Acoustic and resistance measurement shows similar CO_2 front movement, thus can be used to track it until breakthrough point.

- Flow rate has an influence on the displacement of CO_2 with brine in a vertically drilled Gres des Voges (GDV_V). Higher flow rate results in lower saturation of CO_2, lower flow rate allows a higher build up of CO_2 at each beddings boundary. A higher saturation of CO_2 is achieved by lowering the flow rate.

- Permeability changes after the first drainage and imbibition experiments for GDV_V. From 0-1PV CO_2 is detected earlier for all radial channels while the resistance and Vp is lower compared to first experiments.

- Injecting CO_2 perpendicular to bedding plane increases the saturation of CO_2 compared to injecting parallel, but it is slower (49% vs 60% Sco2 for axial from resistivity). High permeable Berea has traits similar to both Gres des Voges (fast movement of CO_2 front, low saturation and Vp axial < Vp radial)

- Fluid distribution inside the pore system affects both acoustic and resistance measurements.

References

Alemu, B. L., Aker, E., Soldal, M., Johnsen, Ø., and Aagaard, P., 2013, Effect of sub-core scale heterogeneities on acoustic and electrical properties of a reservoir rock: a CO2 flooding experiment of brine saturated sandstone in a computed tomography scanner: Geophysical Prospecting, v. 61, no. 1, p. 235-250.

Alexandrov, K. S., Belikov, B. P., and Rysova, T. V., 1966, Vycislenie uprugich parametrov gornich porod po mineralnomu sostavu: Izvestia A. N. SSSR Ser. Geol. Moskva 2, 3-19.

Alkan, H., Cinar, Y., and Ülker, E. B., 2010, Impact of Capillary Pressure, Salinity and In situ Conditions on CO2 Injection into Saline Aquifers: Springer Science+Business Media B. V.

Andre, L., Azaroual, M., Peysson, Y., and Bazin, B., https://hal-brgm.archives-ouvertes.fr/hal-00755091/document, Impact of porous medium desiccation during anhydrous CO2 injection in deep saline aquifers: up scaling from experimental results at laboratory scale to near-well region, *in* Proceedings Energy Procedia, Amsterdam, Netherlands, 2010-09-19 2010, Volume 4, Elsevier, p. 4442-4449.

Balthazor, D. A., 1991, Sedmentology of the Bedford-berea squence (early Mississippian), Williams field, Michigan [Master of Science: Western Michigan University

Baraka-Lokmane, S., Ngwenya, B., and Main, I., Benefit of complementary methods for characterizing sandstone cores, *in* Proceedings SCA Conference Paper2007.

Batzle, M., and Wang, Z., 1992, Seismic properties of pore fluids: GEOPHYSICS, v. 57, no. 11, p. 1396-1408.

Benson, A. K., and Wu, J., 1999, A modeling solution for predicting (a) dry rock bulk modulus, rigidity modulus and (b) seismic velocities and reflection coefficients in porous, fluid-filled rocks with applications to laboratory rock samples and well logs: Journal of Applied Geophysics, v. 41, no. 1, p. 49-73.

Biot, M. A., 1941, General Theory of Three-Dimensional Consolidation: Journal of Applied Physics, v. 12, no. 2, p. 155-164.

Biot, M. A., 1956, Theory of Propagation of Elastic Waves in a Fluid-Saturated Porous Solid. I. Low-Frequency Range: The Journal of the Acoustical Society of America, v. 28, no. 2, p. 168-178.

Carmichael, R. S., 1989, Practical handbook of physical properties of rocks and minerals Boca Raton, Fla, CRC Press, v. Accessed from http://nla.gov.au/nla.cat-vn1960067.

Dawson, G. K. W., Pearce, J. K., Biddle, D., and Golding, S. D., 2014, Experimental mineral dissolution in Berea Sandstone reacted with CO2 or SO2–CO2 in NaCl brine under CO2 sequestration conditions: Chemical Geology.

Francke, H., and Thorade, M., 2010, Density and viscosity of brine: An overview from a process engineers perspective: Chemie der Erde - Geochemistry, v. 70, Supplement 3, no. 0, p. 23-32.

Garg, A., Zwahlen, E., and Patzek, T. W., 1996, Experimental andNumerical Studies of One-Dimensional Imbibition in BereaSandstone the 16th Annual American Geophysical Union Hydrology Days: Fort Colllins, CO, American Geophysical Union.

Gassmann, F., 1951, Über die Elastizität poröser Medien: Vier. Der Natur, v. 96, p. 1-23.

Gebrande, H., Kern, H., and Rummel, F., 1982, Elasticity and inelasticity. , Hellwege, K.-H. (Ed.) Landolt-Börnstein Numerical Data and Functional Relationships in Science and Technology, New Series, Group V. Geophysics and Space Research, Physical Properties of Rocks, Volume 1: Berlin, Springer-Verlag, p. 1-233.

Geertsma, J., 1961, Velocity-Log Interpretation: The Effect of Rock Bulk Compressibility.

Hamilton, E. L., 1970, Sound velocity and related properties of marine sediments, North Pacific: Journal of Geophysical Research, v. 75, no. 23, p. 4423-4446.

Hazlett, R. D., 1995, Simulation of capillary-dominated displacements in microtomographic images of reservoir rocks: Transport in Porous Media, v. 20, no. 1, p. 21-35.

Hill, R., 1963, Elastic properties of reinforced solids: Some theoretical principles: Journal of the Mechanics and Physics of Solids, v. 11, no. 5, p. 357-372.

-, 1964, Theory of mechanical properties of fibre-strengthened materials: I. Elastic behaviour: Journal of the Mechanics and Physics of Solids, v. 12, no. 4, p. 199-212.

IPCC, 2013, Observations: Atmosphere and Surface. In: Climate Change 2013: The Physical Science Basis. Contribution of Working Group I to the Fifth Assessment Report of the Intergovernmental Panel on Climate Change: Cambridge University Press.

Johnson, D. L., 2001, Theory of frequency dependent acoustics in patchy-saturated porous media: The Journal of the Acoustical Society of America, v. 110, no. 2, p. 682-694.

Kim, J., Nakatsuka, Y., Xue, Z., and Matsuoka, T., Monitoring CO2 injected into water-saturated sandstone with P-wave velocity and resistivity, *in* Proceedings 9th SEGJ International Symposium, Sapporo, Japan, 2009, Society of Exploration Geophysicists of Japan.

Kitamura, K., and Xue, Z., 2009, Experimental study on seismic monitoring of residual supercritical CO2 in water-saturated porous sandstones, 9th SEGJ International Symposium: Sapporo, Japan.

Krief, M., Garat, J., Stellingwerf, J., and Ventre, J., 1990, A Petrophysical Interpretation Using The Velocities Of P And S Waves (full-waveform Sonic).

Linstrom, P. J., and Mallard, W. G., NIST Chemistry WebBook, NIST Standard Referencec Database Number 69, National Institute of Standards and Technology, Gaithersburg MD, 20899, http://webbook.nist.gov.

Mavko, G., Effective medium theories.

McKenzie, L. C., Thompson, J. E., Sullivan, R., and Hutchison, J. E., 2004, Green chemical processing in the teaching laboratory: a convenient liquid CO2 extraction of natural products: Green Chemistry, v. 6, no. 8, p. 355-358.

Méheust, Y., Løvoll, G., Måløy, K. J., and Schmittbuhl, J., 2002, Interface scaling in a two-dimensional porous medium under combined viscous, gravity, and capillary effects: Physical Review E, v. 66, no. 5, p. 051603.

Nur, A. M., Mavko, G., Dvorkin, J., and Gal, D., 1995, Critical porosity: The key to relating physical properties to porosity in rocks, SEG Technical Program Expanded Abstracts 1995, p. 878-881.

Omolo, L. O., 2015, Laboratory study on the effect of CO2 flooding on acoustic velocity and resistivity as a means of monitoring sequestrated CO2 in sandstone reservoirs [Master in science: University of Oslo.

Onishi, K., Ishikawa, Y., Yamada, Y., and T., M., 2006, Measuring electric resistivity of rock specimens injected with gas, liquid and supercritical CO2, SEG/New Orleans 2006 Annual Meeting, Volume 2006: New Orleans Society of Exploration Geophysicists.

Pickett, G. R., 1963, Acoustic Character Logs and Their Applications in Formation Evaluation.

Raymer, L. L., Hunt, E. R., and Gardner, J. S., 1980, An Improved Sonic Transit Time-To-Porosity Transform, Society of Petrophysicists and Well-Log Analysts.

Ross, N. L., and Reeder, R. J., 1992, High-pressure structural study of dolomite and ankerite: American Mineralogist, v. 77, no. 3-4, p. 412-421.

Sarda, J.-P., Ferfera, F. M. R., Vincké, O., Beoutéca, M., and Longuemare, P., 1998, Experimental study of the stress paths influence on monophasic permeability evolution, SCA Conference paper: SCA 9827.

Siggins, A. F., Lwin, M., and Wisman, P., 2010, Laboratory calibration of the seismo-acoustic response of CO2 saturated sandstones: International Journal of Greenhouse Gas Control, v. 4, no. 6, p. 920-927.

Woeber, A. F., Katz, S., and Ahrens, T. J., 1963, Elasticity of selected rocks and minerals: Geophysics, v. 28, no. 4, p. 658-663.

Xue, Z., Kim, J., Mito, S., Kitamura, K., and Matsuoka, T., 2009, "Detecting and monitoring CO2 with p-wave velocity and resistivity from both laboratory and field scales", SPE International Conference on CO2 Capture, Storage, and Utilization: San Diego, California, USA, Society of Petroleum Engineers.

Zhang, J., Wong, T.-F., and Davis, D. M., 1990, Micromechanics of pressure-induced grain crushing in porous rocks: Journal of Geophysical Research: Solid Earth, v. 95, no. B1, p. 341-352.

Zhang, J. J., and Bentley, R., 1999, Change of bulk and shear moduli of dry sandstone with effective pressure and temperature: CREWES.

Appendix

Appendix 1

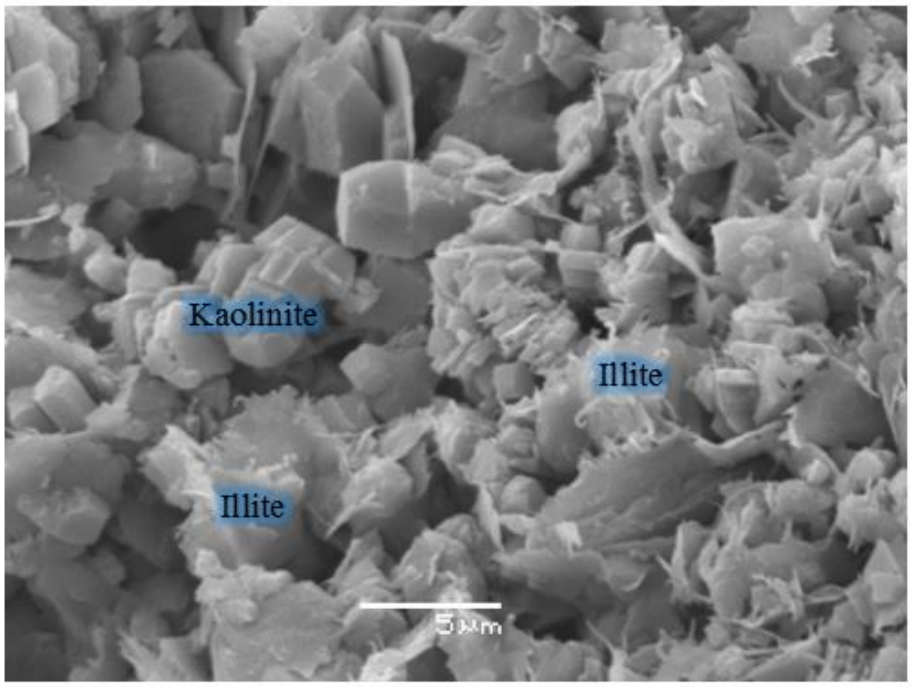

Fig. A1.1 Berea sandstone, kaolinite and illite

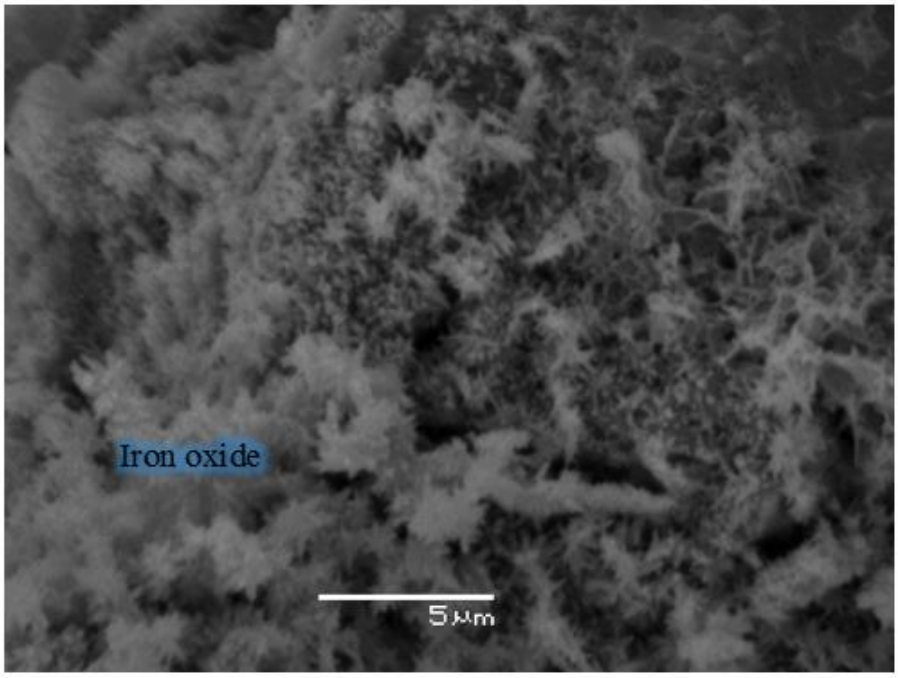

Fig. A1.2 Berea sandstone, iron oxide

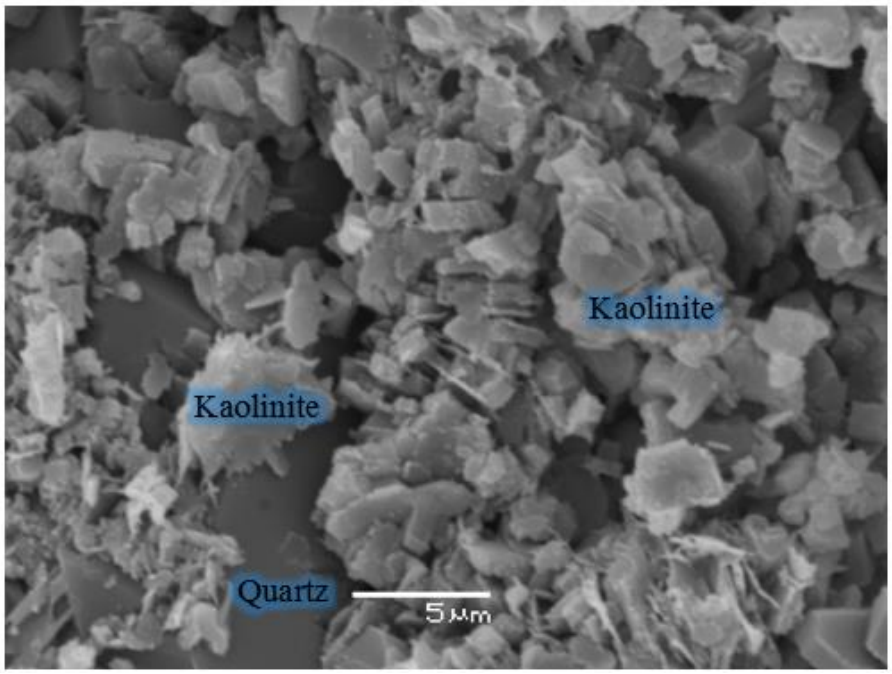

Fig. A1.3 Berea sandstone, kaolinite and quartz

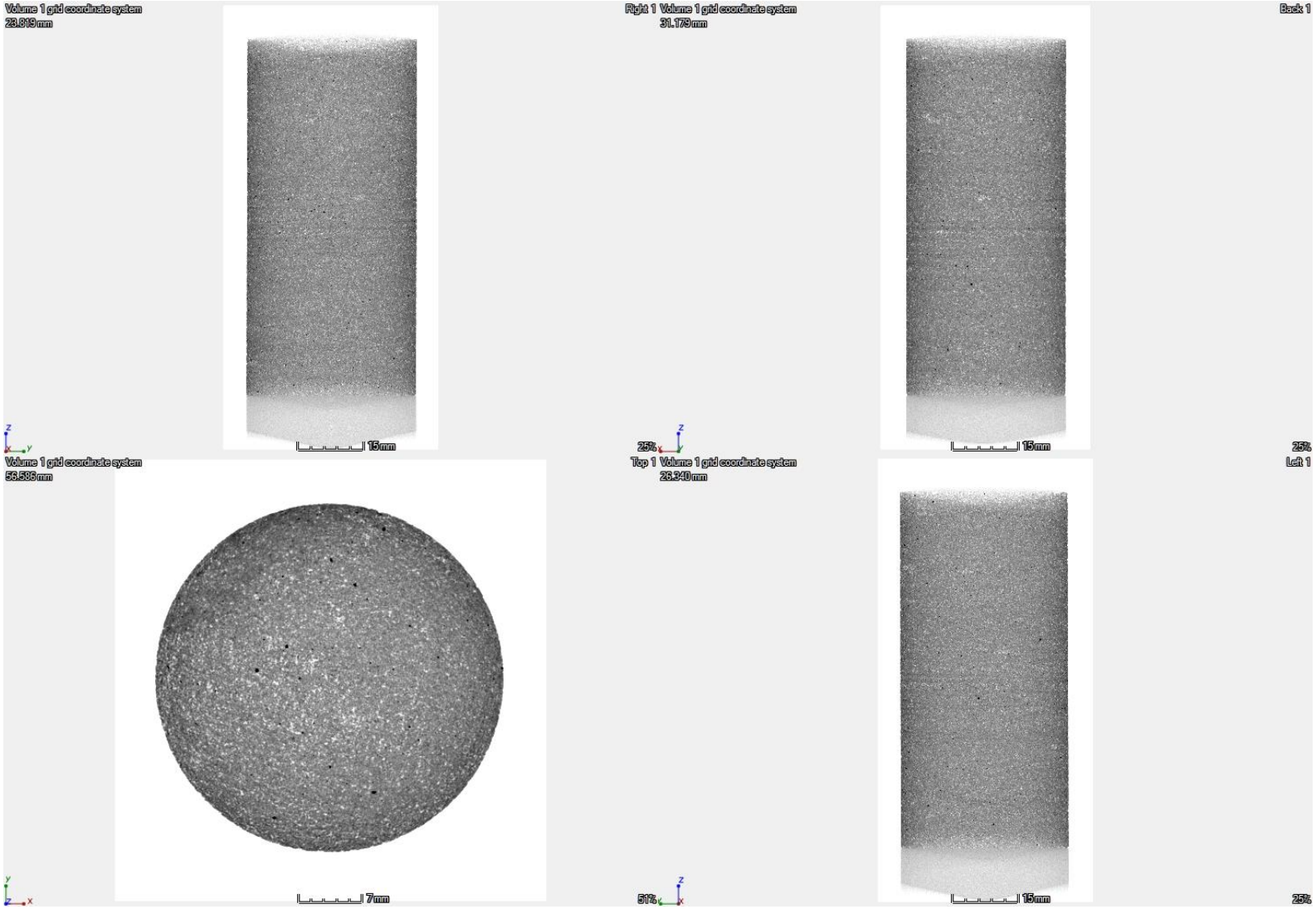

Fig. A1.4 CT-scan of GDV_V

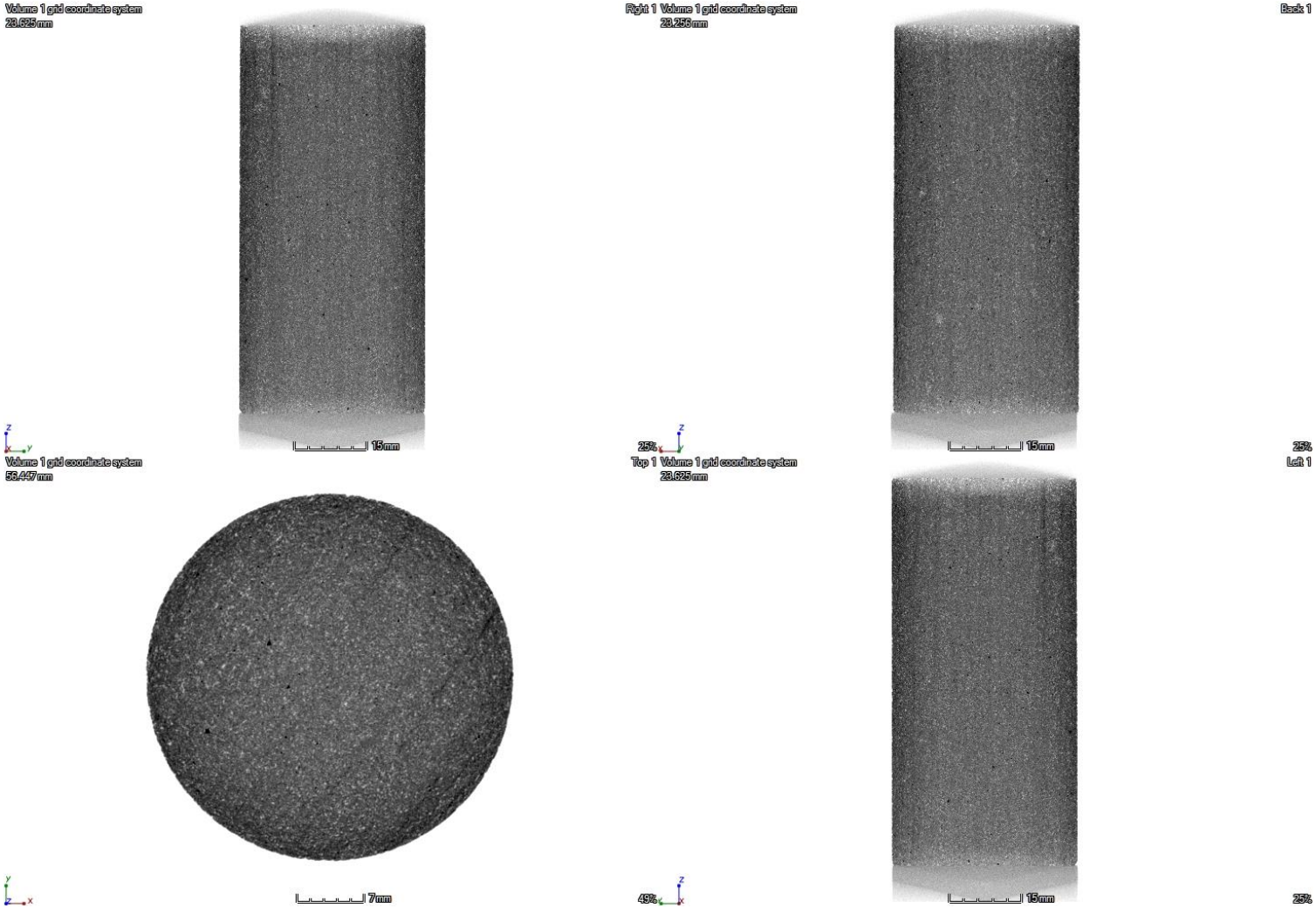

Fig. A1.5 CT-scan of GDV_H

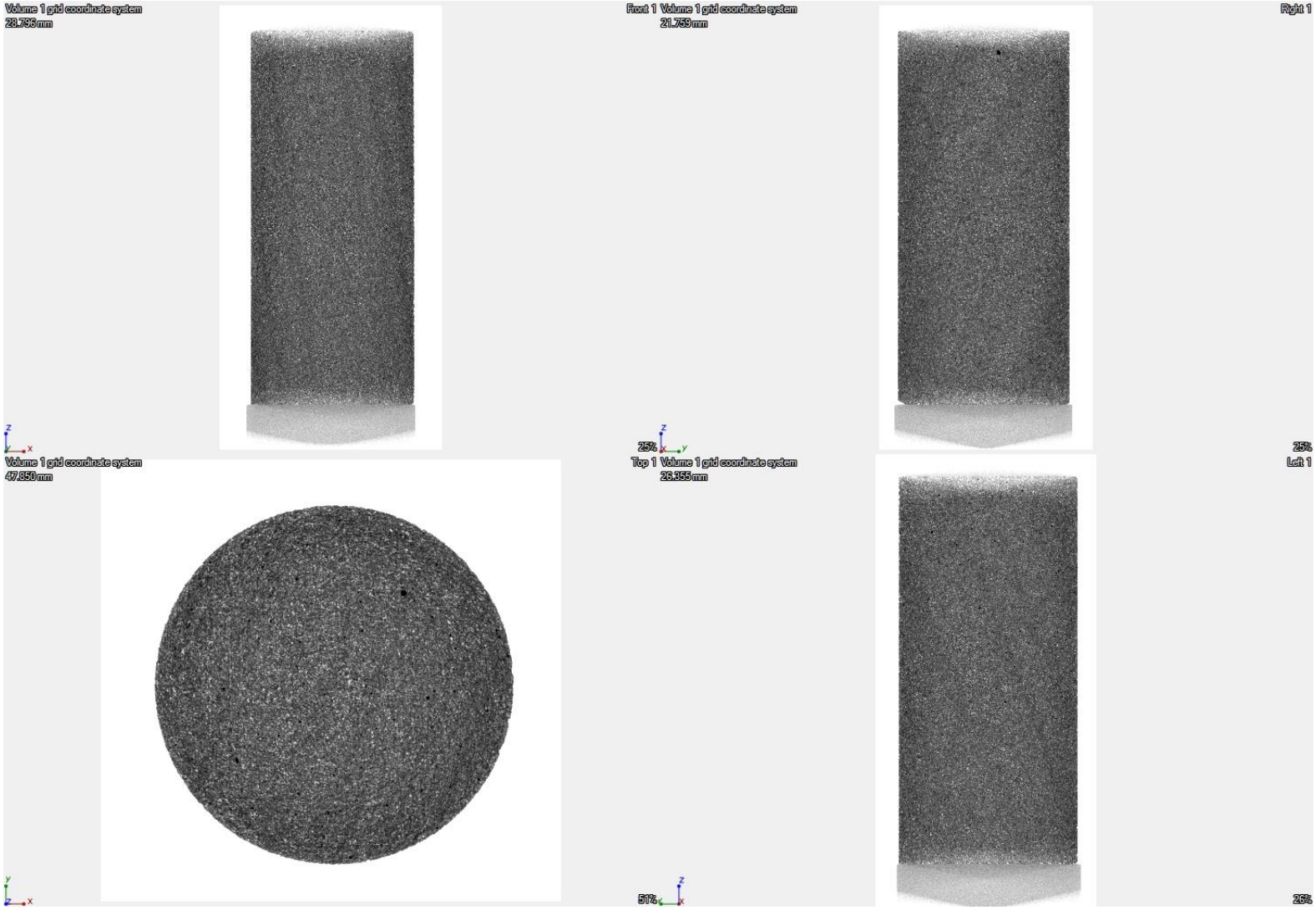

Fig. A1.6 CT-scan of Berea 400mD

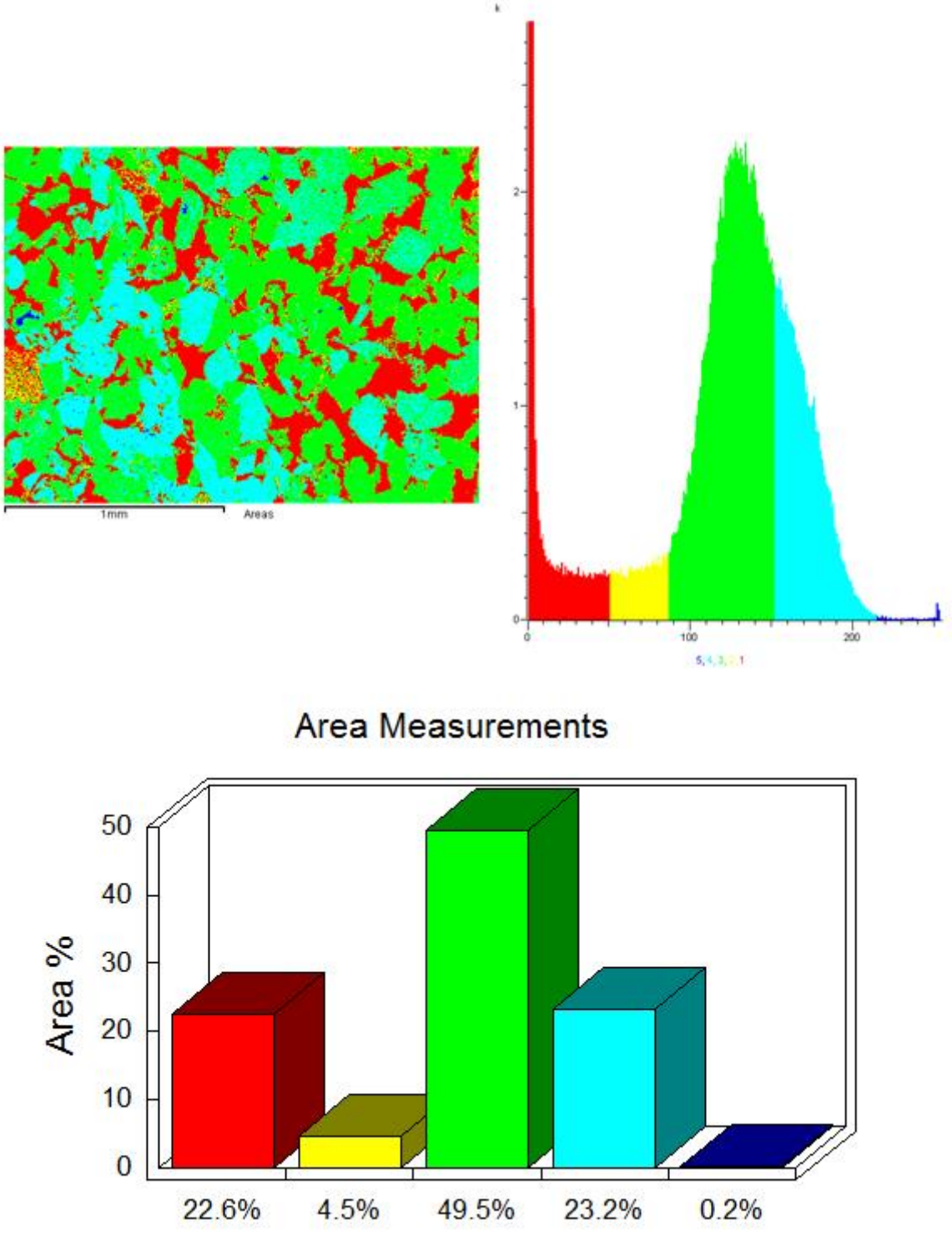

Fig. A1.7 Estimate of minerals and porosity for Gres des Vosges vertical

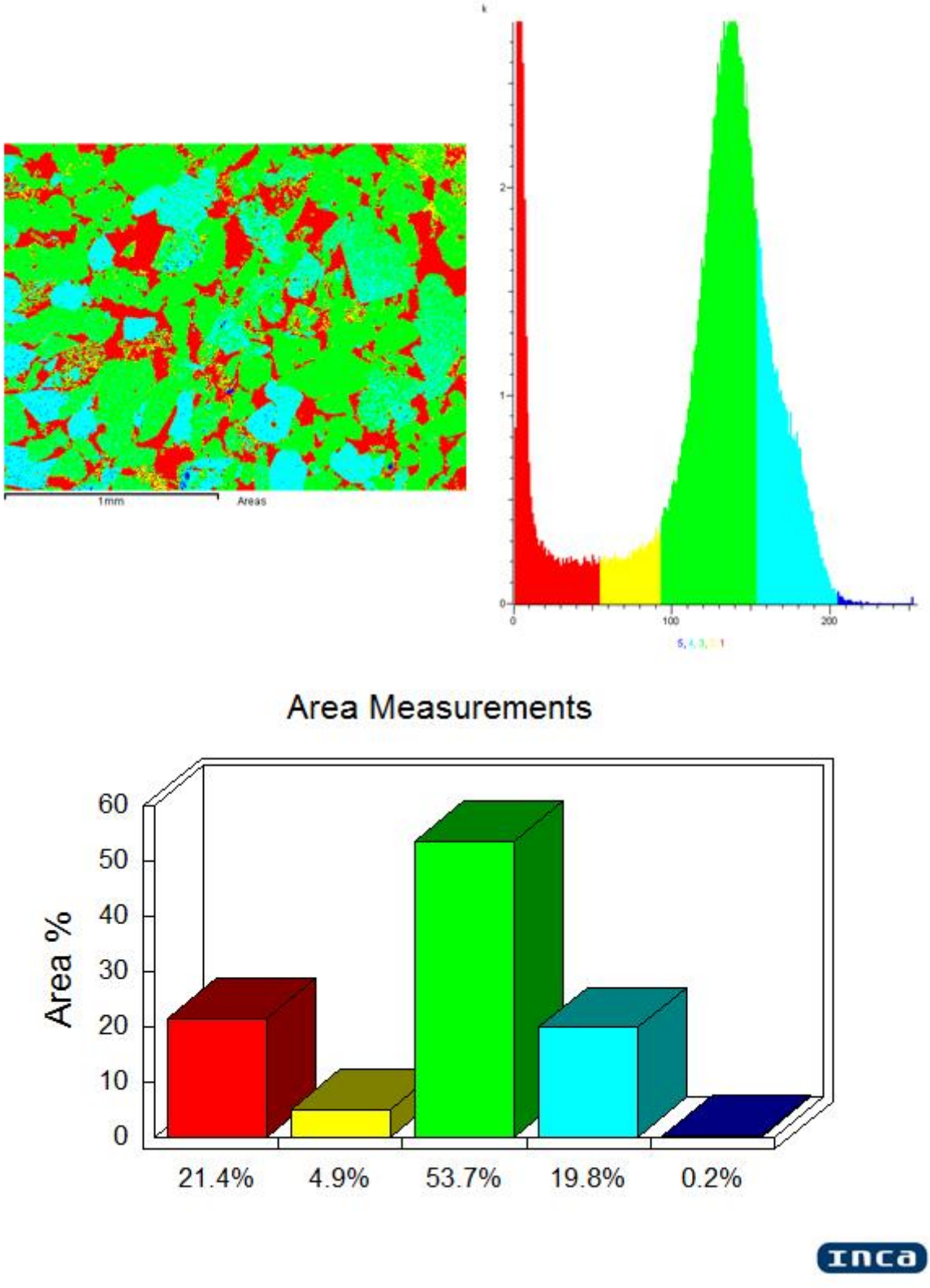

Fig. A1.8 Estimate of minerals and porosity for Gres des Vosges horizont

Matlab code

9.1. Matlab code

9.1.1. Combine_data

```
%Program for reading in text files (resistivity and timepicks into matlabs
a=1;
exitflag=0;
while a==1
   %select type of text file and see if it exist
   checkxlfile=0;
   while checkxlfile==0
      op1='Read in resistivity or timepick? [r]/[t]    ';
      anw1=input(op1,'s');
      resop=strcmpi('r',anw1);
      timeop=strcmpi('t',anw1);
      if timeop==1 %if1
         disp('select text file')
         [checkxlfile,filename,pathname,exitflag]=getfile(checkxlfile,exitflag); %select file
         if exitflag==1
            disp('program closing')
            return
         end
      fprintf('Using textfile %s %s \n',pathname,filename)
      elseif resop==1
         [res,exitflag]=combineRES(resop,exitflag);
         if exitflag==1
            disp('program closing')
            return
         else
             checkxlfile=1;
         end
      elseif (resop+timeop)==0
   [exitflag,checkxlfile]=invalidoption(exitflag,checkxlfile);
         if exitflag==1
            disp('program closing')
            return
         end
      end %end if1
   end %end checkfile

   %select xls file
   checkxlfile=0;
   while checkxlfile==0
      disp('select excel file')
      [checkxlfile,xlfilename,xlpathname,exitflag]=getxlfile(checkxlfile,exitflag); %select file
         if exitflag==1
            disp('program closing')
            return
         end
  fprintf('Using excel file %s %s \n',xlpathname,xlfilename)
   end
```

```
%for resistivity files
if resop==1 %resistivity option
   %load data from file
   [exceldatares] = aquiredata(xlpathname, xlfilename); %from excel

   %set correct time
   limit=4;
   start=1;
   [cor_res,echeck] = findtime(res,exceldatares,limit,start);

   while echeck==1
      [limit,start,echeck]=changelimitstart(limit,start);
         if echeck==20
            fprintf('continue to write to excel file\n')
            break
         end
      [cor_res,echeck] = findtime(res,cor_res,limit,start);%use existing excel array
         if echeck==0
            fprintf('end of txt file \n')
         end
    end

 %print to excel
 flagprint=0;
 flagop5=0;
 while flagop5==0
 op5=('write data to excel sheet? [Y]/[N]   ');
 anw5=input(op5,'s');
 [flagprint,flagop5]=option(anw5);
    if flagprint==0 %last time to regret not saving your readings
       fprintf('changes wont be saved and deleted on next reading\n')
       op11=('continue? [Y]/[N] ');
       anw11=input(op11,'s');
       [flagprint,flagop5]=reverseoption(anw11);
    end
    if flagop5==15
       fprintf('Invalid option, try again')
    end

 end
 printREStoexcel(xlpathname,xlfilename,cor_res,flagprint);

 end %resistivity option

if timeop==1 %timepick option
   %load data
   [timepick] = vel2mat(pathname,filename);%from text file
   [chtxt]= sort_for_each_Ch(timepick);
   [exceldataVEL] = aquiredataVEL(xlpathname, xlfilename); %from excel

%set correct time
   limit=1.3;
   start=1;
   [cor_VEL,echeck,last] = findtimeVEL(chtxt,exceldataVEL,limit,start);

   while echeck==1
      [limit,start,echeck]=changelimitstartVEL(limit,start);
```

```
            if echeck==20
               fprintf('continue to write to excel file\n')
               break

            elseif echeck==1
             [cor_VEL,echeck,last] = findtimeVEL(chtxt,cor_VEL,limit,start);%use existing excel array
                if echeck==0
                   fprintf('end of txt file \n')
                end
            elseif echeck==100
                op17=('type in posistion of single read in  ');
                anw17=input(op17);
                single(1,:)=chtxt(anw17,:);
                [cor_VEL,echeck,last] = findtimeVEL(single,cor_VEL,limit,1);
                   if echeck==0
                   flag15=0;
                   [echeck]=continueORnot(flag15);
                   end
            elseif echeck==25
                   flag=1;
                   stop=length(chtxt);
                   while flag==1
                      [last,stop,flag,echeck]=changelaststop(last,stop,chtxt);
                   end

                   while flag==0 &&echeck==25
                      [co2brine]=checkCO2Brine(last,chtxt,stop); %sort out last timepick in rapid acquisistion and
use it as one reading
                   op12=('Do you want to use these picks? [Y]/[N]  ');
                   anw12=input(op12,'s');
                      if strcmpi('y',anw12)
                         [cor_VEL,echeck,last] = findtimeVEL(co2brine,cor_VEL,limit,1);
                         flag=1;
                         if echeck == 0 && stop < length(chtxt)
                            flag15=0;
                            [echeck]=continueORnot(flag15);
                         end
                      elseif strcmpi('n',anw12)
                         echeck=1;
                         flag=1;
                      else
                         fprintf('Invalid option, try again')
                      end
                   end
            end
         end

      %print to excel
      flagprint=0;
      flagop5=0;
      while flagop5==0
      op5=('write data to excel sheet? [Y]/[N]   ');
      anw5=input(op5,'s');
      [flagprint,flagop5]=option(anw5);
         if flagprint==0 %last time to regret not saving your readings
            fprintf('changes wont be saved and deleted on next reading\n')
            op11=('continue? [Y]/[N] ');
            anw11=input(op11,'s');
            [flagprint,flagop5]=reverseoption(anw11);
```

```
      end
      if flagop5==15
         fprintf('Invalid option, try again')
      end

   end
   printVELtoexcel(xlpathname,xlfilename,cor_VEL,flagprint);

  end %timepick option

   %Check if you want to continue or exit
   flag=1;
   while flag==1
      op3='Continue with more readings? [Y]/[N]    ';
      anw3=input(op3,'s');
      if strcmpi('n',anw3)==1
         disp('program closing')
      return
      elseif strcmpi('y',anw3)==1
         a=1;
         flag=0;
         filename=0;
      else
         disp('invalid option, try again')
      end
   end
end %end main loop/program a
```

9.1.2. Functions for Combine_data

```
%% Import the data from excel time for resistance input
function [exceldatares] = aquiredata(xlpathname, xlfilename)
file = fullfile(xlpathname, xlfilename);
%% Read timestamp in OUTPUT spreadsheet
[~,~,raw] = xlsread(file,'OUTPUT');

%% Create output variable
raw(cellfun(@(x) any(isnan(x)),raw)) = {''}; %remove NaN cells
 ymd = cell2mat(raw(5:end,2)); %Read date in the format dd.mm.yyyy
 hms = cell2mat(raw(5:end,3)); %Read the time as a value

 %Use existing column for resistance to insert new value
 %columns are fixed to a setup in the excel sheet
Axialres=xlsread(file,'OUTPUT','BM:BM'); % Axial measurements
RadialresB=xlsread(file,'OUTPUT','BN:BN'); % Radial bottom measurements
RadialresM=xlsread(file,'OUTPUT','BO:BO'); % Radial middle measurements
RadialresT=xlsread(file,'OUTPUT','BP:BP'); % Radial top measurements
time = datenum(ymd,'dd.mm.yyyy')+hms;
exceldatares=[time,Axialres,RadialresB,RadialresM,RadialresT];
disp(['Data from file ', xlfilename, ' loaded'])
```

```
%% Import data from excel for velocity time picks
function [exceldataVEL] = aquiredataVEL(pathname, filename)
file = fullfile(pathname, filename);
%% Read timestamp in OUTPUT spreadsheet
[~,~,raw] = xlsread(file,'OUTPUT');
```

```
%% Create output variable
% raw(cellfun(@(x) ~isempty(x) && isnumeric(x) && isnan(x),raw)) = {''};
raw(cellfun(@(x) any(isnan(x)),raw)) = {''}; %remove NaN cells
 ymd = cell2mat(raw(5:end,2)); %Reads in date in the format dd.mm.yyy
 hms = cell2mat(raw(5:end,3)); %Reads in time as a value

 %Use existing column for timepicks to insert new value
 %columns are fixed to a setup in the excel sheet
c0=cell2mat(raw(5:end,55)); %column for Vs axial
c1=cell2mat(raw(5:end,56)); %column for Vp axial
c2=cell2mat(raw(5:end,57)); %column for Vp radial bottom
c3=cell2mat(raw(5:end,58)); %column for Vp radial middle
c4=cell2mat(raw(5:end,59)); %column for Vp radial top
time = datenum(ymd,'dd.mm.yyyy')+hms;
exceldataVEL=[time,c1,c2,c3,c4,c0];
disp(['Data from file ', filename, ' loaded'])
```

```
%% Function to change parameters for findtime function
% This gives the option to change where to start and stop matching for
% resistance measurements
function [last,stop,flag,echeck]=changelaststop(last,stop,chtxt)
fprintf('last read pick at position %d and it will stop at %d
\n',last,stop)
fprintf('do you want to use other values? txt file ends at %d
\n',length(chtxt))
op13=('last position [1], where to stop [2], use current values [3] or [4]
to abort  ');
anw13=input(op13);
flag=1;
echeck=25;
        if anw13==1
        op14=('type in new start  ');
        last=input(op14);
        elseif anw13==2
        op15=('type in new stop  ');
        stop=input(op15);
        elseif anw13==3
        flag=0;
        elseif anw13==4
        flag=0;
        echeck=1;
        else
        fprintf('invalid option, try again \n')
        flag=1;
        echeck=1;
        end
end
```

```
%% Function to change parameters for findtime function
% This gives the option to change where to start and stop matching in
% addition to change the timeintervall
function [limit,start,echeck]=changelimitstart(limit,start)
change=0;
while change==0
op6=...
('change start point[1], time interval[2], done/no change[3] and exit[4]');
```

```
anw6=input(op6);
    if anw6==1
    fprintf('start point is %d \n',start)
    op7=('enter new start point ');
    start=input(op7);
    elseif anw6==2
    fprintf('time interval is %d mins\n',limit)
    op8=('enter new time interval ');
    limit=input(op8);
    elseif anw6==3
fprintf('continue with start point %d and time interval %d \n',start,limit)
        echeck=1;
        return
    elseif anw6==4
        echeck=20;
        return
    else
        fprintf('Invalid option, try again\n')
    end
end %while change
end
```

```
%% Option function
% function activates when not all data in txt file (from funcion findtime)
% are properly matched. This function gives the option to change start/stop
% points, using special function checkCO2Brine, do a single matching and
% continue without doing more matching
function [limit,start,echeck]=changelimitstartVEL(limit,start)
change=0;
while change==0
fprintf('what do you want to change?\n')
op6=...
('start[1], time interval[2], done[3], CO2Brine[4], single[5] and no
change[6]');
anw6=input(op6);
    if anw6==1
    fprintf('start point is %d \n',start)
    op7=('enter new start point ');
    start=input(op7);
    elseif anw6==2
    fprintf('time interval is %d mins\n',limit)
    op8=('enter new time interval ');
    limit=input(op8);
    elseif anw6==3
fprintf('continue with start point %d and time interval %d \n',
start,limit)
        echeck=1;
        return
    elseif anw6==4
        echeck=25;
        return
    elseif anw6==5
        echeck=100;
        return
    elseif anw6==6
        echeck=20;
        return
    else
        fprintf('Invalid option, try again\n')
```

```
    end
end %while change
end
```

```
%% Special function for drainage and imbibition measurements
% Use when only one in two or more continously (two or more readings
% seperated by one minute) measurement is desired.
% This function sort out which timepick to put into excel sheet, assumes
% only timepicks from CO2 into brine and brine flushing is lefted.
% NB! THIS FUNCTION WILL SKIP READINGS AT PV = 0, DO SINGLE READING IF
% MEASUREMENT AT PV = 0 IS NEEDED
function [co2brine]=checkCO2Brine(last,chtxt,stop)
newstart=last;
m=0;
flag1=1;
co2brine=[];
pick=[];
while flag1==1
        i=newstart;
        k=1;
        flag=1;
        limit=1/60/24;
        while flag==1
            if (i+1>stop)
                flag=0;
            else
            temp=abs(chtxt(i,1)-chtxt(i+1,1));
                if temp < limit
                i=i+1;
                k=k+1;
                for j=1:5
                pick(j,1)=chtxt(i,j+1);
                end
                else
                flag=0;
                end
            end

        end
    if k>=2
        m=m+1;
        co2brine(m,1)=chtxt(newstart+k-1,1);
        for j=1:5
        co2brine(m,j+1)=pick(j,1);
        end

        newstart=newstart+k-1;

    else
        newstart=newstart+1;
    end
    if newstart==stop
        fprintf('done matching rapid acquisition \n')
        flag1=0;
    end
end
% printing out the picked values into screen, check with txt file + numbers
```

```
% of picks corrosponds to schedule of injection
fprintf('using this array for rapid acquisition\n')
fprintf('date and time           ch1             ch2             ch3
ch4             ch0         \n')

for i=1:length(co2brine(:,1))
    fprintf('%s \t %d \t %d \t %d \t %d \t %d
\n',datestr(co2brine(i,1),21),co2brine(i,2),co2brine(i,3),co2brine(i,4),co2
brine(i,5),co2brine(i,6))
end

end
```

```
%% Combing txt files for resistance
% when resistance files are splitt into four files (axial + three radial)
% a combined array containing all these data are made to eaiser and faster
% write them into excel sheet
% NB! timestamps from axial file are used to match
function [res,exitflag]=combineRES(resop,exitflag)
check=resop;
axial=[]; radbot=[]; radmid=[]; radtop=[];
res=[];
while check==1
disp('select axial res txt file')
[check,filename1,pathname1,exitflag]=getfile(check,exitflag);
if check==1
[axial] = res2mat2(pathname1,filename1);
else
    return
end
disp('select rad res bot txt file')
[check,filename2,pathname2,exitflag]=getfile(check,exitflag);
if check==1
[radbot] = res2mat2(pathname2,filename2);
else
    return
end
disp('select rad res mid txt file')
[check,filename3,pathname3,exitflag]=getfile(check,exitflag);
if check==1
[radmid] = res2mat2(pathname3,filename3);
else
    return
end
disp('select rad res top txt file')
[check,filename4,pathname4,exitflag]=getfile(check,exitflag);
if check==1
[radtop] = res2mat2(pathname4,filename4);
else
   return
end
res=[axial,radbot(:,2),radmid(:,2),radtop(:,2)];

% display selected files before importing values
fprintf('Use textfile %s %s as axial resistance \n',pathname1,filename1)
fprintf('Use textfile %s %s as radial bottom resistance
\n',pathname2,filename2)
```

```
fprintf('Use textfile %s %s as radial middel resistance
\n',pathname3,filename3)
fprintf('Use textfile %s %s as radial top resistance
\n',pathname4,filename4)
    if check==1
        flag=1;
        while flag==1
        op20='Continue with these files? [Y]/[N]    ' ;
        anw20=input(op20,'s');
        if strcmpi('y',anw20)==1
            fprintf('Continuing \n');
            flag=0;
            check=0;
        elseif strcmpi('n',anw20)==1;
            fprintf('Choose resistance files again \n')
            flag=0;
            check=1;
        else
            op21('Invalid option, try again [A] or exit [E] \n  ' );
            anw21=input('E','s');
            if strcmpi('E',anw21)==1
                exitflag =1;
                return
            end
        end
        end
    end
end
```

```
function [echeck]=continueORnot(flag15)
while flag15==0
op15=...
('do you want to continue matching? end of txt file not reached [Y]/[N] ');
anw15=input(op15,'s');
[echeck,flag15]=option(anw15);
        if(flag15==0)
        fprintf('invalid option, try again \n')
        end
end
```

```
%% Match resistance time with excel time
% matching time between resistivity txt file and excel, keeps the time from
% excel as correct time

function [cor_res,echeck] = findtime(res,exceldatares,limit,start)
xt=res(:,1); %date and time form .txt file for matching against excel
cor_res(:,:)=exceldatares(:,:);%import existing time and data column from
                               %excel
j=0;
limdat=limit/60/24;%timewindow for matching given as a value in days

for i=start:length(xt)
    if j>length(exceldatares)%check if within timeset from excelsheet
        if(i<=2)% first time value from txt file does not match with any
                % in the excel sheet
```

```
            fprintf('cant match anything, stops at top of file %s \n'...
                ,datestr(res(start,1),21))
            echeck=1;
            return
        else
k=res(i-2,1);%gives date and time of last data set put into excelsheet
fprintf('cant match everything, stops at time: %s  and position %d \n'...
    ,datestr(k,21),i-2)
echeck=1;
        return
        end
    else
    j=j+1;
    t= (xt(i)== exceldatares(j,1));%true=1 or false=0
        if t==1 %found a match
        cor_res(j,2)=res(i,2);
        cor_res(j,3)=res(i,3);
        cor_res(j,4)=res(i,4);
        cor_res(j,5)=res(i,5);
        else
            while t==0 %didnt find a match, look further down the column
              if (j>length(exceldatares(:,1)))%at end of excel sheet, cant
                                              %find a match, exit loop
                  t=1;
              else
                temp=xt(i)-exceldatares(j,1);
                if abs(temp) <= limdat %within timeframe for readings
                                       %insert txt values in array
                    cor_res(j,2)=res(i,2);
                    cor_res(j,3)=res(i,3);
                    cor_res(j,4)=res(i,4);
                    cor_res(j,5)=res(i,5);
                    t=1;
                else
                  j=j+1; %keep searching
                end
              end
            end
        end
    end
end
echeck=0;
end
```

```
%% Match acoustic measurement time with excel time
% matching time between time pick txt file and excel, keeps the time from
% excel as correct time

function [cor_VEL,echeck,last]=findtimeVEL(chtxt,exceldataVEL,limit,start)
xt=chtxt(:,1); %date and time form .txt file for matching against excel
cor_VEL(:,:)=exceldataVEL(:,:);%use existing time+date column from excel
j=0;
limdat=limit/60/24;%timewindow for matching
%exceldataVEL=[time,ch1,ch2,ch3,ch4,ch0]
last=0;
for i=start:length(xt)
    if j>length(exceldataVEL)%check if within timeset from excelshee
        if(i<=2)% first time value from txt file does not match with any
```

```
                % in the excel sheet
            fprintf('cant match anything, stops at top of file %s \n'...
                ,datestr(chtxt(start,1),21))
            echeck=1;
            return
        else
k=chtxt(i-2,1);%gives date and time of last matched data set
fprintf('cant match everything, stops at time: %s  and position %d \n'...
    ,datestr(k,21),i-2)
echeck=1;
last=i-2;
        return
        end
    else
    j=j+1;
    t= (xt(i)== exceldataVEL(j,1));%true=1 or false=0
        if t==1 %found a match
        cor_VEL(j,2)=chtxt(i,2); %ch1
        cor_VEL(j,3)=chtxt(i,3); %ch2
        cor_VEL(j,4)=chtxt(i,4); %ch3
        cor_VEL(j,5)=chtxt(i,5); %ch4
        cor_VEL(j,6)=chtxt(i,6); %ch0
        else
            while t==0 %didnt find a match, look further down the column
              if (j>length(exceldataVEL(:,1)))%at end of excel sheet, cant
                                              %find a match, exit loop
                  t=1;
              else
                temp=xt(i)-exceldataVEL(j,1);
                if abs(temp) <= limdat %within timeframe for readings
                                       %insert txt values in array
                    cor_VEL(j,2)=chtxt(i,2); %ch1
                    cor_VEL(j,3)=chtxt(i,3); %ch2
                    cor_VEL(j,4)=chtxt(i,4); %ch3
                    cor_VEL(j,5)=chtxt(i,5); %ch4
                    cor_VEL(j,6)=chtxt(i,6); %ch0
                    t=1;
                else
                  j=j+1; %keep searching
                end
              end
            end
        end
    end
end
echeck=0;
end
```

```
%% pop-up window to select txt file
function [check,filename,pathname,exitflag]=getfile(check,exitflag)
filename=0;
flag=1;
    while flag==1
        [filename,pathname] = uigetfile('*.txt','Select the text file');
        if filename==0 %no file selected,
            flag2=1;
            while flag2==1
                op2='No file selected, try again? N for exit[Y]/[N]   ';
                anw2=input(op2,'s');
```

```
                if strcmpi(anw2,'n')==1
                exitflag=strcmpi(anw2,'n');
                check=0;
                return
                elseif strcmpi(anw2,'y')==1
                check=0;
                exitflag=0;
                flag2=0;
                else
                disp('invalid option, try again')
                end
            end
        else
        check=1;
        exitflag=0;
        flag=0;
        end
    end
end
```

```
%% pop-up window to select excel file
function [check,xlfilename,xlpathname,exitflag]=getxlfile(check,exitflag)
xlfilename=0;
flag=1;
    while flag==1
        [xlfilename,xlpathname] =...
            uigetfile({'*.xlsx';'*.xls'},'Select the excel file');
        if xlfilename==0 %no file selected,
            flag2=1;
            while flag2==1
                op2='No file selected, try again? N for exit[Y]/[N]    ';
                anw2=input(op2,'s');
                if strcmpi(anw2,'n')==1
                exitflag=strcmpi(anw2,'n');
                return
                elseif strcmpi(anw2,'y')==1
                check=0;
                exitflag=0;
                flag2=0;
                else
                disp('invalid option, try again')
                end
            end
        else
        check=1;
        exitflag=0;
        flag=0;
        end
    end
end
```

```
%% invalid option function
% used to continously use the program without exiting due to inserting of
% non-exsisting option
function [exitflag,checkfile]=invalidoption(exitflag,checkfile)
```

```
flag=0;
  while flag==0
    op4='Invalid option,try again? N for exit [Y]/[N]      ';
    anw4=input(op4,'s');
    if strcmpi('n',anw4)==1
        exitflag=1;
        return
    elseif strcmpi('y',anw4)==1
        checkfile=0;
        return
    end
  end
end
```

```
%% a switchS
function [value,flag]=option(anw)
value=15;
    if strcmpi('n',anw)
        value=0;
        flag=1;
    elseif strcmpi('y',anw)
        value=1;
        flag=1;
    else
        flag=0;
    end

end
```

```
%% Write in data to excel
% write resistance measurements to the excel file
function printREStoexcel(xlpathname,xlfilename,cor_res,flagprint)
    if flagprint==1
    fprintf('Writing data to %s %s...\n',xlpathname, xlfilename)
    filename = fullfile(xlpathname, xlfilename);
    Ar = {'1000.0Hz','1000.0Hz','1000.0Hz','1000.0Hz';'Resistance', ...
        'Resistance','Resistance','Resistance';'Axial','Radial(B)',...
        'Radial(M)','Radial(T)';'[ohm/m]','[ohm/m]','[ohm/m]','[ohm/m]'};
    Ar(5:4+length(cor_res),1)=num2cell(cor_res(:,2));
    Ar(5:4+length(cor_res),2)=num2cell(cor_res(:,3));
    Ar(5:4+length(cor_res),3)=num2cell(cor_res(:,4));
    Ar(5:4+length(cor_res),4)=num2cell(cor_res(:,5));
    sheet = 'Res';
    xlRange = 'BM1';
    xlswrite(filename,Ar,sheet,xlRange)
    fprintf('Done writing data to %s %s...\n',xlpathname, xlfilename)
    fclose('all');
    end

end
```

```
%% Write in data to excel
% write acoustic time picks measurements to the excel file
```

```
function printVELtoexcel(xlpathname,xlfilename,cor_VEL,flagprint)
    if flagprint==1
        fprintf('Writing data to %s %s...\n',xlpathname, xlfilename)
        filename = fullfile(xlpathname, xlfilename);
        Ar = {'Ch5','Ch1','Ch2','Ch3','Ch4';'S-wave','P-wave','P-wave',...
         'P-wave','P-wave';'Tsax','Tpax','Tprad(b)','Tprad(m)','Tprad(b)'};
        Ar(5:4+length(cor_VEL(:,1)),1)=num2cell(cor_VEL(:,6));
        Ar(5:4+length(cor_VEL(:,1)),2)=num2cell(cor_VEL(:,2));
        Ar(5:4+length(cor_VEL(:,1)),3)=num2cell(cor_VEL(:,3));
        Ar(5:4+length(cor_VEL(:,1)),4)=num2cell(cor_VEL(:,4));
        Ar(5:4+length(cor_VEL(:,1)),5)=num2cell(cor_VEL(:,5));
        sheet = 'OUTPUT';
        xlRange = 'BC1';% position of first colon
        xlswrite(filename,Ar,sheet,xlRange)
        fprintf('Done writing data to %s %s...\n',xlpathname, xlfilename)
    end
end
```

```
%% Import resistivity file,
% use if only one type of measurement in one txt file, eg. only axial
% measurement
function [res] = res2mat2(pathname,filename)
file = fullfile(pathname, filename);
delimiter = ';';
startRow = 2;

%% Format string for each line of text:
formatSpec_data = '%*s %*f %f %[^\n\r]';
formatSpec_date = '%s %[^\n\r]';

%% Load data
FID = fopen(file,'r');
data = textscan(FID, formatSpec_data, 'Delimiter', delimiter,...
    'HeaderLines' ,startRow-1, 'ReturnOnError', false);
fclose(FID);
FID = fopen(file,'r');
date = textscan(FID, formatSpec_date, 'Delimiter', delimiter,...
    'HeaderLines' ,startRow-1, 'ReturnOnError', false);
fclose(FID);

%% Create output variable
data = [data{1:end-1}];
date = [date{1:end-1}];

time = datenum(date,'yyyymmdd_HHMMSS'); %convert date/time a value
res = [time, data];
disp(['Data from file ', filename, ' loaded'])
```

```
%% reverse option, value is now 1 for n
function [value,flag]=reverseoption(anw)
value=15;
    if strcmpi('n',anw)
        value=1;
        flag=1;
    elseif strcmpi('y',anw)
        value=0;
```

```
        flag=1;
    else
        flag=0;
    end

end
```

```
%% Separate all five measurement into five column
% sort time picks after channels Vs and Vp for axial + three radial
% NB! use timestamp for Vs as matching time with excel time
function [chtxt]= sort_for_each_Ch(timepick)
ch0=zeros(length(timepick)/5,2);
ch1=zeros(length(timepick)/5,2);
ch2=zeros(length(timepick)/5,2);
ch3=zeros(length(timepick)/5,2);
ch4=zeros(length(timepick)/5,2);
j=0; k=0; l=0; m=0; n=0;

for i=1:length(timepick)
    check=timepick(i,1);
    if check==5
        j=j+1;
        ch0(j,1)=timepick(i,2);
        ch0(j,2)=timepick(i,3);
    elseif check==1
        k=k+1;
        ch1(k,1)=timepick(i,2);
        ch1(k,2)=timepick(i,3);
    elseif check==2
        l=l+1;
        ch2(l,1)=timepick(i,2);
        ch2(l,2)=timepick(i,3);
    elseif check==3
        m=m+1;
        ch3(m,1)=timepick(i,2);
        ch3(m,2)=timepick(i,3);
    else
        n=n+1;
        ch4(m,1)=timepick(i,2);
        ch4(m,2)=timepick(i,3);
    end
end
chtxt=[ch0(:,1),ch1(:,2),ch2(:,2),ch3(:,2),ch4(:,2),ch0(:,2)];
end
```

```
%% Import time picks, different format than for resistivity
function [timepick] = vel2mat(pathname,filename)
file = fullfile(pathname, filename);
%delimiter = ';';
delimiter = '\t';
startRow = 11;

%% Format string for each line of text:
formatSpec_data = '%*f Ch%f %*f %f %*[^\n\r]';
%formatSpec_date = '%*f %*s %*f %*f %*f %*f %*s %*7s%19s%*[^\n\r]';
```

```
formatSpec_date = '%*f %*s %*f %*f %*f %*f %*s %s%*[^\n\r]';
%% Load data
FID = fopen(file,'r');
data = textscan(FID, formatSpec_data, 'Delimiter', delimiter,...
    'HeaderLines' ,startRow-1, 'ReturnOnError', false);
fclose(FID);
FID = fopen(file,'r');
date = textscan(FID, formatSpec_date, 'Delimiter', delimiter,...
    'HeaderLines' ,startRow-1, 'ReturnOnError', false);
fclose(FID);


%% Create output variable
ch   = [data{1}];
picks = [data{2}];
date2 = [date{1}];
a=length(date2);
date3=zeros(a,1);
% timestamp as "Ch418 2015-01-12 16:03:16"  "" , but want format as
% YYYY-mm-ddHH:MM:SS, work for any number of measurements and not limited
% to under 100 measurements
for i=1:a %format timestamp to desired format
    y=date2{i,1}; %take single character string
    temp=strrep(y,'"',' '); % remove "
    temp2=sscanf(temp,'%*s %s %s'); % removes Ch### from string
    date3(i,1)=datenum(temp2,'YYYY-mm-ddHH:MM:SS');%string to value
end
timepick = [ch, date3, picks];
disp(['File ', filename, ' loaded'])
```

Submitted and accepted abstract for TCCS

TRACKING CO_2 FRONT DEVELOPMENT WITH ELECTRICAL RESISTIVITY MEASUREMENTS-AN EXPERIMENTAL STUDY

T. Tran[1], L.O. Omolo[1], M. Soldal[2], N.H. Mondol[1,2], J. Park[2] and Ø. Johnsen[3]

[1]Department of Geosciences, University of Oslo, P.O. Box 1047 Blindern, 0316 Oslo
[2]Norwegian Geotechnical Institute (NGI), P.O. Box 3930 Ullevål Stadion, 0806 Oslo
[3]Polytec Research Institute, Sørhauggata 128, 5527 Haugesund, Norway

Corresponding author's e-mail address: truongxt@student.geo.uio.no

Keywords: CO2, resistivity, monitoring

ABSTRACT

Subsurface storage of carbon dioxide (CO_2) is considered to be a possible solution to reduce atmospheric CO_2 emissions and to mitigate global warming. Saline aquifers and depleted hydrocarbon reservoirs can be good candidates for storing large amount of CO_2. Due to the variable depths of possible geological storage of CO_2, direct monitoring of change in the fluid properties is not feasible. Several authors (Alemu et al., 2013; Onishi et al., 2006; Xue et al., 2009) have studied electrical resistivity monitoring as an indirect method that could help to detect saturation changes of CO_2 storage reservoirs. In this experimental study, resistivity changes during injection of both liquid CO_2 and brine (30g/l NaCl) are measured across and at three different locations along a sandstone core plug (Gres des Vosges Sandstone from France). The tested core plug has an average porosity of 20% and the height and diameter are 79 mm and 38 mm respectively.

The experiment is conducted in a hydrostatic pressure vessel in which the confinement pressure is hydraulically controlled by a pressure controller to keep it at 25MPa. The sandstone core plug is placed inside a nitril rubber sleeve with mounted LVDT for radial and axial strain measurement, and possibility of measuring resistance in the axial and three radial positions (top, middle and bottom of the sample shown in Fig**.** 1a. To avoid gravity segregation, liquid CO_2 is injected from the top of the sample and during imbibition brine is injected from the bottom (Fig**.** 1b). Both liquids are pressurized to 10 MPa, and volumes corresponding to a certain number of pore volumes (0.1, 0.3, 0.5, 0.7, 0.9, 1.0, 2.0, 4.0, 6.0, 8.0, 9.0 and 10 PV) are injected and subsequent measurements of electrical resistivity are made. For 0-1 PV and 1-10 PV the injection rate were set at 0.5 mL/min and 2.5 mL/min respectively.

The measured electrical resistivity during drainage and imbibition are shown in Fig**.** 1c and 1d. The axial resistivity increases steadily until 9 PV during drainage, while it decreases until 4 PV during brine imbibition. The radial resistivity measurements are able to detect the CO_2 front during drainage; a resistivity increase is first seen at the sensor nearest the injection point and then gradually towards the outlet. During imbibition resistivity decreases for bottom (brine inlet) and middle part at 0.1 PV injected while for the top it is at 0.2 PV. After 10 PV of brine imbibition the measured resistivity is approximately as it was at the start of drainage.

From our experimental study, we conclude the electrical resistivity method and sensor array configuration is a handy tool to track development of CO_2 front during CO_2 injection. The flow rate influences the saturation of CO_2 as the resistivity development before and after 1 PV does not match (Fig**.** 1c). Imbibition of 0.2 PV brine is enough to decrease the resistivity by about 70%, but pushing the remaining CO_2 out requires injection of several pore volumes of brine. The change in flow rate does not seem to have a big impact during imbibition due to the gravity effect. More work will be done in this study on sandstones with varying anisotropy focusing more closely on the effects of injection rate.

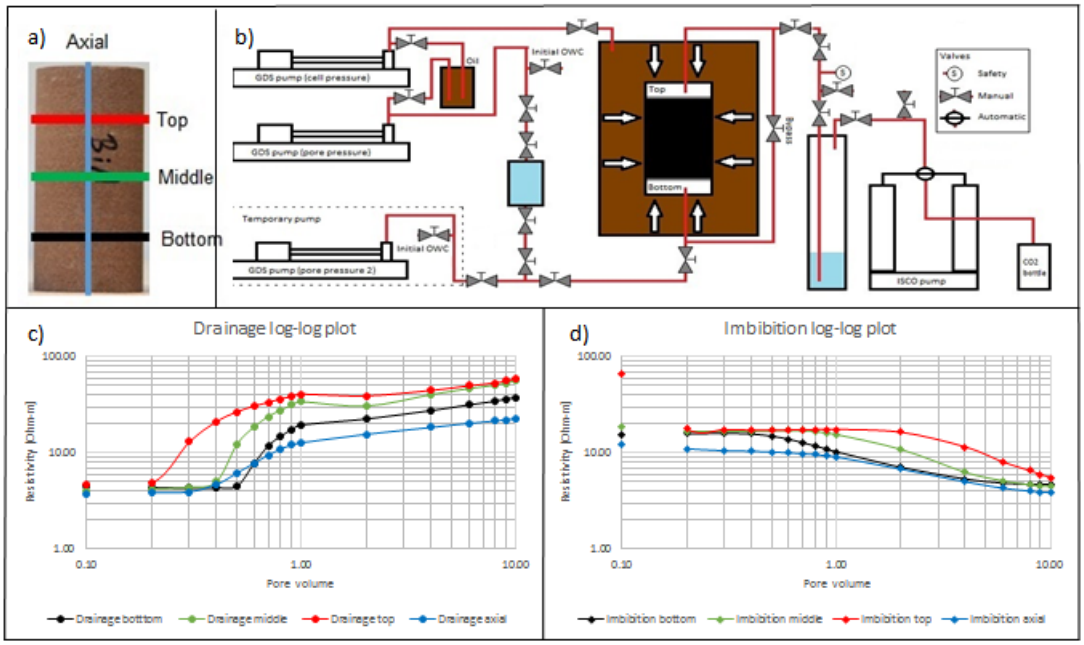

Fig. 1: a) Gres des Vosges Sandstone core plug, b) Experimental set up, c) Measured electrical resistivity during drainage of CO2 and d) Measured electrical resistivity during imbibition of brine.

ACKNOWLEDGEMENTS

We appreciate the support from SUCCESS FME centre for CO2 storage under grant 193825/S60 from Research Council of Norway (RCN). We also thank for the financial and scientific contributions from NGI GBV Project 20120265.

REFERENCES

Alemu, B. L., Aker, E., Soldal, M., Johnsen, Ø., and Aagaard, P., 2013, Effect of sub-core scale heterogeneities on acoustic and electrical properties of a reservoir rock: a CO2 flooding experiment of brine saturated sandstone in a computed tomography scanner: Geophysical Prospecting, v. 61, no. 1, p. 235-250.

Onishi, K., Ishikawa, Y., Yamada, Y., and Matsuoka, T., 2006, Measuring Electric Resistivity of Rock Specimens Injected With Gas, Liquid And Supercritical CO2, Society of Exploration Geophysicists.

Xue, Z., Kim, J. W., Mito, S., Kitamura, K., and Matsuoka, T., 2009, Detecting and Monitoring CO2 With P-Wave Velocity and Resistivity From Both Laboratory and Field Scales, Society of Petroleum Engineers.

ACOUSTIC VELOCITY MEASUREMENT DURING DRAINAGE AND IMBIBITION OF CO_2 IN SANDSTONES

L.O. Omolo[a], T. Tran[a], M. Soldal[b], N. H. Mondol[a,b], L. Grande[b], J. Park[b] and Ø. Johnsen[c]

[a]Department of Geosciences, University of Oslo, [b]Norwegian Geotechnical Institute (NGI) Oslo, [c]Polytec Research Institute, Haugesund, Norway

Corresponding author's e-mail address: lamechoo@mail.uio.no

Keywords Vp –Vs relation, imbibition, drainage.

ABSTRACT

Subsurface storage of CO2 is considered to have a large potential to mitigate and reduce anthropogenic CO2 emission. Some of the best candidates for large scale CO2 storage includes saline aquifers and depleted hydrocarbon reservoirs. Several laboratory-based studies have been carried out in recent years to find the influence of CO2 on the acoustic properties of reservoir rocks including Lei and Xue (2009), Nakagawa et al. (2013) and Siggins et al. (2010). They show that Gassmann's prediction of both P- and S-wave velocities during fluid substitution can be proven by experimental results. The success of CCS (Carbon Capture and Storage) technique depends, among other thing on, storage capacity and injectivity of CO2 without any leakage to the surface. Indirect geophysical monitoring can provide information about the CO2 behavior including distribution, migration and change in saturation (Kitamura et al., 2014), and estimate the CO2 storage volume in a given reservoir.

In this experimental study, we investigate the potential of seismic techniques for monitoring and quantifying saturation changes in the space-time domain for CO2 reservoirs by simulating 1 km deep reservoir with a pore pressure of 10 MPa using three well-known sandstones: Berea, Red Wildmoor and Gres des Vosges. The experiment protocol comprises of mechanical loading phase, succeeded by a CO2 drainage and imbibition phase. The inherent and stress-induced material anisotropy, the effect of pore fluid composition, as well as the dynamic changes during CO2 drainage and imbibition are quantified, mechanically and in terms of rock physical signatures.

The experimental laboratory investigations are conducted in a hydrostatic pressure vessel (Fig. 1c) with a confining pressure of 25 MPa. Pressure sensors measure confining pressures and pore pressures, and Linear Variable Differential Transformer (LVDT) mounted directly onto the nitrile sleeve with an array of P- and S-wave piezo-ceramic crystals embedded at three different levels across the length in order to measure velocity both in axial and radial directions (Fig. 1d). The pore pressure is controlled using an ISCOTM pump. To avoid dropping in pressure during drainage, we used a GDS pump for maintaining backpressure.

Prior to CO2 injection, the samples underwent cyclic hydrostatic loading from 1MPa to 15 MPa for dry, fully CO2 saturated, and fully brine saturated conditions to characterize the mechanical properties. During both drainage and imbibition, we use a flow rate of 0.5 ml/min from 0 pore

volume (PV) to 1 PV in 0.2 PV steps and increased the flow rate to 2.5 ml/min from 2 PV to 8 PV in 2 PV steps. Liquid CO2 was injected from top of the sample during drainage while brine was injected from the bottom during imbibition to avoid gravity segregation.

During both drainage and imbibition, axial Vs does not change much and this is attributed to non-response nature of Vs during fluid substitution. The axial Vp decreases from 0-1 PV then flattens out during drainage while bottom and middle radial Vp sensors record drastical decrease from 0-1 PV then stabilizes up to 8 PV as compared to top Vp sensor. In the imbibition phase, the axial Vp increases gradually with the greatest increment occurring between 2-9 PV. For the radial Vp, all the three (top, middle and bottom) measurements are more or less stable between 0-1 PV. Bottom Vp increases most between 1 and 4 PV as compared to the rest then stabilizes up to 9 PV.

From our experimental results, we clearly see opposite tendencies in Vp and Vs during drainage and imbibition. The acoustic P-wave velocities decreases during drainage (Figs. 1a and 1b) due to negative change in bulk modulus and density as a result of pore fluid substitution (brine to CO2) and this is in agreement with Gassmann's prediction (Gassmann, 1951). According to Mavko et al. (1995), presence of reservoir fluid is identified on seismic data using relationships between the P- and S-wave arrival times and attenuation. At the end of imbibition, Vp does not recover fully to a pre-drainage due to the effect of residual trapped CO2. These results are consistent with previous studies on Vp-Vs relation suggested by Han et al. (1986) and Kitamura et al. (2014). By analyzing the experimental data, we can clearly see the effect of injected CO2 on the formation, which should be critical in interpreting geophysical field data in practice including mapping its distribution.

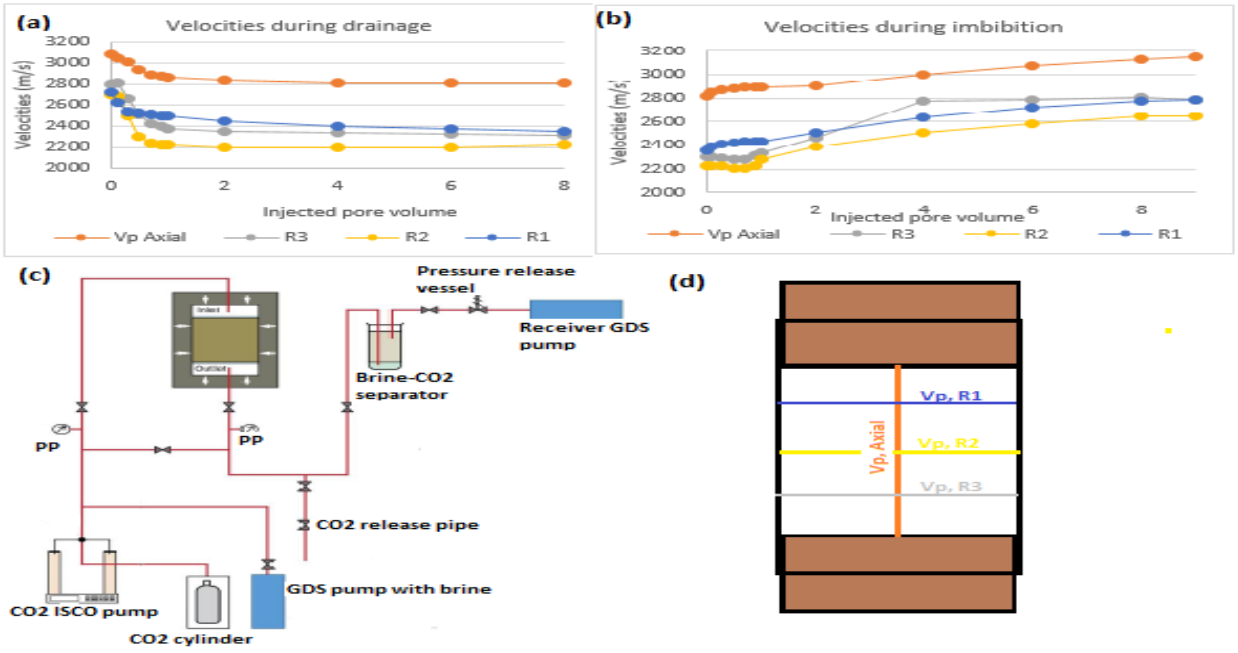

Figure 1: a) Measured velocities during drainage, (b) Measured velocities during imbibition. (c) Experimental setup and (d) schematic diagram showing measurement direction, R1, R2 and R3 refers to Vp measurements at the top, middle and bottom respectively.

ACKNOWLEDGEMENTS

We appreciate the support from SUCCESS FME centre for CO2 storage under grant 193825/S60 from Research Council of Norway (RCN). We also thank for the financial and scientific contributions from NGI GBV Project 20120265.

BACHU, S. 2000. Sequestration of CO2 in geological media: Criteria and approach for site selection in response to climate change. Energy Conversion and Management, 41, 953-970.

GASSMANN, F. 1951. Uber die Elastizitat poroser Medien, Zurich, Vierteljahrsschrift der Naturforschenden Gesellschaft.

HAN, D.-H., NUR, A. & MORGAN, D. 1986. Effects of porosity and clay content on wave velocities in sandstones. Geophysics, 51, 2093-2107.

KITAMURA, K., XUE, Z., KOGURE, T. & NISHIZAWA, O. 2014. The potential of Vs and Vp–Vs relation for the monitoring of the change of CO2-saturation in porous sandstone. International Journal of Greenhouse Gas Control, 25, 54-61.

LEI, X. & XUE, Z. 2009. Ultrasonic velocity and attenuation during CO2 injection into water-saturated porous sandstone: Measurements using difference seismic tomography. Physics of the Earth and Planetary Interiors, 176, 224-234.

MAVKO, G., MUKERJI, T. & GODFREY, N. 1995. Predicting stress-induced velocity anisotropy in rocks. Geophysics, 60, 1081-1087.

NAKAGAWA, S., KNEAFSEY, T. J., DALEY, T. M., FREIFELD, B. M. & REES, E. V. 2013. Laboratory seismic monitoring of supercritical CO2 flooding in sandstone cores using the Split Hopkinson Resonant Bar technique with concurrent x-ray Computed Tomography imaging. Geophysical Prospecting, 61, 254-269.

SIGGINS, A. F., LWIN, M. & WISMAN, P. 2010. Laboratory calibration of the seismo-acoustic response of CO2 saturated sandstones. International Journal of Greenhouse Gas Control, 4, 920-927.

Submitted and accepted abstract for 3IWRP

CO2 flooding experiment of reservoir sandstones-monitoring changes in acoustic and electric properties

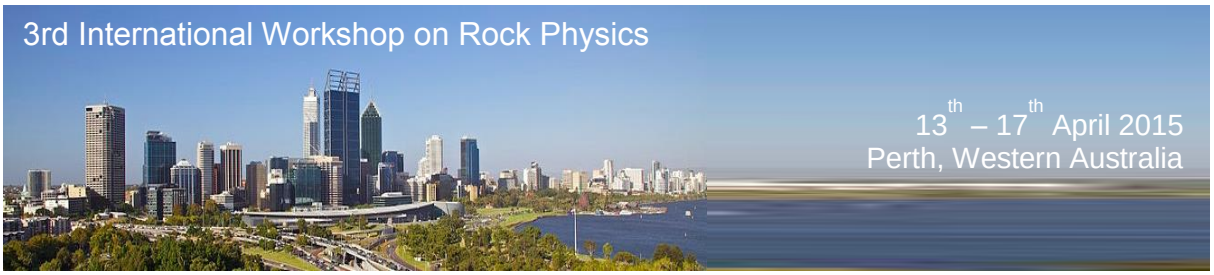

CO2 flooding experiment of reservoir sandstones-monitoring changes in acoustic and electric properties

M. Soldal[a], L.O.Omolo[b] and T.Tran[b], Ø. Johnsen[c], N.H.Mondol[b,a], I. Viken[a], L. Grande[a] and J. Park[a]

[a]*Norwegian Geotechnical Institute (NGI), Postboks 3930 Ullevål Stadion, 0806 Oslo;* [b]*Department of Geosciences, P.O box 1047Blindern0316 OSLO,* [c]*Polytec Research Institute, Sørhauggata 128, 5527 Haugesund, Norway. Contact email: magnus.soldal@ngi.no*

Summary

We present an advanced laboratory work to measure electrical resistivity, acoustic velocity (ultrasonic frequency) and anisotropy during injection of liquid CO2 into initially brine saturated reservoir core samples. A novel measurement system has been developed, where velocity and resistivity are measured at different points along the specimen axial direction. The changes in velocity and resistivity observed during the CO2 injection will be a critical element in interpreting geophysical field data to understand reservoir behaviour.

Introduction

Geological storage of carbon dioxide (CO2) is considered one of the main options for reducing anthropogenic CO2 emission from large scale point sources. Saline aquifers and producing/abandoned hydrocarbon reservoirs are good candidates for large scale CO2 geological storages (e.g. those in North Sea). Success of such techniques is dependent primarily on the storage capacity and injectivity of these repositories to store CO2 without any leakage and incident through cap rock and overburden. Initially, most of injected CO2 is mobilized and trapped hydro-dynamically in formation pore space. Therefore, the fundamental mechanisms of multiphase flow through porous media is a critical element to understand and apply. In addition, the injected CO2 influences the formation petrophysical properties, which are also important in characterization and monitoring of reservoir and cap rock during and after injection (Alemu *et al*. 2013). Direct measurement of the petrophysical properties is, however, not a common practice during geological injection due to technical and cost issues. Instead, indirect measurement through geophysical field survey is applied. Geophysical field data can provide temporal and spatial variations of seismic velocity, electrical resistivity, density and anisotropy of the formation, which in turn can provide the changes in the formation petrophysical properties through relevant rock physics models (Alnes *et al*. 2011, Arts *et al*. 2008, Chadwick *et al*. 2005, Park *et al*. 2014).

In this study, we present a rock physics laboratory work to measure electrical resistivity, acoustic velocity (ultrasonic frequency) and their anisotropy during injection of liquid CO_2 into initially brine saturated reservoir core samples. For this purpose, a novel measurement system has been developed. The system measures velocity and resistivity at different points along the specimen axial direction. Saturation levels and fluid distribution pattern within the porous system are also be mapped using a high resolution X-ray Computed Tomography (CT) scanner (Alemu *et al*. 2013). The study is still on-going and more results will be published in near future. The current focus of the study is only CO2 geological storage. As a long term plan, the same framework will be applied to CO2 injection for enhanced oil recovery (EOR).

Method

The tests are conducted in a hydrostatic pressure vessel and the injected CO2 is in the liquid state (see Figure 1). Pressure sensors measure confining and pore pressures, and LVDT strain gages mounted onto the samples give accurate measurements of axial and radial deformation. Two parallel experiments are performed on each sample; one utilizing a core sleeve with copper electrode rings embedded for sequential resistivity measurements (Figure 1b) and one utilizing a sleeve with LVDTs mounted directly onto it and with an array of P-wave piezo-ceramic crystals embedded into it at three different levels across the sample length (Figure 1c). The two in-parallel experiments make it possible to quantify the stress dependency, anisotropy and fluid composition of P-wave velocity (Vp), S-wave velocity (Vs), and electrical resistivity (R) during hydrostatic loading and CO_2 flooding. The rock physical signature interpreted from geophysical measurements are cross-correlated against actual CO2 distribution pattern retrieved from flooding experiments conducted inside the CT scanner.

Test specimens are selected from well-known permeable sandstones (Red Wildmore, Gres des Vosges and Berea) with homogeneous and heterogeneous mineralogical compositions. Core plugs are drilled parallel and perpendicular to bedding plane in order to study the impact of material type on the mechanical and linked physical responses and impact of anisotropy (Table in Figure 2). Prior to CO2 injection, the samples experience hydrostatic loading cycles in dry conditions, fully CO2 saturated conditions and fully brine saturated conditions to characterize the mechanical response.

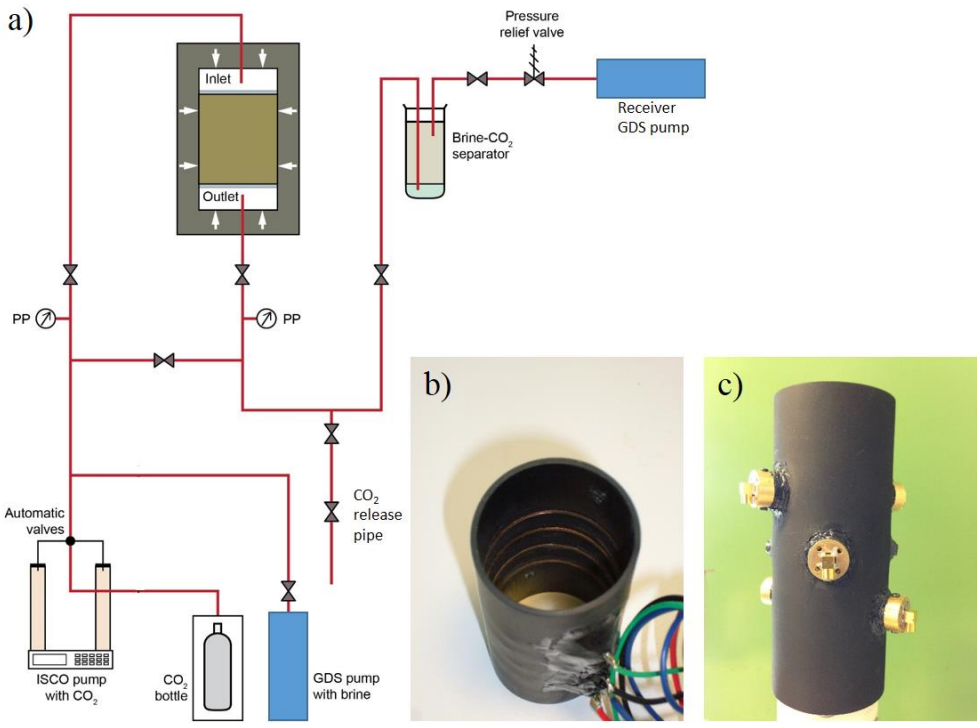

Figure 1. A) flow chart of the experimental setup; b) sleeve with 5 copper electrode rings embedded for sequential resistivity measurements, and c) sleeve with array of acoustic P-wave piezo elements.

Results

Figure 3 and 4 shows the rock physics response to CO_2 injection for the sensor configurations Figure 1 a) and b) respectively for a vertically drilled Red Wildmore sandstone (V, $\perp$ to bedding). Both resistivity and acoustic techniques are efficient in tracing the CO_2-brine front, and we find from the curves that

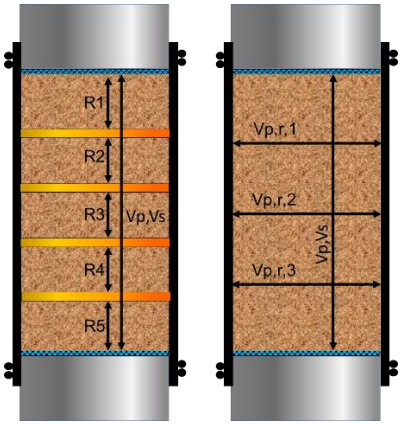

Sample material	Drilling directions	Sleeve 1	Sleeve 2
Red Wildmoore	**V, ⊥ to bedding**	**P⊥, S⊥, R 1-5⊥**	**P⊥, S⊥,P∥ 1-3**
	H, ∥ to bedding	**P ∥ , S ∥ , R 1-5 ∥**	**P ∥ , S ∥ , P⊥ 1-3**
Gres Des Vosges	**V, ⊥ to bedding**	**P⊥, S⊥, R 1-5⊥**	**P⊥, S⊥,P∥ 1-3**
	H, ∥ to bedding	**P ∥ , S ∥ , R 1-5 ∥**	**P ∥ , S ∥ , P⊥ 1-3**
Berea	**V, ⊥ to bedding**	**P⊥, S⊥, R 1-5⊥**	**P⊥, S⊥,P∥ 1-3**
	H, ∥ to bedding	**P ∥ , S ∥ , R 1-5 ∥**	**P ∥ , S ∥ , P⊥ 1-3**

Figure 2. Sleeve configuration for resistivity and velocity measurement (Sleeves 1 and 2, respectively); Permutations of rock physics measurements

breakthrough. As the front advances along the length of the sample the measured normalized resistivity increases from unity in an in a sequential fashion from R1 through R5 (Figure 3) revealing the front position as the saturation of conducting phase (brine) decreases (Archie, 1942) locally. Similarly the acoustic P-wave velocity decreases due to negative change in bulk modulus for the rock/fluid system as well a negative change in density, in accordance with common mixing laws (Brie 1995). The behaviour is naturally reversed in the case of reimbibition of brine.

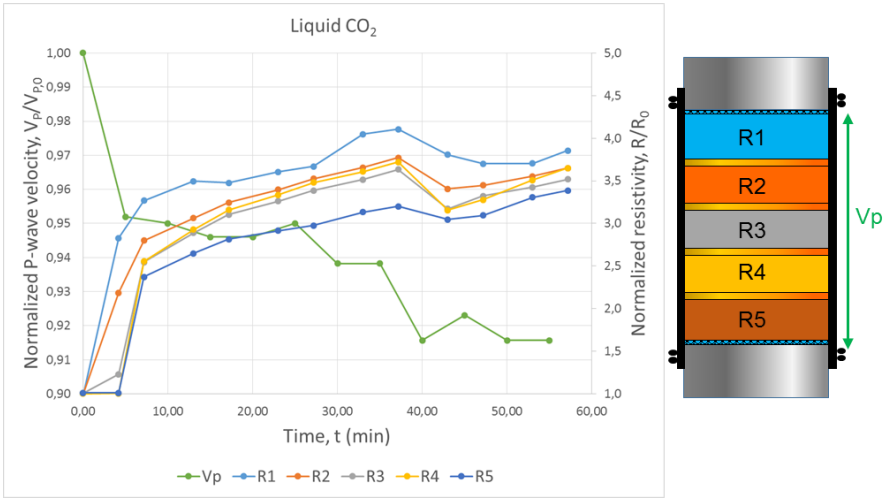

Figure 3. Resistivity and axial P-wave velocity during injection of liquid CO_2. Measured V_P and R are normalized with the initial fully brine saturated reference value $V_{P,0}$ and R_0.

After first registering the displacement front by radial V_P measurements or altered resistivity in segment 1-5 there is considerable change in measured quantities over time as injection continues, suggesting a good sweep efficiency and a stable displacement, i.e. capillary forces dominant thus suppression of viscous fingering / channeling. Mixing of the phases also contributes and in being in nature a time function becomes more important with time even after breakthrough of CO_2. This is confirmed by flow experiments conducted in a CT scanner (Alemu et al, 2013).

Conclusions

In this study, we present a novel approach to measure seismic velocity and resistivity during CO2 flooding experiment in a rock physics framework. Liquid CO2 is injected into initially brine saturated

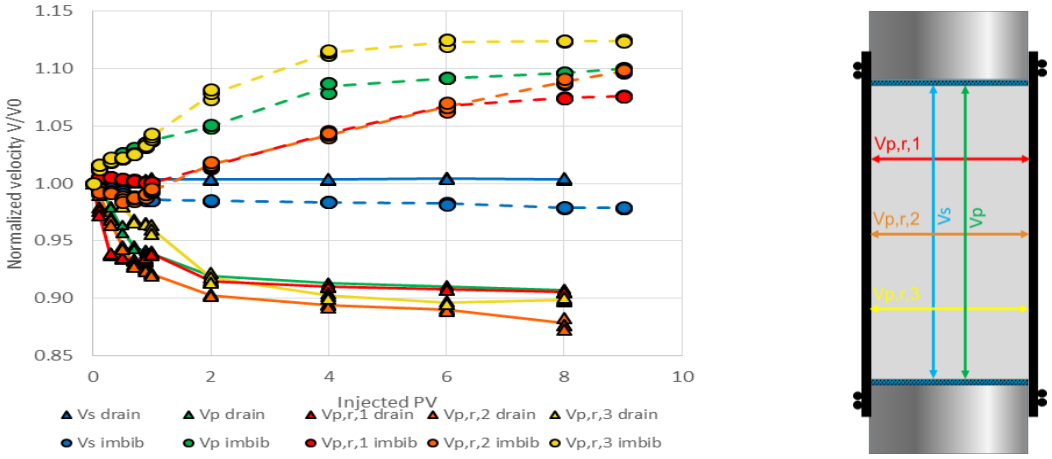

Figure 4: Axial P- and S-wave, and radial P-wave velocities measured during injection of liquid CO_2, vs injected pore volume (PV) of CO_2 (drainage) and brine (reimbibition). Measured velocities are normalized with measured velocity just before injection; fully saturated with brine before injecting CO_2 and partial brine/CO_2 saturation before reimbibition with brine.

reservoir core samples. Results show promising aspects of the developed system. By analyzing the measure data, we can clearly see the effect of injected CO2 on the formation, which should be critical in interpreting geophysical field data in practice. The study is still on-going and more results will be published in near future.

Acknowledgements

We appreciate the support from SUCCESS FME centre for CO2 storage under grant 193825/S60 from Research Council of Norway (RCN). We also thank for the financial and scientific contributions from NGI GBV.

References

1. Alemu, B.L., Aker, E., Soldal, M., Johnsen, Ø. and Aagaard, P. [2013] Effect of sub-core scale heterogeneities on acoustic and electrical properties of a reservoir rock: a CO2 flooding experiment of brine saturated sandstone in a computed tomography scanner, Geophysical Prospecting, 61(1), 235-250.
2. Alnes, H., Eiken, O., Nooner, S., Sasagawa, G., Steinvold, T. and Zumberg, M. [2011] Results from Sleipner gravity monitoring: Updated density and temperature distribution of the CO2 plume. Energy Procedia, 4, 5504-5511.
3. Archie, G.E. 1942. The Electrical Resistivity Log as an Aid in Determining Some Reservoir Characteristics.
4. Arts, R., Chadwick, A., Eiken, O., Thibeau, S. and Nooner, S. [2008] Ten years' experience of monitoring CO2 injection in the Utsira Sand at Sleipner offshore Norway, First Break, 26, 65-72.
5. Brie, A., Pampuri, F., Marasala, A.F. & Meazza, O. 1995. Shear sonic interpretation in gasbearing sands. *Society of Petroleum Engineers* SPE No. 30595.
6. Chadwick, R.A., Arts, R. and Eiken, O. [2005] 4D seismic quantification of a growing CO2 plume at Sleipner, North Sea, In: Doré, A.G. & Vining, B. (editors), Petroleum Geology: North-West Europe and Global Perspectives – Proceedings of the 6th Petroleum Geology Conference, 1385-1399.
7. Park, J., Vanneste, M., Bohloli, B., Viken, I., Bjørnarå, T.I. [2014] In situ resistivity of CO2 plume at Sleipner from CSEM and gravity data, Fourth EAGE CO2 Geological Storage Workshop, 22-24 April 2014, Stavanger, Norway